UNIVERSITÀ
DEGLI STUDI
DI PADOVA

DIPARTIMENTO
DI INGEGNERIA
DELL'INFORMAZIONE

DIPARTIMENTO DI INGEGNERIA DELL'INFORMAZIONE

CORSO DI LAUREA MAGISTRALE IN BIOINGEGNERIA

NEURONAL DAMAGE AND COGNITIVE IMPAIRMENT IN PARKINSON'S DISEASE: THE RELATION AMONG SERUM BIOMARKERS, BRAIN ATROPHY AND COGNITIVE PERFORMANCE

Relatore: Ch.ma Prof.ssa Alessandra Bertoldo
Correlatore: Dott. Simone Cauzzo

Laureando: Andrea Ribattezzato

ANNO ACCADEMICO 2023 – 2024

Data di laurea 05/12/2024

Contents

ABSTRACT

Parkinson's disease (PD) is the second most widespread neurodegenerative pathology after Alzheimer's one. During the early stages it presents highly heterogeneous features and, as time progresses, it leads patients to present symptoms of a not only motor nature. Among the main motor symptoms, it is possible to find cognitive impairment, apathy, depression, anxiety, impulse control disorders, sleep disturbance, fatigue, pain, visual hallucinations and autonomic dysfunction. At present, the mechanism by which these collateral symptoms can develop during the disease progression and/or what type of physiological factors they are linked to, is not yet well understood. The development of new magnetic resonance imaging techniques has had a great impact on the characterization of many neurodegenerative pathologies, including Parkinson's disease.

The objective of this thesis is to carry out a morphometric analysis on the patients' magnetic resonance images and to investigate the relationship between morphometric results, blood parameters and cognitive status.

To do this, it was considered a cohort of 57 PD patients, part of which affected by mild cognitive impairment (MCI), while another part characterized by a normal cognitive state (NC). The structural images considered were acquired using high-field magnetic resonance imaging and the sequences used for the morphometry were mainly T1-weighted and FLAIR T2-weighted. The biomarkers considered were nuerofilament light chain (NFL), Glial fibrillary acidic protein (GFAP), phosporilated Tau 181 and the GFAP/NFL ratio, while the cognitive scales used were the Montreal Cognitive Assessment (MOCA) and the Mini Mental State Examination (MMSE). To obtain brain morphometrics both a surface-based/voxel-based hybrid model on FreeSurfer and a voxel-based model on SPM were used. The morphometry results of the two models were compared. From the statistical parameters of the morphometry, the brain volumes were extracted and, so, the correlations between those of MCI and those of NC patients were calculated. Then, the correlations between volumes and biomarkers were evaluated and comparisons on the values of the biomarkers, dividing the population by gender, cognitive state and score on the cognitive scales were carried out.

The results showed that there is a significant linear correlation between FreeSurfer and SPM results for most of the cortical volume estimates, although a scaling factor is present, while the situation in the subcortex is much more heterogenous, presenting areas for which there is little or no correlation. The morphometrics obtained with Freesurfer are in line with the literature.

Gray matter atrophy was found in the cingulate, entorhinal, fusiform, parahippocampal and temporal cortex, other than in the orbital regions and in the paracentral lobule.

Trends were observed between volumes and blood biomarkers and statistical tests suggested links between biomarker values and demographic parameters like age, gender and cognitive status. However, applying the Bonferroni-Holm multiple testing correction method, the significance values found earlier did not survive.

Although the study was limited by the relatively small size of the dataset available, these preliminary results highlight how this line of research could reveal new insights in the specificity of these biomarkers and further studies could lead to a clearer picture of the neurodegenerative phenomenon dictated by Parkinson's disease in all its aspects.

Chapter 1

INTRODUCTION

1.1 NEUROIMAGING

The field of neuroimaging deals with the study of the brain through visual representations of its structure, function and connectivity (1). The visualization of the brain in two or three dimensions allows a human user (e.g. a physician) to draw results for diagnostic or research purposes. This need calls for the use of a variety of visualization and image processing techniques to process images and to make them more understandable and more useful for human users.

The main objective of neuroimaging is to better understand the functioning of the brain, both in normal and pathological conditions, through the direct observation of its activities and anatomical characteristics (2).

Neuroimaging techniques such as structural magnetic resonance imaging (sMRI) and computed tomography (CT) enable detailed visualization of the anatomical structure of the brain, including brain tissues, lesions, and structural anomalies (3). Techniques such as functional magnetic resonance imaging (fMRI), electroencephalography (EEG), and magnetoencephalography (MEG) allow real-time observation of brain activity at rest or during cognitive, emotional, or behavioural tasks (4). Through diffusion tensor imaging (DTI) it is possible to map neural connections in the brain and study the brain circuits involved in various cognitive and behavioural functions (5).

The field of neuroimaging has important applications in scientific research, clinical practice, neurology, and psychiatry. Neuroimaging can be used to better understand the neural bases of neurological and psychiatric diseases, diagnose brain lesions, monitor the progression of certain clinical conditions, and evaluate the effectiveness of pharmacological or therapeutic treatments(6). Moreover, neuroimaging is crucial for the development and improvement of neurotechnologies, such as neurofeedback, non-invasive brain stimulation, and brain-computer interfaces, which have the potential to transform the treatment of various neurological and psychiatric conditions (7).

1.1.1 MAGNETIC RESONANCE IMAGING

Magnetic Resonance Imaging (MRI) consists of a set of techniques that, by exploiting the magnetic and electrical properties of the electron, allows the study of biological tissues through the assessment of the absorption of radiofrequency and microwave energies by the electron subjected to an external magnetic field (8). A fundamental characteristic of Magnetic Resonance Imaging (MRI) is the use of low-energy electromagnetic radiation that does not alter or destroy the substances under study and has no harmful effects on biological molecules.

The main components of a magnetic resonance imaging (MRI) system include:

1. **Magnet**: The magnet is the primary component of the MRI system and generates a uniform static magnetic field within which the patient is positioned during the examination.
2. **Radiofrequency coils**: These coils emit radiofrequency pulses used to manipulate the magnetic field within the patient and to detect signals generated by protons in the body during the examination.
3. **Gradient magnetic system**: This system consists of magnetic gradients that allow the creation of weak but directed magnetic fields in different directions. These gradients are used to encode spatial information during image acquisition.
4. **Computer and image processing software**: After signals are detected by the radiofrequency coils, they are sent to a computer that uses specialized software to process the data and generate final images.
5. **Control console**: This is the interface that allows operators to control the MRI system, set examination parameters, and monitor the patient during the scan.
6. **Patient bed**: The bed on which the patient is positioned slides in and out of the MRI machine during the examination.

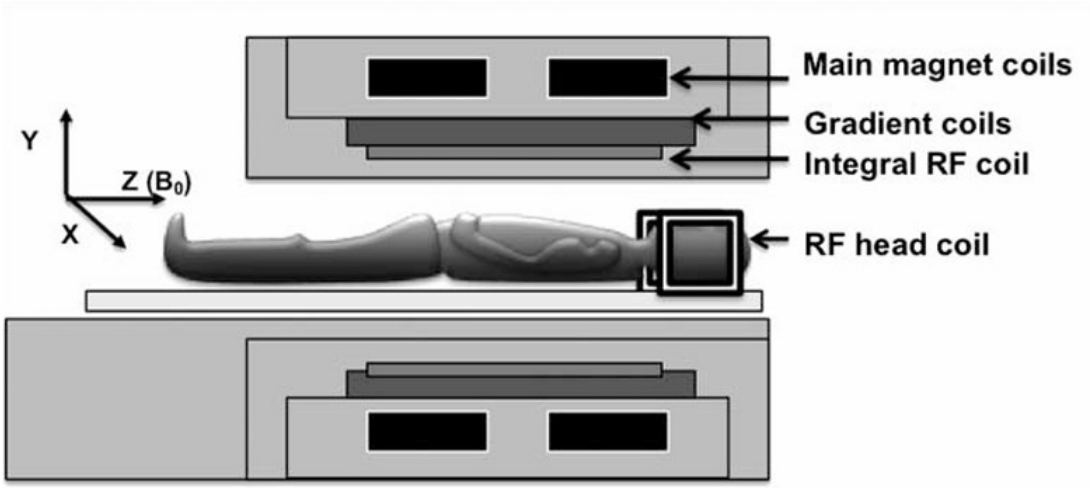

Figure 1: Schematic representation of the MRI coils and the relative position of the patient (image from (9))

When the patient is positioned inside the MRI machine, the protons present in the body tissues are aligned with the static magnetic field. A radiofrequency pulse is applied, causing a temporary disturbance in the alignment of the protons. When the pulse is turned off, the protons release energy and gradually return to their initial state of alignment to the static magnetic field. The MRI machine detects the signals emitted by the protons as they return to their state of magnetic alignment. These signals are processed to create detailed images of the body tissues. The reference system adopted in this technology is the one reported below (Figure 1). In these figures, the one on the right side describe the reference system and the terminology adopt while the image on the left describe how it is applied the static magnetic field from the main coil that produce the polarization of all the magnetic dipoles relative to each molecule and atoms. This magnetic field lead to the same orientation of all the magnetic dipoles inside our body. This is a crucial step, which we will describe it later deeply, to have the same position and orientation for all the dipoles of our body.

Figure 2: MRI Reference System. M0, or B0, is the static magnetic field. The reference system is organized in such a way that the z axis coincides with the direction and direction of B0 (or M0), while the x and y axes lie on a plane perpendicular to z

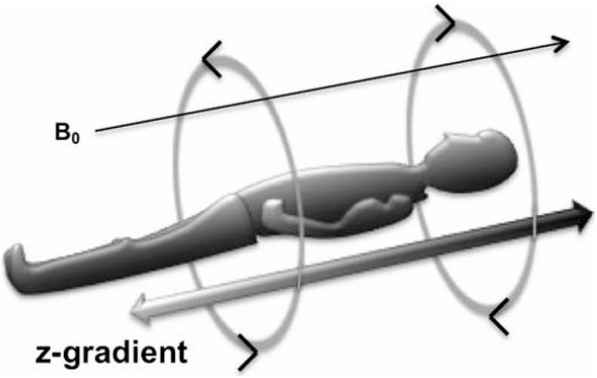

Figure 3: Orientation of the main magnetic. The reference system z axis of is parallel to B0 and longitudinal with respect to the patient (image from (9))

When an atom, with an odd number of protons and/or neutrons, is placed in a magnetic field, its nucleus aligns either parallel or antiparallel to the direction of the field lines, and it rotates around its axis at a specific frequency (Larmor frequency). By providing energy in the form of radio waves tuned to the Larmor frequency, the nucleus absorbs this energy and enters an unstable state. After the RF pulse is ceased, the nucleus returns to its initial condition, emitting a radio wave that can be captured and analysed by the apparatus.

Since the human brain is predominantly composed of water, there is an abundance of free hydrogen protons. At rest, these hydrogen protons rotate around their own axis and, being positively charged, induce a small polar magnetic field known as the magnetic moment or spin. The spin (also called angular momentum) is a vector quantity, which has a value of +/- 1/2. In the absence of an external magnetic field, each proton aligns randomly in space, resulting in a zero magnetic moment, but applying an external magnetic field (homogeneous and constant over time), individual particles align themselves according to the direction of the magnetic field, much like the needle of a compass aligns itself with the direction of the Earth's magnetic field, positioning itself parallel or antiparallel (10).

Considering that the magnetic axis of the proton tends to align itself with the direction of the magnetic field in an oscillating manner, and that this oscillation combines with the rotational motion inherent to the particle (spin), we will have a complex movement of rotation on a conical surface with the axis being the direction of the magnetic field. The movement is very similar to that of a spinning top, which oscillates around its own axis of rotation. It's important to know the speed of this movement measured as the precession frequency (the number of precessions per second) (10). The speed of the precession movement, measured as a frequency, increases

proportionally with the intensity of the external magnetic field and varies from atom to atom depending on the gyromagnetic constant (10). The relationship that links these quantities is called the Larmor equation:

$$\omega_0 = \gamma * B_0$$

where

$\omega_0 = precession\ angular\ speed\ or\ precession\ frequency$

γ =gyromagnetic constant

$B_0 = static\ \ magnetic\ field\ intensity$

By positioning a patient in an MRI machine, like in any magnetic field, the patient behaves like a magnet, forming its own magnetic field. We cannot quantify longitudinal magnetization, as it presents a direction parallel to that of the external magnetic field. So, it is necessary to disturb this system so that a new magnetization is generated in the transverse direction to the previous one. To achieve this, a short-duration electromagnetic wave, which we call an RF pulse, is sent to the patient. This pulse is intended to disturb the protons uniformly, aligning them parallel to the external magnetic field. Not all radiofrequency pulses disturb the alignment of protons, but only some can change their energy. Only when the RF pulse and the protons have the same frequency, the protons can absorb energy from the radio pulse (a phenomenon called resonance). The pulse must have the same frequency: if it were not the case, the energy exchange would be lower or impossible because it would not match the speed of the protons. The Larmor equation allows to calculate this frequency so as to determine the frequency of the RF pulse to be sent.

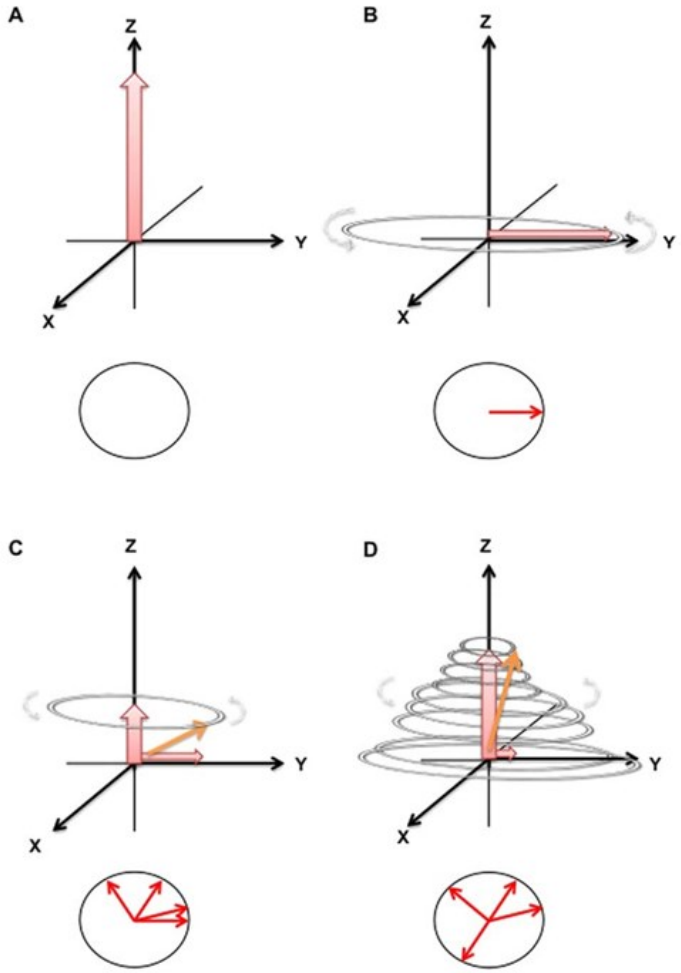

Figure 4: Protons longitudinal magnetisation recovery following a 90° radiofrequency (RF) pulse (image from (9))

The radio wave has two effects on the protons:

- It causes some protons to transition to a higher energy level (they align downwards).
- It causes the protons to precess in phase. The first effect results in a decrease in longitudinal magnetization. The second effect establishes a new magnetization in the "X-Y" plane, transverse, which moves around with the precessing protons.

Once the RF pulse is turned off, the system tends to return to equilibrium (reaching its state of minimum energy) by releasing the energy absorbed during excitation. This occurs through two independent processes: longitudinal relaxation and transverse relaxation.

Longitudinal relaxation, also known as spin-lattice relaxation or T1 relaxation, is named after the time constant that governs this process. T1 relaxation refers to the process of recovering longitudinal magnetization through the exchange of energy with the surrounding environment.

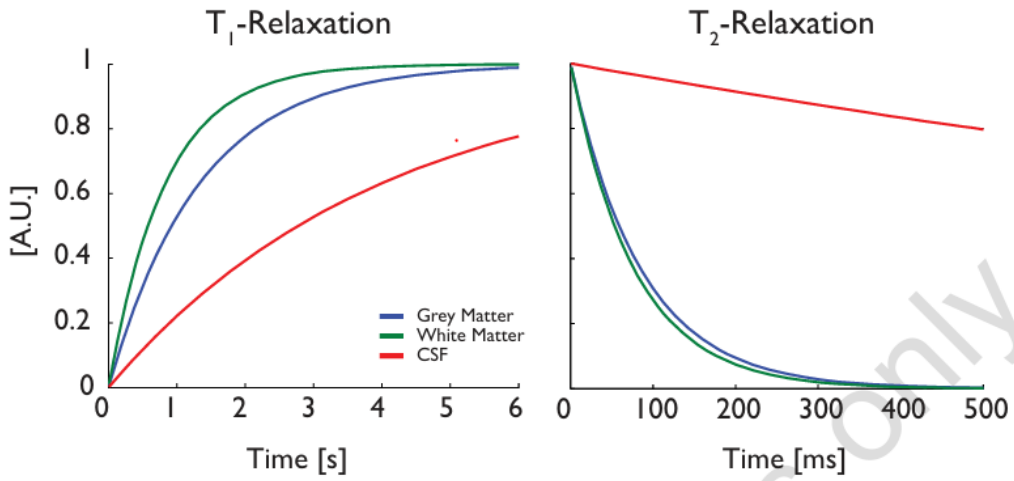

Figure 5: T1 and T2 relaxation rates for different brain tissue classes (image form (8))

T1 is the longitudinal relaxation time (thermal relaxation time or spin lattice relaxation time). The T1 relaxation time characterizes the rate at which the Mz component recovers its initial magnetization $M0$.

$$M_z(t) = M_0(1 - e^{-\frac{t}{T_1}})$$

Transverse relaxation, also known as T2 relaxation, describes the process of losing phase coherence between spins, effectively destroying the transverse component of the magnetization vector. This is caused by the presence of local magnetic fields produced by neighbouring nuclear and electronic spins.

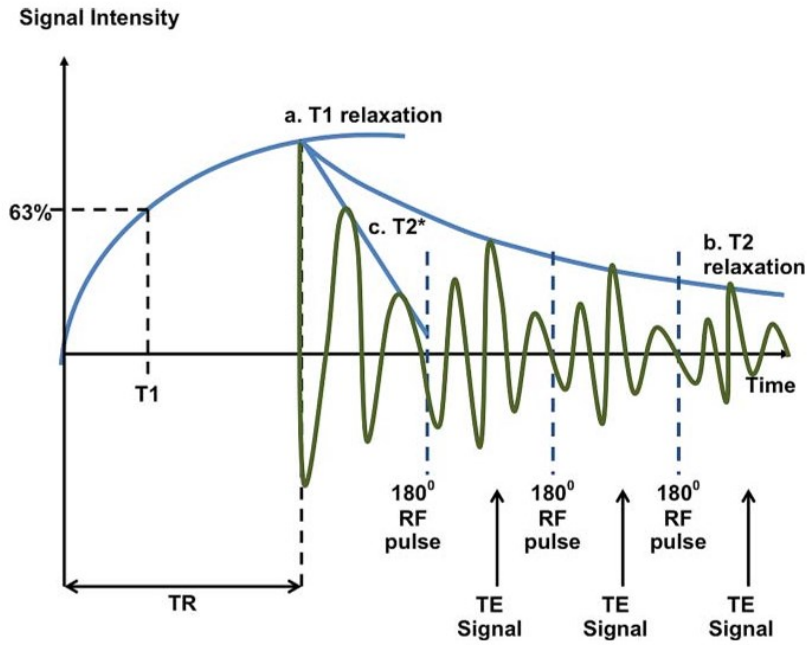

Figure 6: T1, T2 and T2 relaxation (image from (9))*

T_2 is also known as the transverse relaxation time (spin – spin relaxation time). The T_2 relaxation time characterizes the rate at which the M_{xy} component decays.

$$M_{xy}(t) = M_0\, e^{-\frac{t}{T_2}}$$

Both T1 and T2 relaxations are exponential processes. Since T1 and T2 depend on the surrounding environment of the spins, they tend to vary with tissue characteristics: water is bound differently in different tissues. This leads to differences in the rate of T1 and T2 relaxation in different tissues, generating contrast in the image. T1 and T2 relaxations are independent processes that operate on different time scales and depend on the strength of the magnetic field.

Two other important parameters in MRI acquisition sequences are the "Echo Time" (TE) and "Repetition Time" (TR). They allow for the adjustment of contrast, spatial resolution, and motion sensitivity in the obtained images and their choice depends on the scan's objective and the characteristics of the tissues one aims to visualize.

Repetition Time (TR): TR is the time interval between the emission of two successive radiofrequency (RF) pulses during the image acquisition sequence. In other words, it's the time taken to repeat the entire sequence of RF pulses and image acquisition. This parameter primarily influences the tissue contrast weighting in the final image. A longer TR tends to produce greater tissue contrast as it allows more time for longitudinal relaxation (T1) of protons in tissues.

Echo Time (TE): TE is the time elapsed between the radiofrequency pulse and the moment when the MRI signal is measured. This parameter mainly affects tissue contrast weighting and

sensitivity to motion. A shorter TE tends to produce images with greater contrast between tissues with different transverse relaxation times (T2), while a longer TE can provide information about lesions that may have different T2 relaxation times compared to surrounding tissues.

In T1 sequence a short TR and a short TE are used. T1 images provide excellent anatomical resolution and are effective in visualizing details of anatomical structures. Tissues containing many proteins and fats, such as fat, appear bright in T1 images.

In T2 sequence, a long TR and a long TE are used. T2 images are useful for highlighting tissues containing water, such as soft tissues. These tissues appear bright in T2 images. T2 sequences are often used to diagnose inflammatory lesions, edema, tumor lesions, and many other conditions.

While T2 identifies the transverse relaxation time, due to fluctuations in the magnetic field within the tissue (due to the interaction of the magnetic fields of neighboring protons), there is a second cause which involves the loss of phase of the transverse magnetic moment (9). The static magnetic field B_0, indeed, is not homogeneous over the entire control volume (9). So according to Currie et al. "magnetic field variations result in slightly different Larmor frequencies for protons at different locations within the field" (9). It is possible to consider both factors in estimating the loss of transverse magnetization, incorporating the phenomena into a single time variable indicated with T2*. Thus, since T2* considers both T2 relaxation and the de-phasing that results from inhomogeneity in B0, it determines the actual rate of decay observed when measuring a free induction decay signal (9).

1.1.2 ANATOMICAL MRI

Anatomical MRI provides an overview of the brain structure and its static characterization (8,11). It's an imaging technique that gives information about shape, size and tissue integrity (8). The type of images commonly used for this purpose are T1, T2 and Flair (12).

According to Bloomfield et al. "T1-w images provide good contrast between grey matter (GM) and white matter (WM), while high water content media (e.g., Cerebrospinal Fluid (CSF)) and bones appear dark. T1-w images are typically used for tissue segmentation and registration purposes and are often acquired using a 3D sequence with isotropic voxel size (e.g., 1x1x1 mm^3)." (8)

T2 weighted images are characterized by a marked contrast between tissues and fluid substances (13). Brain tissues appear dark (or grey), while high water content media are bright (8,13). Since many pathologies cause an increase in local water, T2 weighted images have proven to be very useful in clinical diagnostics (14). Lesions, such as demyelination or inflammation, are sensitively detected with a hyperintense signal change (15). According to Bloomfield et al., when used for clinical purposes, "T2w images are often acquired with high in-plane resolution relative to the slice thickness (e.g., voxel size of 0.5x0.5x3 mm^3)" (8).

Depending on the type of structures you want to analyze and, thus, highlight, it's possible to use other types of sequences. An example of these is the flair, which allows clinicians and researchers to visualize the brain with T2 weighting image and suppression of the cerebrospinal fluid signal (16).

1.1.3 FUNCTIONAL MRI

Functional MRI (fMRI) is a neuroimaging method designed to provide a real-time indirect measure of brain activity (8). It operates on the premise that neural activity requires metabolic support of oxygenated blood (neurovascular coupling). Gradient-echo sequences sensitive to the variation in magnetic polarization of tissues are able to capture differences in magnetic susceptibility dictated by blood oxygenation levels (17). Since neuronal activity is evaluated on variations in the magnetic field which depends on the degree of oxygenation of the tissues due to the blood flow, the fMRI operating principle is known as blood-oxygen-level-dependent (BOLD) contrast technique (8) (17). So, the magnitude of the BOLD signal is an indirect measure of neuronal activity which offers a non-invasive means to provide unique insights into brain functions (17) whether under specific conditions or during rest, thereby complementing the information provided by anatomical or diffusion MRI (8) (17) (18).

1.1.4 DIFFUSION MRI

In addition to anatomical and functional ones, there are other techniques capable of providing images with relevant features in the clinical and research field. Among these, the Diffusion MRI techniques has played an important role in clinical diagnostics thanks to their property to use the movement of water molecules within biological tissues to generate images with distinct contrast compared to the ones discussed previously (19). The simplest technique in diffusion

imaging is diffusion-weighted imaging (DWI), while its advanced form is diffusion tensor imaging (DTI) (8,19).

Although image contrast is based on differences in the magnitude of diffusion of water molecules within the brain both in DWI and in DTI, the second one analyses the three-dimensional shape of the diffusion, also known as diffusion tensor (19). The DTI instead is based on simpler model of water molecules diffusion, offering good but less detailed images (19).

Diffusion MRI is able to produce a non-invasive characterization of the brain architecture and heterogeneity at a fiber level, not achievable through conventional imaging methods (8). However, since it is very complex to interpret DWI and DTI, it is necessary to use post-processing techniques on this type of image (8,20).

Thus, numerous software for the post-processing of diffusion images have been created both by research centers and by scanner suppliers and made available by them. These processing tools are very different from each other in terms of pre-processing steps, models, and statistical analysis approaches.

1.2 MRI MORPHOMETRY

Magnetic Resonance Imaging (MRI) Morphometry is a field of neuroscience that deals with analysing the shape and dimensions of brain structures using images obtained through magnetic resonance imaging. This type of analysis is crucial for understanding structural variations in the human brain in relation to pathological conditions, normal development, aging, and more. There are two main approaches used in brain morphometry: voxel-based and surface-based.

1.2.1 SURFACE-BASED MORPFHOMETRY

In the surface-based method, the interface between gray matter and white matter is modelled as a three-dimensional surface. This approach focuses on analysing the geometric and topological characteristics of brain surfaces, such as surface area, cortical thickness, and the shape of gyri and sulci (24). Analysis of brain surfaces can reveal subtle changes in cortical morphology associated with various neurological or pathological conditions. Measurements obtained from brain surfaces are often considered more sensitive than voxel-based measurements for detecting localized variations in the brain (25). Statistical analysis of surface measurements is used to

identify specific regions of the brain that show significant differences between groups of individuals or are associated with clinical variables.
In summary, while the voxel-based approach focuses on analysing differences in signal intensity in the voxels of the brain image, the surface-based approach focuses on analysing the geometric characteristics of brain surfaces (24). Both approaches are complementary and can provide valuable information about brain morphology in relation to various clinical and biological conditions (24).

1.2.2 VOXEL-BASED MORPFHOMETRY

In the voxel-based method, the brain image is divided into three-dimensional volume units called voxels (volumetric pixels). This approach focuses on analysing differences in signal intensity between voxels in brain images of different individuals or the same individual at different times. Differences in signal intensity may reflect variations in the density or concentration of brain tissue, such as the presence of lesions, atrophy, or changes in neuron density. Statistical analysis is used to compare voxels between different groups of individuals or to evaluate correlations between brain signal patterns and clinical or behavioural variables. The voxel-based approach is often used to detect global or diffuse changes in the brain.

One of the most used software for voxel-based morphometric analysis is SPM (Statistical Parametric Mapping) (21). SPM is a statistical analysis technique primarily used in neuroscience to analyse neuroimaging data, such as images obtained from functional magnetic resonance imaging (fMRI) or positron emission tomography (PET) (21). SPM allows for comparing brain imaging data between different experimental conditions or groups of subjects to identify patterns of brain activation associated with specific cognitive processes or pathologies (21).
Through the CAT12 toolbox, included in SPM, it is possible to implement a technique known as "optimized" voxel-based morphometry (VBM)(22).

It is necessary for the images to be spatially normalized, segmented into different tissue classes, and smoothed before conducting statistical tests (23). The "optimized" preprocessing strategy involves spatially normalizing the brain images of subjects to a standard space by matching the gray matter in these images with a reference gray matter. The historical motivation behind this approach was to reduce the confounding effects of non-brain structural variability (e.g., scalp) on registration (21). Tissue classification in SPM requires that the images be registered with tissue probability maps (21). After registration, these maps represent the prior probability of

different tissue classes being found at each location in an image. Bayes' rule can then be used to combine these priors with tissue type probabilities derived from voxel intensities to provide the posterior probability (21).

This procedure is inherently circular because registration requires an initial tissue classification, and tissue classification requires an initial registration. This circularity is resolved here by combining both components into a single generative model. This model also includes parameters that account for image intensity nonuniformity, although it is now quite standard to include intensity nonuniformity correction in segmentation and registration methods. Estimating the model parameters (for a maximum a posteriori solution) involves alternating among classification, bias correction, and registration steps. This approach provides better results than simple serial applications of each component.

1.3 PARKINSON'S DISEASE

Parkinson's disease (PD) was first described by Dr. James Parkinson in 1817 as a "shaking palsy" (26). It is the second most widespread neurodegenerative pathology after Alzheimer's one (27). PD is highly heterogeneous in early clinical features and later outcomes because it is characterised by both cardinal motor and non-motor symptoms (28). Resting tremor, rigidity, and bradykinesia are the most frequent motor indicators of the presence of PD (29). Cognitive impairment, apathy, depression, anxiety, impulse control disorders, sleep disturbance, fatigue, pain, visual hallucinations and autonomic dysfunction are among the main symptoms of a non-motor nature that can arise throughout disease course (28) (30).
The motor symptoms of PD are attributed to the loss of striatal dopaminergic neurons, although the presence of nonmotor symptoms supports neuronal loss in non-dopaminergic areas as well (31). The term *parkinsonism* is a symptom complex used to describe the motor features of PD, which include resting tremor, bradykinesia, and muscular rigidity. PD is the most common cause of parkinsonism, although a number of secondary causes also exist, including diseases that mimic PD and drug-induced causes (31).

1.3.1 COGNITIVE STATES

Cognitive decline is, among non-motor symptoms in PD, the one impacting the most on life quality, and in the PD population it is six times more frequent than in the healthy population (32). Cognitive decline can involve different domains, with heterogeneous impact and patterns

across the PD population (33), nonetheless decline is most frequently observed in executive domain, in particular in early stages, due to fronto-striatal degeneration (34).
Cognitive decline in PD is defined as a spectrum ranging from no cognitive impariment (NC) to mild cognitive impairment (MCI) to dementia (PDD) (35,36). With MCI, daily life activities are preserved. Nonetheless, cognitive impairment is present and represents a risk factor for dementia, with 60% of diagnosed PD-MCI turning to PDD in a 5 year follow-up (37). The diagnosis is based on a global cognitive scale and a battery of neuropsychological tests at first level, covering five cognitive domains. When the patient obtains deficitary scores for at least two domains, the diagnosis is positive.

1.3.2 BIOMARKERS IN PARKINSON'S DISEASE

MRI

Typically, a standard brain MRI will appear normal during the early stages of Parkinson's disease, or it may reveal alterations associated with ageing (38). Cortical atrophy in either the frontal or temporal lobe may become evident (39). These areas of atrophy can be evaluated quantitatively by measuring diameters and areas or by utilising voxel-based morphology (VBM), which employs a 3D isotropic voxel T1 sequence such as T1 MP-RAGE sequence (40).VBM facilitates the detection of differences between groups in an operator-independent and automated manner (41). Studies using VBM have documented grey matter decline in cortical regions within the frontal lobe in individuals with Parkinson's disease (42). Cortical atrophy could potentially contribute to the onset of dementia in Parkinson's disease, particularly when regions like the limbic/paralimbic areas, anterior cingulate, and subcortical grey matter are affected (43). However, VBM's application in routine clinical diagnostic procedures is restricted due to the absence of well-defined or validated diagnostic criteria (40).

SERUM BIOMARKERS

PD biomarkers are heterogenous and can be classified in four macro-categories: genetical biomarkers, clinical biomarkers, imaging biomarkers and biochemical biomarkers. Among clinical biomarkers, the triad bradykinesia/akinesia, tremor and rigidity is the most relevant, and can be quantified with PD-specific scales such as the Unified Parkinson's Disease Rating Scale (UPDRS) (44,45). For neuroimaging, single-photon emission computerized tomography (SPECT) is the clinical standard for detecting the lower expression of dopamine in the striatum in PD, even before the expression of motor symptoms (46). MRI is instead still understudied in

PD and underused in clinical practice, being it mostly limited to the differentiation of parkinsonisms (47).

In recent years, the search for proteins in biological fluids has gained attention in neurodegeneration research. Once based on invasive CSF sampling, nowadays advances in the sensitivity of serum and plasma analysis made blood-based research on protein biomarkers of neurodegeneration a hot topic, despite the lower concentrations of biomarkers in blood with respect to CSF. Some proteins, such as Neurofilament Light Chain (NfL), Glial Fibrillary Acidic Protein (GFAP), phosphorylated-tau181 (pTau181) and pTau217, have already been associated to neurodegenerative processes in Alzheimer's disease (48). The search for blood biomarkers of Parkinson's disease is instead still limited to preliminary works, assessing the possibility to help in the early diagnosis and in the differentiation of parkinsonisms, as well as in predicting cognitive decline (49). Blood biomarkers can be measured in both the serum and the plasma components of blood (i.e., the corpuscolar and the liquid component of blood). The measures obtained from serum and plasma are strongly correlated and are both used in literature (50).

NfL is a protein composing the neuronal cytoskeleton, particularly expressed at axonal level. NfL is released in the interstitial fluid in proportion to neuronal and axonal damage (51), with values in blood that are strictly correlated to those found in CSF, possibly representing thus a cheap, non-invasive biomarker (52). Higher NfL values have been observed in the blood of PD patients rather than in the blood of atypical parkinsonim patients (53), but higher in PD with respect to healthy controls (54). The latter study indicated plasma NfL as the best predictor for the evolution of motor symptoms after two years follow-up, overperforming age, sex, disease duration and other factors.

GFAP is a structural protein present in the cytoskeleton of astrocytes, which is released in high quantities into the CSF and in blood flow during the process of astrogliosis. For that reason, the large presence of this protein in plasma was proposed by Yang, Z., & Wang, K. K. (55) as a possible nonspecific biomarker of neurodegeneration. The validity of this biomarker has already met evidence in some degenerative diseases such as the Alzheimer's one, where a strong correlation has been found between the concentrations of GFAP in plasma and those of beta-amyloid protein (Aβ42) in CSF (56). Studies regarding connections between the GFAP protein and Parkinson's are still limited. Studies regarding connections between the GFAP protein and Parkinson's are still in their early stages, so not much is available about it in the scientific literature (50). Two studies, in particular, have returned considerable results in order to consider possible relationships between this biomarker and PD. The first study, conducted by Lin et al. (57), showed that PD patients have higher plasma GFAP concentrations than healthy controls.

The second study, conducted by the same group (58), was focused on the ability of plasma GFAP to differentiate motor subtypes of PD and possibly predict their evolution over time. At two-year follow-up, patients with subtype characterized by akinesia, rigidity, postural instability and disturbances gait (PIGD) show higher plasma GFAP levels compared to patients with tremor-dominant (TD) subtype. Furthermore, patients with TD, who already present, at the beginning of the follow-up period, higher concentrations of GFAP in plasma tend to evolve towards a PIGD phenotype during time. Conversely, patients with PIGD and lower initial GFAP levels in plasma tend to convert to TD or other undefined subtypes.

The Tau protein is a fundamental protein for the stabilization of microtubules which are intracellular structures that constitute the neuronal cytoskeleton. PTau refers to an abnormal phosphorylation of the Tau protein. The pTau protein plays a key role in some neurodegenerative diseases, triggering neuronal death. The mechanism of hyperphosphorylation of the Tau protein is not yet perfectly clear, however, it seems to be connected to the accumulation of the Aβ42 protein and the interaction with it. A strong presence of pTau and the Aβ42 proteins was found in patients suffering from Alzheimer disease. With the introduction of innovative measurement techniques that have made it possible to measure the levels of pTau181 in the blood, it has been demonstrated that, through the estimation of the values of this protein, it is possible to distinguish patients with Alzheimer's disease from healthy controls, even earlier of the onset of memory disorders (59,60). Moreover, the measure of pTau181 levels can anticipate the confirmation of neuropathological diagnosis post-mortem (59,60). Alzheimer's neuropathology is well documented in the brains (analysed post-mortem) of PD patients suffering from dementia (61). So, the pTau181 protein could be a good non-invasive biomarker to identify PD patients at risk of dementia or, at least, of the onset of cognitive disorders.

Chapter 2

AIM OF THE THESIS

The aim of this study is to perform on PD patients a preliminary evaluation on the association between blood biomarkers (NFL, GFAP, pTau181, GFAP/NFL), cognitive state, and grey matter morphometry based on structural magnetic resonance imaging. In this way, it was possible to evaluate if the results suggested some kind of correlation between the variables involved and the evolution of Parkinson's disease. My analysis was focused on the search for a biomarker that could give possible indications on the disease and/or its evolution in patients suffering from it in such a way as to be able to open up new perspectives in the way of diagnosing it. So, the results of the patients' blood tests were used to understand if there was a link with the regression of the gray matter or with the cognitive state in subjects suffering from Parkinson's disease.

Secondly, I investigated any differences attributable to the subjects' gender, comparing populations with the same cognitive state and different gender and vice versa, in relation to each biomarker used. In this way it was possible to understand whether it was necessary to evaluate the possibility of differentiating the diagnosis of patients based on gender or cognitive state in the future studies.

Finally, I related the results of the MOCA and MMSE cognitive tests with biomarkers, to evaluate a possible link between the patients' physiological parameters and the way in which the cognitive state is assessed.

More generally, my study was based not only on seeking a connection between the patients' physiological parameters and the morphometric analysis, but also on the possibility of finding a connection between the subjects' pathophysiology and their cognitive functions.

Chapter 3

METHODS

3.1 PARTICIPANTS

A cohort of 57 PD patients were recruited at the Parkinson Disease and Movement Disorders Unit, Neurology Clinic in Padua, and at the San Camillo Hospital, Venice. PD was diagnosed according to the clinical diagnostic criteria. All subjects underwent a comprehensive neuropsychological battery (level II criteria of the MDS guidelines as described (62)) specifically designed to target PD-cognitive deficits, which allow us to classify patients as PD-NC, PD-MCI, or PD with dementia (PDD). All examinations were approved by the Venice Research Ethics Committee, Venice, Italy, and completed in accordance with the Helsinki Declaration.

3.2 ACQUISITION

3.2.1 MRI

Structural MRI acquired within 5 years from the date of blood sampling at the Neurology Clinic in Padua and at the San Camillo Hospital in Venice were collected. All images were acquired on 3T Philips Ingenia scanners. Structural images include at least one T1 structural image with 1 mm isotropic voxel size, and, for 55 patients a T2 FLAIR image with similar resolution, and for 2 patients a T2 image with similar resolution.

3.2.2 COGNITIVE ASSESSMENT

All participants underwent second-level neuropsychological evaluation, in order to characterize their cognitive profile. The cognitive diagnosis has been produced following the guidelines in Litvan et al. 2012 for MCI (63), and that in Dubois et al. 2007 for PDD (64). In particular, two scales of global cognition were used, the Montreal Cognitive Assessment (65,66) and the Mini Mental State Examination (67,68).

3.2.3 SERUM

All subjects underwent blood sampling at the Neurology Clinic in Padua. Serum was extracted and processed using the commercial single-molecule assay (SIMOA™) kit developed by Quanterix (69). NfL, GFAP and pTau181 concentrations were expressed in ng/L. One additional biomarker was defined as the ratio NfL/GFAP.

3.3 ANALYSIS

Before starting our analyses, a preliminary study was carried out on the available images to verify their suitability. The dataset was provided in DICOM format, the most widespread standard in the field of medical imaging. In the DICOM format, datasets are stored in 2D images, one for each slice acquired on the acquisition plane, each bearing standardized metadata describing the subject and the acquisition protocol. To be processed with the most used MRI processing software, DICOM data need to be reconstructed as 3D images. MRI images were converted to NIFTI format, using the popular dcm2niix software. Once the files had been converted, we moved on to a qualitative evaluation of the T1-weighted and T2-weighted FLAIR images in the Freesurfer viewer "Freeview" aimed at verifying that they met the minimal requirements to be included in the analysis, i.e.,

- Full brain coverage;
- Voxel size of 1mm isotropic or close to this value (sub-millimetric voxel sizes were accepted, as well as non-cubic voxel shapes non exceeding 1.5 mm3;
- Absence of excessive Gibbs ringing / movement-related artefacts.

In this process, I was assisted by the automatic evaluation performed by the software BAAD (and by CAT12) on nifti images (70), which provides a quality score from A (optimal) to D (worst) based on resolution, contrast and noise. After this preliminary quality check through which the original dataset was skimmed, we then moved on to the actual morphometric analysis. The morphometry software used were FreeSurfer (71) and BAAD (Brain Anatomical Analysis using Diffeomorphic deformation). The latter is a wrapper of SMP CAT12 routines integrated with Alzheimer disease score calculation (72). Testing both software allowed to gain experience on both a voxel based and a surfaced based approach and to have the possibility to compare them.

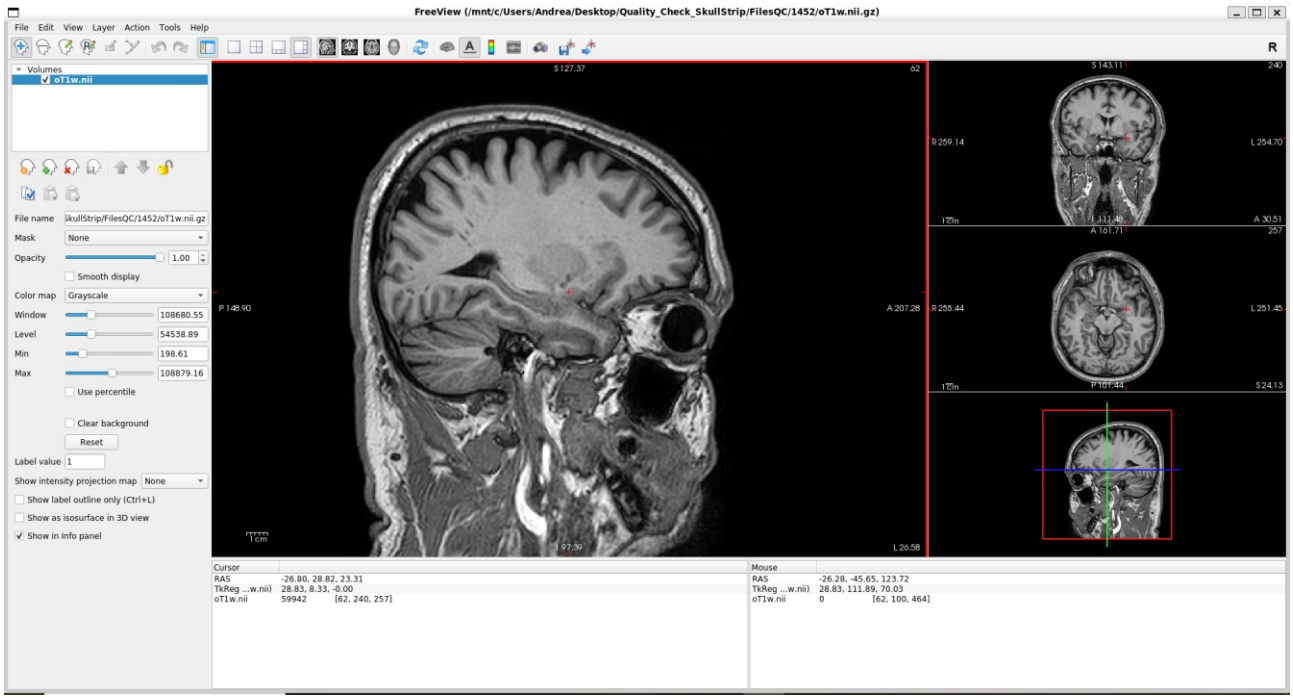

Figure 7: xample of the Freeview GUI used to evaluate the quality of structural images, here used to visualize on a three-plane view the T1-weighted image of subject 1452.

3.3.1 SURFACE-BASED MORPHOMETRY

PREPROCESSING

In order to achieve the parcellation and segmentation of the brain and extract the data of interest it was necessary to preprocess the images, carrying out normalization, registration, removal of the artifacts, such as bias field, and skull-stripping. Indeed, when we perform the parcellation and segmentation, each brain area must be classified within an atlas.

MRI images generally have different dimensions and orientation based on how the patient is positioned inside the machine or based on the MRI features itself.

The normalization aim is to bring the image back to a unit of measurement that is easily interpretable, and which allows the areas of a subject's brain to match or be framed dimensionally within an atlas(73).

Image registration, also known as image fusion, matching or warping, consists of aligning two images, so that common features overlap and differences, should there be any, between the two are emphasized and readily visible to the naked eye (74). We used it to insert the brain into a measurement system similar to that of the atlas, in such a way to ensure that the reference atlas and the brain are not translated or rotated during the superposition.

Since magnetic resonance images are affected by numerous artefacts including Gibbs-ringing (75) and bias field (76), segmentation algorithms may have problems classifying some parts of the image. Moreover, to classify the components of the patients' brain in an atlas it is necessary to remove the skull and, in general, what is not part of the brain itself. So, in our analysis two preparatory operations were carried out for normalization and registration. On the one hand we used the N4 algorithm to perform bias field correction (77), on the other hand, we implemented skullstripping by using a combination of FreeSurfer's SynthStrip algorithm, based on neural networks (78), and the optiBET approach (79), which performs preliminar normalization to the MNI template and applies the inverse registration to the brain tissue mask of the MNI template to obtain a brain tissue mask at subject level. The logical OR between the results of the two algorithms allows to obtain a conservative skull-stripping, with reliable cut level at the medulla as obtained from optiBET.

In order to carry out preprocessing on the images we used a unified tissue classification model proposed by John Ashburner and Karl J. Friston (80). In their work, they underlined that to get brain matter classification there's a first step where the image is registered with a tissue probability map (81), which is the prior probability of different tissue classes being found at each location in an image (82). Bayes rule can then be used to combine these priors with tissue type probabilities derived from voxel intensities to provide the posterior probability (80). To execute the registration, it's required an initial tissue classification, and the tissue classification requires an initial registration: so, it leads to build a procedure inherently circular. This circularity was resolved by Ashburner and Friston. by combining both components into a single generative model which includes parameters that account for image intensity nonuniformity (80). According to Ashburner and Friston, "estimating model parameters (for a maximum a posteriori solution) involves alternating among classification, bias correction, and registration steps. This approach provides better results than simple serial applications of each component" (80). The objective function used by Ashburner et al. is constituted by a mixture of Gaussians (MOG). The algorithm is set up in such a way as to search for the minimum of the objective function, finding the optimal values of its parameters.

The objective function used by Ashburner et al. is constituted by a mixture of Gaussians (MOG). The algorithm is set up in such a way as to search for the minimum of the objective function, finding the optimal values of its parameters. Thus, the cost function takes on an expression of the type

$$\varepsilon = -\sum_{i=1}^{I} log\left(\varrho_i(\boldsymbol{\beta})\sum_{k=1}^{K}\frac{\gamma_k}{2\pi\sigma_k^2}exp\left(-\frac{(\varrho_i(\boldsymbol{\beta})y_i-\mu_k)^2}{2\sigma_k^2}\right)\right) \quad (1)$$

Where:

- γk is the prior probability of any voxel, irrespective of its intensity, belonging to the kth Gaussian, given the proportion of voxels that belong to that Gaussian
- μk and σk2 are the mean and the variance of the kth Gaussian
- ρ is a scale factor
- β is a vector of unknown parameters
- K is the number of Gaussians (clusters)
- I is the number of elements of observed data y

Through particular formulations of the priors and **β** it is possible to manipulate equation (1) in such a way as to be able to find the optimal parameters that minimize the cost function. Thus, based on the type of boundary conditions that are established to solve the problem, and, therefore, based on the mathematical expression of the priors and beta, it will be possible to come to different results.

In addition to optimization, the algorithm used carries out a regularization, reducing, where possible, the number of parameters considered in order to avoid pernicious interactions among the parameter estimates. By reducing the number of parameters, indeed, regularization prevents the algorithm from relying too much on the measured data (affected by errors and noise) and thus avoiding the problem of overfitting.

FREESURFER

We used the software FreeSurfer as a reference point for each step of our analysis. Through it we carried out a quality check of the images in the preliminary preprocessing phase and in all subsequent phases (including segmentation and data extrapolation).

FreeSurfer requires data to be stored within a specific hierarchy of folders which use standard naming. In a study folder defined using a global variable, each subject corresponds to a folder

named with the prefix “subj” and the code identifying the subject. In the folder specific to a subject, the T1-weighted image is stored in a “mri/orig” subfolder. Images are first processed using the N4 and Synthstrip algorithms (figure 8), then organized in the folder hierarchy.

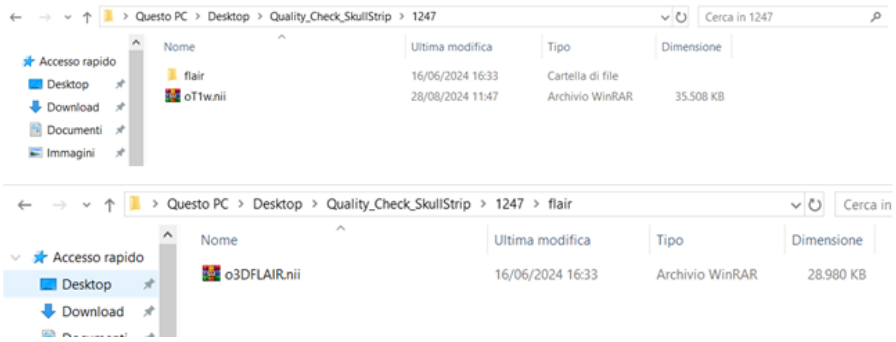

Figure 8: T1 and the flair order within the folders so that FreeSurfer can process them, carrying out Gibbs-ringing and bias field correction, skullstripping, parcellation and segmentation

The workflow was divided into two steps, skullstripping and actual morphometry. Before skullstripping, both the T1-weighted and T2FLAIR images were corrected for bias field using the N4 correction as implemented in ANTs software and wrapped in FreeSurfer. Then, the two images were rigidly co-registered. Skullstripping was implemented with a combination of standard and machine-learning based approaches. The FreeSurfer routine mri_synthstrip (78) performs skull-stripping using a pre-trained deep-learning model. The routine was observed to provide good results in general, and it was chosen as a starting point for the optiBET algorithm (79). The optiBET algorithm extracts the brain by normalizing the T1 image to the MNI template, then using the inverse transform to bring a dilated MNI mask to the subject space. With respect to the output of mri_synthstrip, optiBET ensures that the medulla is cut at a replicable level, the one determined by the extent of the MNI template. OptiBET was observed to be far more conservative than mri_synthstrip in including some non-brain areas, but happened to cut some external gyri in the upper central cortex. Nonetheless, the final brain extraction result is obtained with a logical OR between the mask extracted with mri_synthstrip and that extracted with optiBET, in order to be sure to include all parts of the brain. A mask of the medulla was created to ensure that no addition from mri_synthstrip was introduced in that region. FreeSurfer, in fact, has an interface, Freeview, that allows you to analyse not only volumes, but also surfaces in three-dimensional, axial, sagittal and coronal views. Furthermore, it is possible to simultaneously load not only several different images (for example a T1 and the corresponding skullstrip), but also volumes and surfaces, allowing you to make overlaps between them.

Figure 9: Subject 1410 T1 loaded on Freeview

All the views through which it is possible to analyze T1 images in FreeSurfer are respectively represented in figures 9,10 and 11. In these and subsequent images, I have shown the results obtained on MRI sequences of one of the subjects (n°1410) who were included in the study.

The Skullstripping outcomes are represented in figure 12, where it's possible to appreciate the precision of the algorithm and the height where it cut the brainstem.

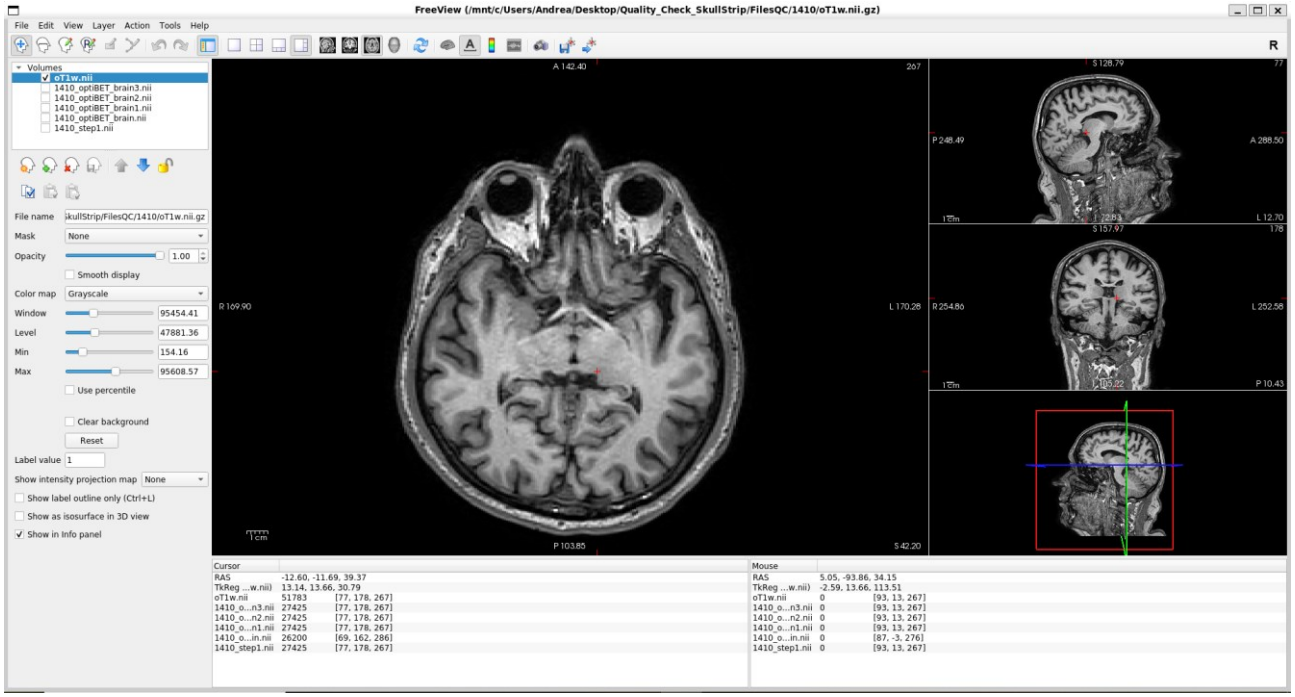

Figure 10: 1410 subject Axial View on Freeview

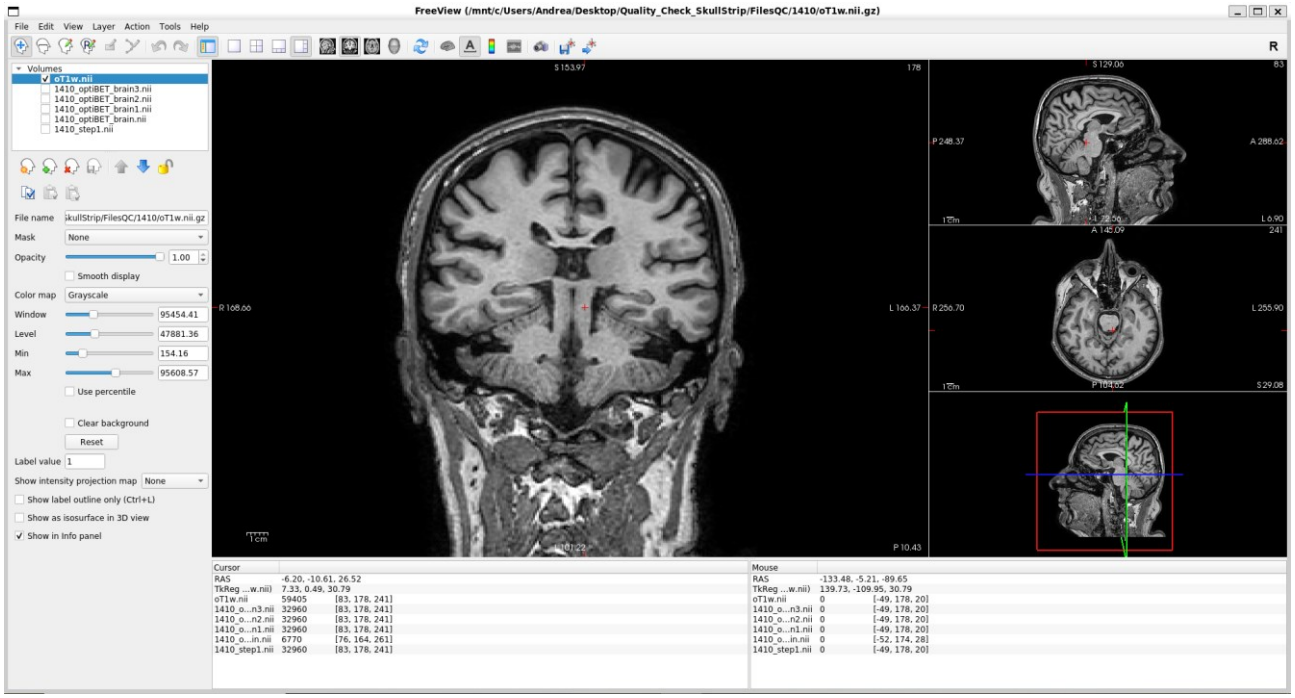

Figure 11: 1410 subject Coronal View on Freeview

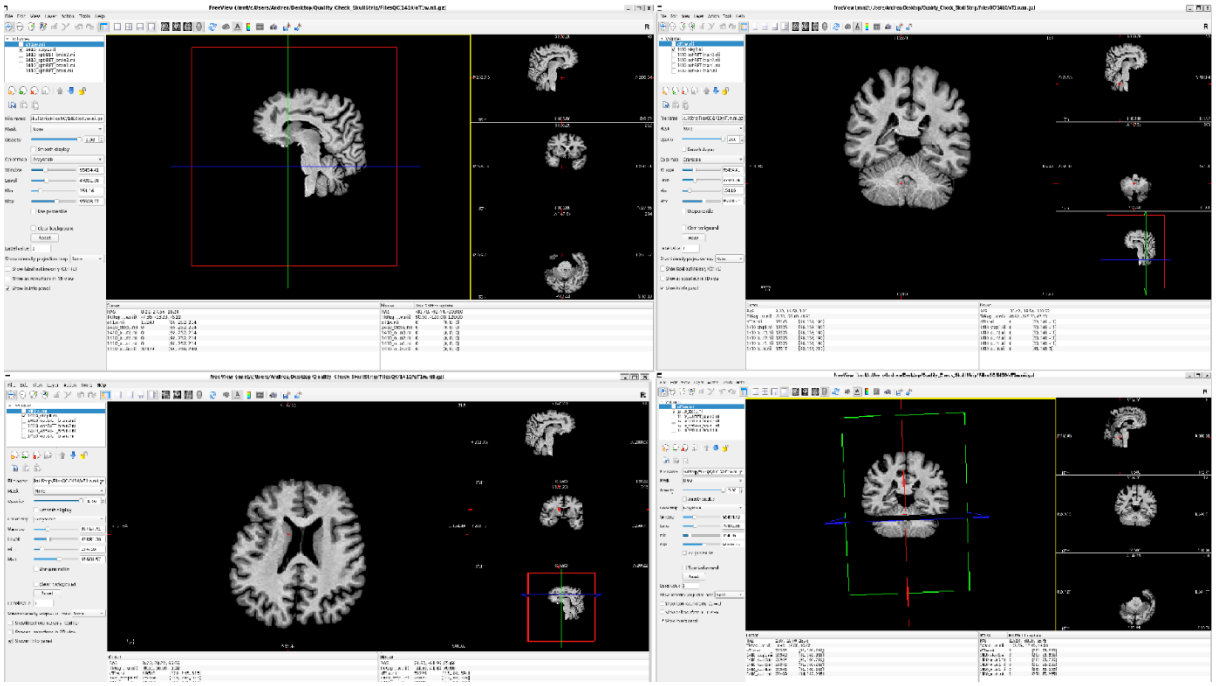

Figure 12: Subject 1410 Skullstripping result

Figure 13: Superposition of the T1 and the brain image of patient 1410 obtained through the skullstrip

Freeview allows to superimpose different images to compare them with the naked eye by adjusting their opacity and colormap. I used this functionality to verify that skullstripping had been performed correctly on each subject, checking, in particular, that no parts of the telencephalon, cerebellum or a significant portion of the brainstem had been eliminated. Figure 13 shows how I overlapped the subject 1410 T1 with its respective skullstrip image, increasing the opacity of the T1 and setting a heat colormap for the extracted brain. In this way I was able to supervise each slice in the three main views (sagittal, axial and coronal) ensuring that the quality of the result could be acceptable to move on to parcellation and segmentation operations.

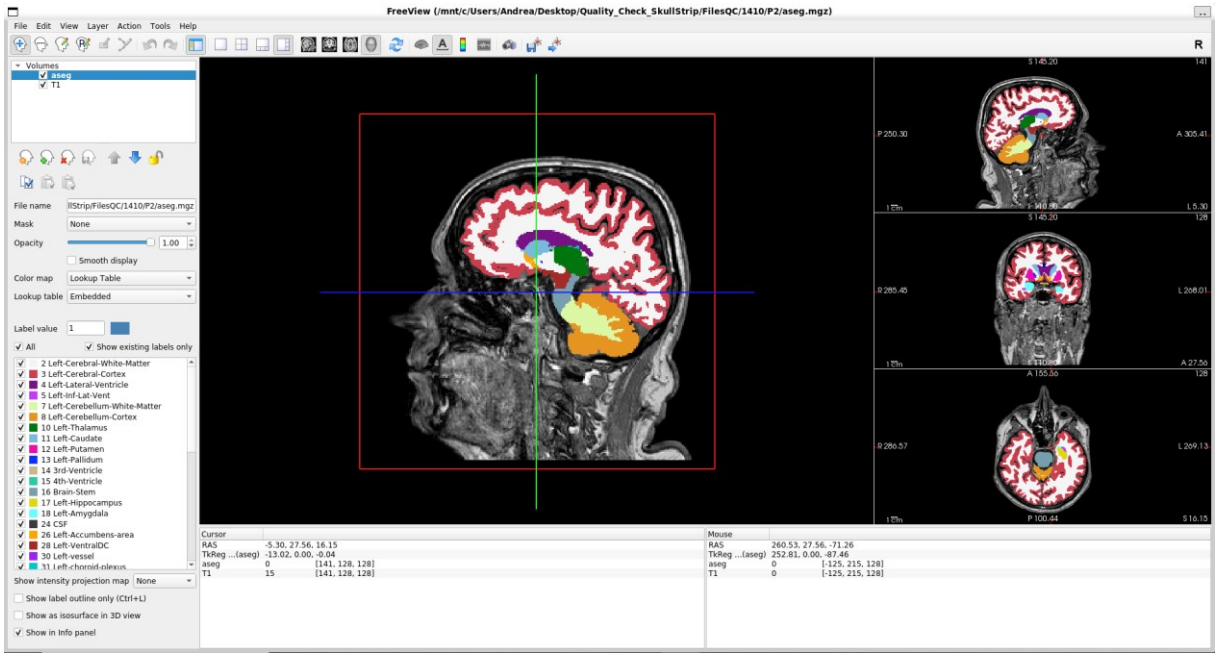

Figure 14: Parcellation and Segmentation results on subject 1410. The image presents the results displayed in Freeview: each part of the brain has been cataloged and marked with a color. Labels with a corresponding color have also been attributed to the cerebellum and brainstem. The list of volumes is visible in the bottom left pane of Freeview.

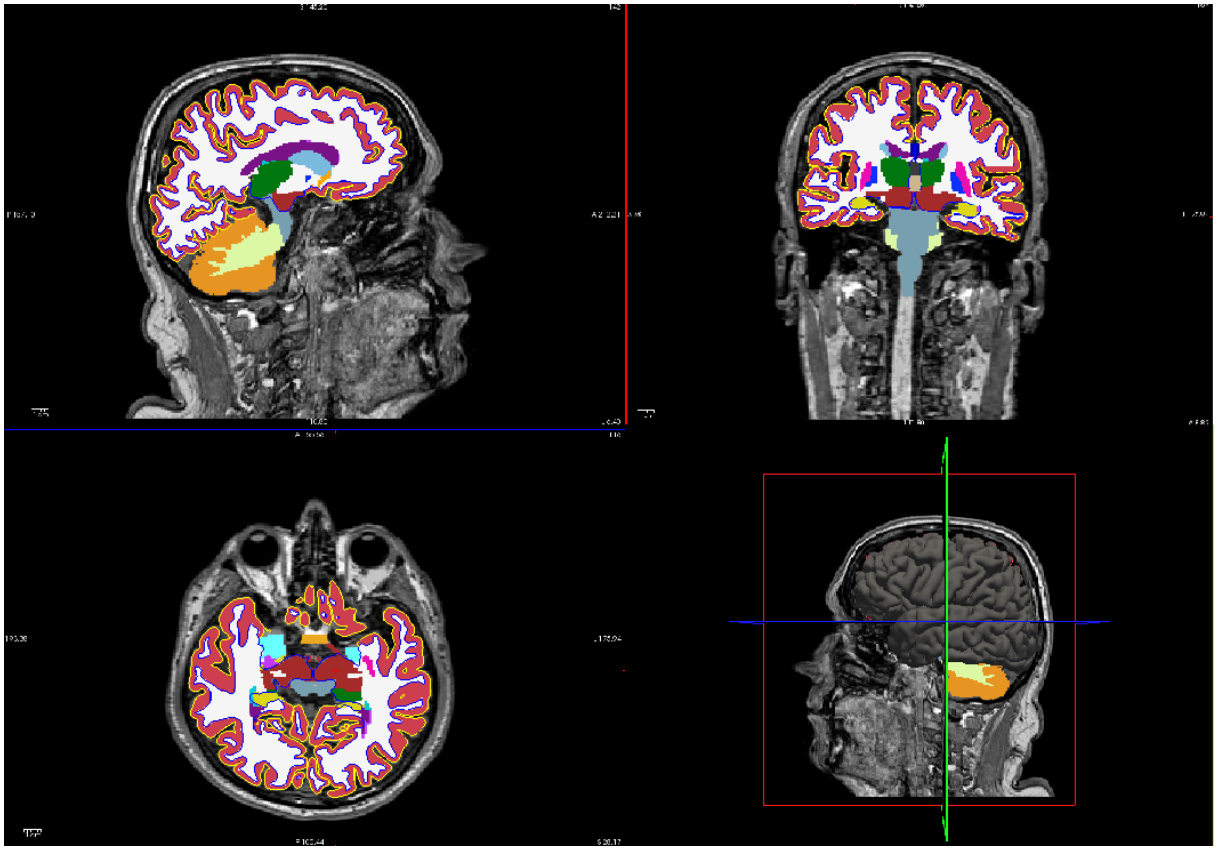

Figure 15: Parcellation and Segmentation performed with FreeSurfer and visualized in FreeView. The separating surface between the cortical part and what surrounds the telencephalon is in yellow. The separation surface between the cortical and subcortical parts is in blue. In the bottom right view it is possible to see a three-dimensional reconstruction of the patient's brain, made possible through a surfaced-based morphometry model used to obtain the aforementioned separation surfaces.

At the end of the morphometric analysis obtained with FreeSurfer, I performend the parcellation of the cortical part and the segmentation of the subcortical part (figure 14). The cortical areas

were parcelled with two atlases: the Desikan-Killiany-Tourville Atlas (83) and the Destrieux Atlas (a2009s). As it possible to see in figure 15, the algorithm had automatically assigned a label to every brain volume and other important parts of central nervous system (cerebellum and brainstem). Freeview also allows us to overlay surface-modeled images onto volume-modeled images. I used this tool for a visual analysis not only of the level of quality achieved in dividing the cortical part from the subcortical one, but also to better appreciate the result of the previous skullstrip. In figure 15, in addition to the parcellation and segmentation carried out on subject 1410, I've also shown the separation surfaces obtained (respectively in yellow the one that divides the cortex from what is external and in blue the separation between the cortical and subcortical part). In the same figure (in the bottom right view) there is the three-dimensional modeling of the cerebral cortex. To reconstruct the cortical surface, the skullstripping pre-process was essential: in fact, having previously extrapolated the brain, it was possible to reconstruct the external surface by interpolating the border points of each slice.

Once the parcellation and segmentation processes were completed, I obtained a spreadsheet with a table reporting subjects' telencephalon volumes parameters (surface area, gray volume, average thickness, standard deviation of the thickness, etc.). So, I used the gray matter volume values for each cortical and subcortical area for subsequent statistical considerations.

3.3.2 VOXEL-BASED MORPHOMETRY

BAAD is a software for voxel-based morphometry based on diffeomorphic deformations and on the CAT Computational Anatomy Toolbox for the popular SPM software (84). This method enables registering and comparing structural magnetic resonance imaging (MRI) images of individual brains to identify differences or changes in brain anatomy. This can be useful for studying anatomical variations associated with neurological, psychiatric conditions, or developmental processes.

For the morphometric processing addressed in this thesis work, BAAD was utilised as follows:

- The corresponding NIfTI files of the magnetic resonance imaging scans conducted on the patients were imported for a multichannel segmentation (using the command import). Specifically, T1 and FLAIR images were used.
- After loading the list of patients with all T1 images, it was possible to associate their corresponding FLAIR images through the command.

- Afterwards, the parameters for Voxel-Based Morphometry (VBM) were configured. The use of FLAIR images was set as an option for White Matter Lesion (WML) correction. It was analysed both white and grey matter. BAAD has used the same age by decade as control group through the command “Auto select”. Finally, the volumetric Desikan-Killiany atlas as provided with the popular software AFNI was selected as custom template for ROI analysis.
- Through the "analyse" button, the VBM analysis was initiated.

Following the multichannel analysis of T1 and FLAIR images, BAAD provides a parcellation of the subject’s brain and relative brain morphometrics, expressed both in absolute terms (ml) and in Z-scores, using internally stored normative values.

BAAD provides an easy implementation for CAT12-based voxel-based morphometry, as all preprocessing steps (skull stripping, bias field correction, T1-FLAIR coregistration and normalisation) are automatically executed once input data are given. This solution was used for comparison between different approaches. The comparison was conducted in two terms:

- On absolute volumes, by computing the distance between Freesurfer volumes and BAAD volumes, in mm^3.
- On normalized volumes, comparing the Z-scores extracted by BAAD using its internal normalization based on age decades, sex and estimated intracranial volume, and the Z-scores extracted from Freesurfer volumes using the tables published in Potvin et al. (85,86).

3.3.3 ANALYSIS OF BIOMARKERS

Once the morphometric parameters for the subjects had been obtained, it was possible to compare them with the serological data.

To do this, I loaded both the tables with the statistical values of brain volumes and those containing the results of the blood tests on Matlab. Subsequently, I created some matrices where there were reported each subject gender, cognitive state, values of each of the 4 biomarkers and results of the morphometry. In this way it was possible to make considerations not only on the possible connections between serum and brain volumes, but also on any influence related to sex and/or cognitive state.

Once the data were grouped, I performed a check on them by first verifying whether they were normally distributed. Since the normality test gave me a negative result, it was not possible for me to calculate the correlation between volumes and biomarkers with the Pearson coefficient. Thus, I used a non-parametric test, obtaining the Spearman correlation coefficient and the relative p-value for each biomarker volume pair. I carried out this type of correlation analysis first on non-normalized volumes and then on volumes normalized with respect to normative values. Thirdly, I also performed a partial correlation between non-normalized volumes and biomarkers, in such a way as to verify the type of results in the absence of influence from sex, age and eTIV (estimated Total Intracranial Volume).

The correlation coefficient values obtained from each volume-biomarker comparison were plotted on a correlation matrix. I used a color scale to allow the most correlated pairs to be visually captured.
As regards the p-values, instead, I developed brain maps through *freesurfer_statsurf_display* toolbox, the areas of which were divided based on the volumes being compared. Subsequently, I associated the corresponding p-value to each volume, obtaining a map showing how the significance of the comparisons is distributed.

The statistical tests conducted are single tests for each biomarker volume pair and the significance level of each test was set to 0.05 (5% significance). Once I obtained the volume-biomarker pairs whose p-value was below the threshold, I plotted them on scatterplots to verify their distribution with respect to the reference population.
Since the tests were carried out as single tests, each characterized by a significance level of 5%, I had to correct this value by bringing it back to the case of multiple comparisons. To do this I used the *MultipleTestingToolbox* on Matlab, through which I carried out corrections with Bonferroni-Holm method.

Following the correlation analysis between volumes and biomarkers, I looked for possible links between the biomarkers and the cognitive state of patients divided by gender.
The subjects were first divided into two fundamental cognitive categories: those suffering from mild cognitive impairment (MCI) and those with a normal cognition (NC). Secondly, these two groups were further divided by gender.
Once this initial classification of subjects had been defined, I calculated the mean and standard deviation of each biomarker for each group.

Thus, I carried out comparisons between these groups, analyzing whether there were any significant differences in serological results between the populations considered. First, I carried out a T-test for each couple (male vs female, MCI, male vs female NC, male MCI vs male NC, female MCI vs NC, MCI vs NC, PD-men vs PD women) setting a level of significance for a single test equal to 5%.
Secondly, I developed boxplots to compare the populations that had a p-value less than or equal to the threshold to have a visual confirmation of the differences in statistical terms.

Thirdly, I corrected the significance value using multiple comparisons correction method of Bonferroni-Holm, in such a way as to be as cautious as possible.

Finally, I calculated the correlation coefficient (and the relative p-value) between the biomarker values and the subjects scores on the cognitive scales object of this study (Montreal Cognitive Assessment and Mini-Mental State Examination).

Chapter 4

RESULTS

4.1 DATASET DESCRIPTION

To carry out our analyses we considered a population consisting of 57 subjects. Among the patients recruited for this study 36 are men and 21 are women (Table 1). In terms of cognitive state, it's possible to see that 20 are PD-MCI patients and 36 are PD-NC patients, while for one subject it was not possible to retrieve a cognitive evaluation.

	MCI	NC	TOT
Male	12	23	36
Female	8	13	21
TOT	20	36	56

Table 1: Numerosity of the dataset divided for gender and for cognitive state

The dataset appears unbalanced towards males and NC. To investigate any age differences related to the two grouping variables of table 1 (gender and cognitive state), unpaired, two-tailed, two-samples t-tests were performed, setting the significance level to 5% (Matlab function ttest2). With x and y being the two sub-groups to be compared, the null hypothesis for the t-test is that the data in x and y comes from independent random samples from normal distributions with equal means and equal but unknown variances. The alternative hypothesis is that the data in x and y comes from populations with unequal means. From the p-values found in the tables 2 and 3 we can see that not only there is no significant difference in terms of age between men and women in the whole PD sample, but neither there are differences between men and women within the PD-NC subgroup and within the PD-MCI subgroup. Furthermore, I also tested age difference between PD-MCI and PD-NC, disregarding sex, and found no significant difference (table 3).

The only significant difference was found when comparing the PD-MCI male subjects with PD-NC male ones (table 4). The p-value found with a t-test is equal to 0.006. By correcting the

significance level of the test using Bonferroni-Holm, a significant difference in the age distribution between the two populations is confirmed.

	Male Mean	Male STD	Female Mean	Female STD	P-value Male VS Female	TOT Mean	STD Mean
MCI	69,92	5,68	63,75	8,65	0,07	67,45	7,47
NC	62,17	8,11	65,15	10,54	0,35	63,25	9,03
TOT	65,14	8,27	64,62	9,66	0,83		

Table 2: Table showing the comparison of ages between the male and female populations. The table shows first the p-value obtained from the comparison between MCI men and women, then NC and finally between men and women in general. The table also indicates the mean and variance values of each population considered and of their totality (e.g. the total mean of the MCI population represented in the average of all subjects, men and women, affected by mild cognitive impairment)

	MCI Mean	NC Mean	P-value MCI VS NC
Male and Female Subjects	67,45	63,25	0,08

Table 3: Comparison between the ages of PD-MCI (men and women) and PD-NC subjects

	MCI Mean	NC Mean	P-value MCI VS NC
Male Subjects	69,92	62,17	0,006 *

*Table 4: Comparison between the ages of PD-MCI and PD-NC male subjects. The * mark denotes a significant p-value with 95% confidence.*

	MCI Mean	NC Mean	P-value MCI VS NC
Female Subjects	63,75	65,15	0,76

Table 5: Comparison between the ages of PD-MCI and PD-NC female subjects

4.2 MORPHOMETRY OF PD AND COGNITIVE STATES

Once the morphometric data of each patient had been obtained, I performed an analysis aimed at searching for any differences between PD patients and normative data computed on healthy subjects, and between PD-MCI and PD-NC subjects.

First, I combined the results obtained with the subcortical volumetric parcellation with those obtained using the cortical Desikan-Killiany-Tourville Atlas (DKT) parcellation. Volumes combined in this way were organized in a matrix having subjects along rows and brain labels along columns. Data were normalized for age, gender and Estimated Total Intracranial volume (eTIV) values as explained in the methods section.

Then, I divided the PD-MCI subjects from the PD-NC ones and obtained the mean and standard deviation of each brain volume for each group (figure 16).

	1 MCI mean	2 MCI std	3 NC mean	4 NC std	5 p-value
1 SC_Left-Lateral-Ventricle	8.4620e+04	5.2012e+04	8.0777e+04	5.3115e+04	0.7949
2 SC_Left-Inf-Lat-Vent	1.4083e+03	1.7313e+03	1.4532e+03	1.7816e+03	0.9276
3 SC_Left-Thalamus	0.0049	1.8584	-0.1676	1.4532	0.7020
4 SC_Left-Caudate	-0.4090	0.9893	-0.4836	1.1055	0.8028
5 SC_Left-Putamen	-0.7944	1.0416	-0.7509	0.8626	0.8675
6 SC_Left-Pallidum	2.6313	1.3278	2.1184	0.8960	0.0908
7 SC_3rd-Ventricle	1.1669e+04	2.5399e+03	1.2180e+04	6.2529e+03	0.7284
8 SC_4th-Ventricle	-0.3861	0.7369	-0.1524	1.3065	0.4650
9 SC_Brain-Stem	0.7454	1.5956	0.3118	0.9448	0.2060
10 SC_Left-Hippocampus	-0.1431	2.3274	-0.4073	1.2579	0.5823
11 SC_Left-Amygdala	-0.3018	1.2602	-0.2836	1.4873	0.9632
12 SC_Left-Accumbens-area	-0.2545	0.9038	-0.1724	0.6840	0.7032
13 SC_Left-VentralDC	1.0436	1.5744	0.6819	1.0658	0.3111
14 SC_Right-Lateral-Ventricle	7.8989e+04	5.3669e+04	7.2282e+04	4.9029e+04	0.6372
15 SC_Right-Inf-Lat-Vent	1.2945e+03	1.3667e+03	1.2722e+03	1.6039e+03	0.9584
16 SC_Right-Thalamus	0.4734	2.3704	0.2856	1.8776	0.7456
17 SC_Right-Caudate	-0.1007	1.1441	0.0229	1.1295	0.6977
18 SC_Right-Putamen	-0.3943	1.1542	-0.5646	0.9280	0.5493
19 SC_Right-Pallidum	2.8238	1.4585	2.0653	1.1425	0.0357
20 SC_Right-Hippocampus	-0.6120	1.2145	-0.6184	1.6156	0.9877
21 SC_Right-Amygdala	0.3977	0.9401	0.3827	1.1639	0.9608
22 SC_Right-Accumbens-area	-0.3752	0.8387	-0.3982	0.9605	0.9291
23 SC_Right-VentralDC	1.3046	1.5954	0.7414	1.0805	0.1220
24 L_caudalanteriorcingulate	-1.5551	0.7755	-1.3272	1.3078	0.4802
25 L_caudalmiddlefrontal	-0.0979	1.4634	-0.4697	0.9869	0.2622
26 L_cuneus	0.2731	1.2169	0.0921	1.1388	0.5804

Figure 16: Extract from the table obtained from the morphometric data of the subjects

To compare morphometrics of PD-NC patients with those of PD-MCI patients, I performed an unpaired two tailed t-test for each area, setting a significance level at 5%.

The p-values smaller than the significance level of each t-test have been reported on an inverted logarithmic scale for visualization purposes, applying a –log10 transform to express higher significance with higher values in the figure 17.

P-values lower than 0.05 were observed for left and right supramarginal and transversetemporal volumes, although no p-value survived correction for multiple comparisons or FDR (false discovery rate). The correction was performed using the Bonferroni-Holm method which sorts the p-values from smallest to largest and adjusts the significance level for each test in a stepwise manner. This method is ideal when there are a few very significant results among many results not significant (87).

In a similar way I performed on the whole dataset of PD patients a one-sample two-tailed t-test for each area, setting a significance level at 5%. Since I used Z-scored data, the result is a statistical comparison between the morphometrics of PD patients and the normative morphometrics computed from age-, gender-, and eTIV-matched controls (figure 18). The cortical areas in red, in Figure 18, and those in the subcortical most deviated from zero, correspond to the areas with the greatest atrophy. In this way it is possible to note the regions of the brain most affected by Parkinson's disease. The regions in Figure 18, with p-values lower

than 0.05 (t-tests significance) are 66. By correcting the significance value with the Holm-Bonferroni method, the volumes below the threshold become 44.

They are:

1. 'SC_Left-Lateral-Ventricle'
2. 'SC_Left-Inf-Lat-Vent'
3. 'SC_Left-Caudate'
4. 'SC_Left-Putamen'
5. 'SC_Left-Pallidum'
6. 'SC_3rd-Ventricle'
7. 'SC_Left-VentralDC'
8. 'SC_Right-Lateral-Ventricle'
9. 'SC_Right-Inf-Lat-Vent'
10. 'SC_Right-Putamen'
11. 'SC_Right-Pallidum'
12. 'SC_Right-VentralDC'
13. 'L_caudalanteriorcingulate'
14. 'L_entorhinal'
15. 'L_fusiform'
16. 'L_inferiorparietal'
17. 'L_inferiortemporal'
18. 'L_isthmuscingulate'
19. 'L_lateralorbitofrontal'
20. 'L_lingual'
21. 'L_middletemporal'
22. 'L_parahippocampal'
23. 'L_paracentral'
24. 'L_parsopercularis'
25. 'L_posteriorcingulate'
26. 'L_rostralanteriorcingulate'
27. 'L_rostralmiddlefrontal'
28. 'L_superiortemporal'
29. 'L_insula'
30. 'R_caudalanteriorcingulate'
31. 'R_entorhinal'
32. 'R_fusiform'

33. 'R_inferiorparietal'
34. 'R_inferiortemporal'
35. 'R_isthmuscingulate'
36. 'R_lingual'
37. 'R_middletemporal'
38. 'R_parahippocampal'
39. 'R_paracentral'
40. 'R_parsorbitalis'
41. 'R_parstriangularis'
42. 'R_postcentral'
43. 'R_posteriorcingulate'
44. 'R_rostralanteriorcingulate'
45. 'R_superiorparietal'
46. 'R_superiortemporal'
47. 'R_transversetemporal'
48. 'R_insula'

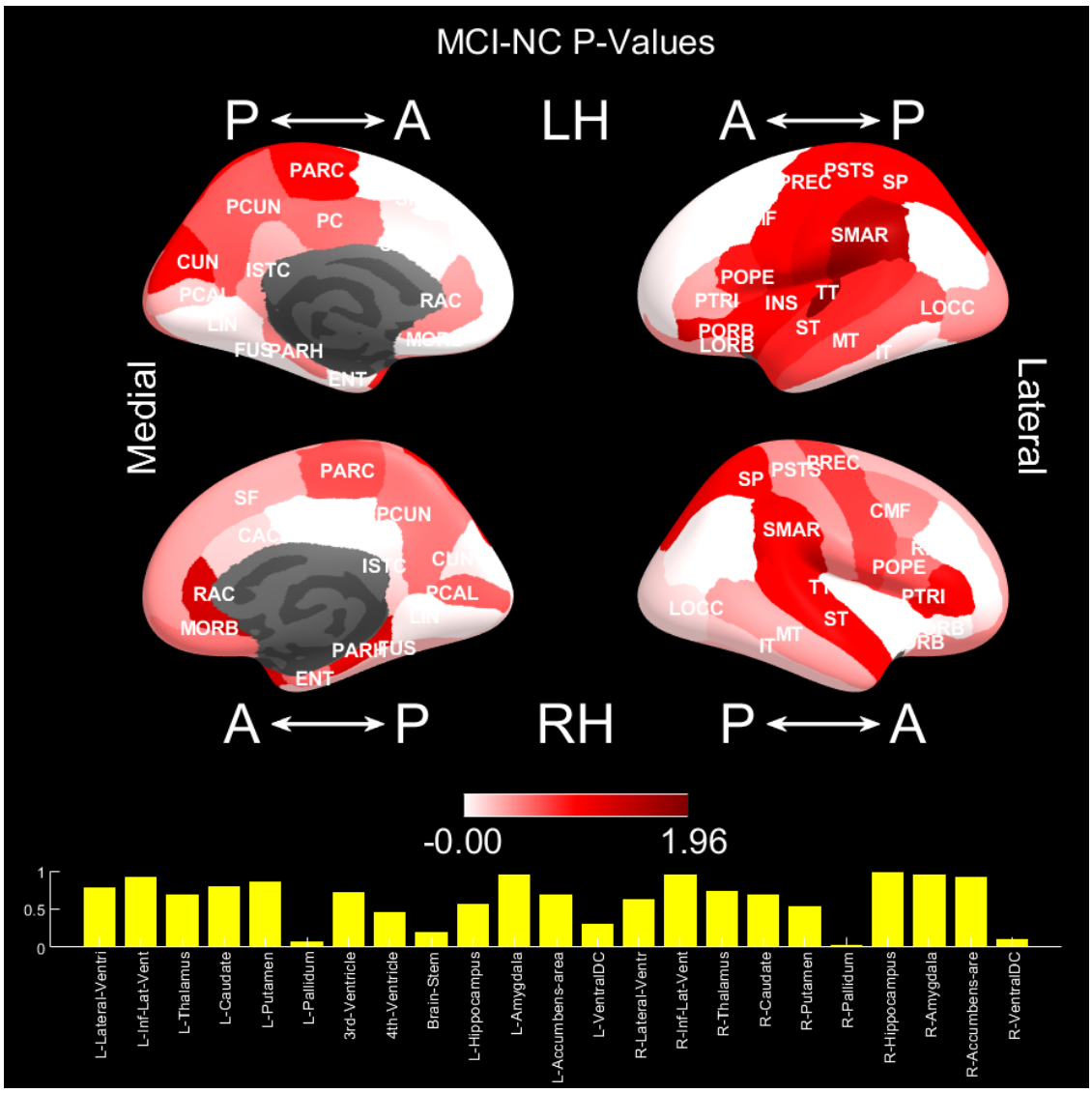

Figure 17: Comparison between MCI and NC of Normalised brain volumes. In the upper part of the figure, -log10(p-value) is expressed with colors ranging from white (not significant) to red (approaching significance). In the lower part of the figure an histogram summarizes data for subcortical structures, using again -log10 transform for the p-values. The acronyms that identify the various brain volumes have the following meanings: AC: Caudal anterior cingulate, CMF: Caudal middle frontal, CUN: Cuneus, ENT: Entorhinal, FUS: Fusiform, INFP: Inferior parietal, INS: Insula, ISTC: Isthmus cingulate, IT: Inferior temporal, LIN: Lingual, LOCC: Lateral occipital, LORB: Lateral orbito-frontal, MORB: Medial orbito-frontal, MT: Middle temporal, PARC: Paracentral lobule, PARH: Parahippocampal, PC: Posterior cingulate, PCAL: Pericalcarine, PCUN: Precuneus, POPE: Pars opercularis, PORB: Pars orbitalis, PREC: Precentral, PSTS: Postcentral, PTRI: Pars triangularis, RAC: Rostral anterior cingulate, RMF: Rostral middle frontal, SF: Superior frontal, SMAR: Supramarginal, SP: Superior parietal, ST: Superior temporal, TT: Transverse temporal

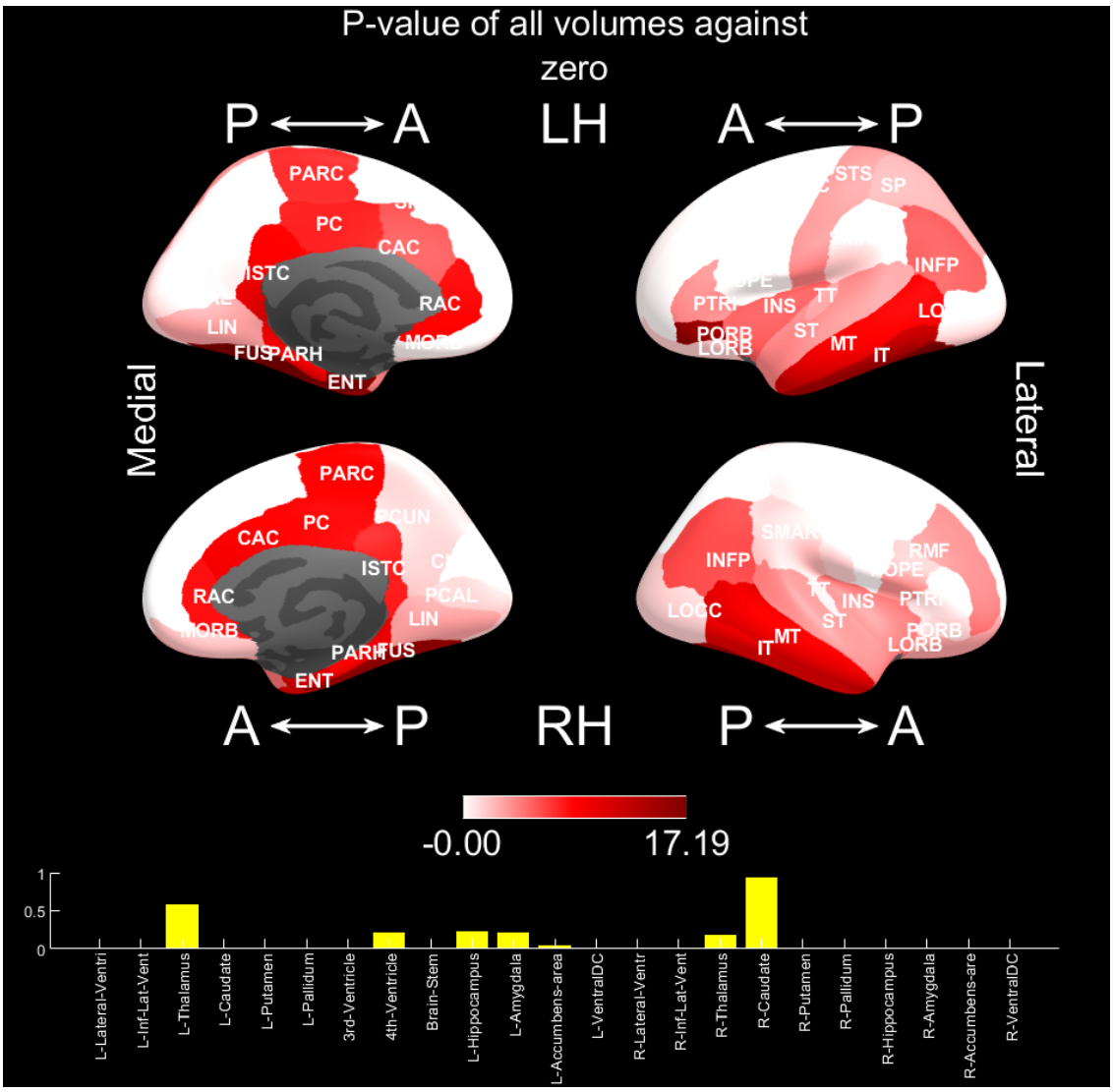

Figure 18: P-values of all z-scored volumes against zero. The graph was obtained by carrying out a T-test of the normalized volumes to check whether there were any values for which their normalized means (according to normative parameters) deviated from a null value. In the upper part of the figure, -log10(p-value) is expressed with colors ranging from white (not significant) to red (approaching significance). In the lower part of the figure an histogram summarizes data for subcortical structures, using again -log10 transform for the p-values. The acronyms that identify the various brain volumes have the following meanings: CAC: Caudal anterior cingulate, CMF: Caudal middle frontal, CUN: Cuneus, ENT: Entorhinal, FUS: Fusiform, INFP: Inferior parietal, INS: Insula, ISTC: Isthmus cingulate, IT: Inferior temporal, LIN: Lingual, LOCC: Lateral occipital, LORB: Lateral orbito-frontal, MORB: Medial orbito-frontal, MT: Middle temporal, PARC: Paracentral lobule, PARH: Parahippocampal, PC: Posterior cingulate, PCAL: Pericalcarine, PCUN: Precuneus, POPE: Pars opercularis, PORB: Pars orbitalis, PREC: Precentral, PSTS: Postcentral, PTRI: Pars triangularis, RAC: Rostral anterior cingulate, RMF: Rostral middle frontal, SF: Superior frontal, SMAR: Supramarginal, SP: Superior parietal, ST: Superior temporal, TT: Transverse temporal

4.3 COMPARISON BETWEEN VOXEL-BASED AND SURFACE-BASED MORPHOMETRY

We performed the same analysis using instead the BAAD software, i.e., employing voxel-based morphometry. The correlation coefficients between non-normalized volumes obtained from BAAD and FreeSurfer estimations are visualized for each region of interest in Figure 19. Except for right cingulate cortexes and fusiform gyrus, all cortical parcels obtained correlation coefficients above 0.7, while the situation in the subcortex is much more heterogenous, with ventricles and brainstem appearing to be totally uncorrelated.

To assess whether there is consistent overestimation for one of the algorithms with respect to the other, we computed the ratio between the two set of estimated volumes and subtracted it from the unit. The median of this measure is visualized in Figure 20. We can see that volumes estimated with SPM are consistently smaller, about 75% of those estimated with freesurfer on average, in particular around the central sulcus and in the superior part of the temporal cortex, as well as in the pericalcarine. In the subcortex, the ventral diencephalon, the 4th ventricle and the choroid plexus and the optic chiasm are the only regions being larger in SPM, while in the cortex this is true only for the rostral middle frontal cortex.

In the absence of a gold standard, we used as a first indication of quality, the correlation between morphometrics and scores obtained at the MOCA scale.

Figure 21 shows the correlation coefficient values calculated respectively between the volumes obtained with FreeSurfer and MOCA, and the volumes obtained with SPM and MOCA.

When we are analysing volumes and applying partial correlations, FreeSurfer achieves larger correlation values for its morphometrics with MOCA scores. In particular, it is able to catch the relation between MOCA scores and the lingual gyrus and rostral anterior cingulate, and the anticorrelation with ventricles expansion. BAAD might be better for subcortical regions, as it is better in finding correlation with putamen when using normalizations, the correlation with MOCA is basically the same.

The results confirm that BAAD does not estimate cortical volumes as well as FS, while in the subcortex it could return significantly more relevant results.

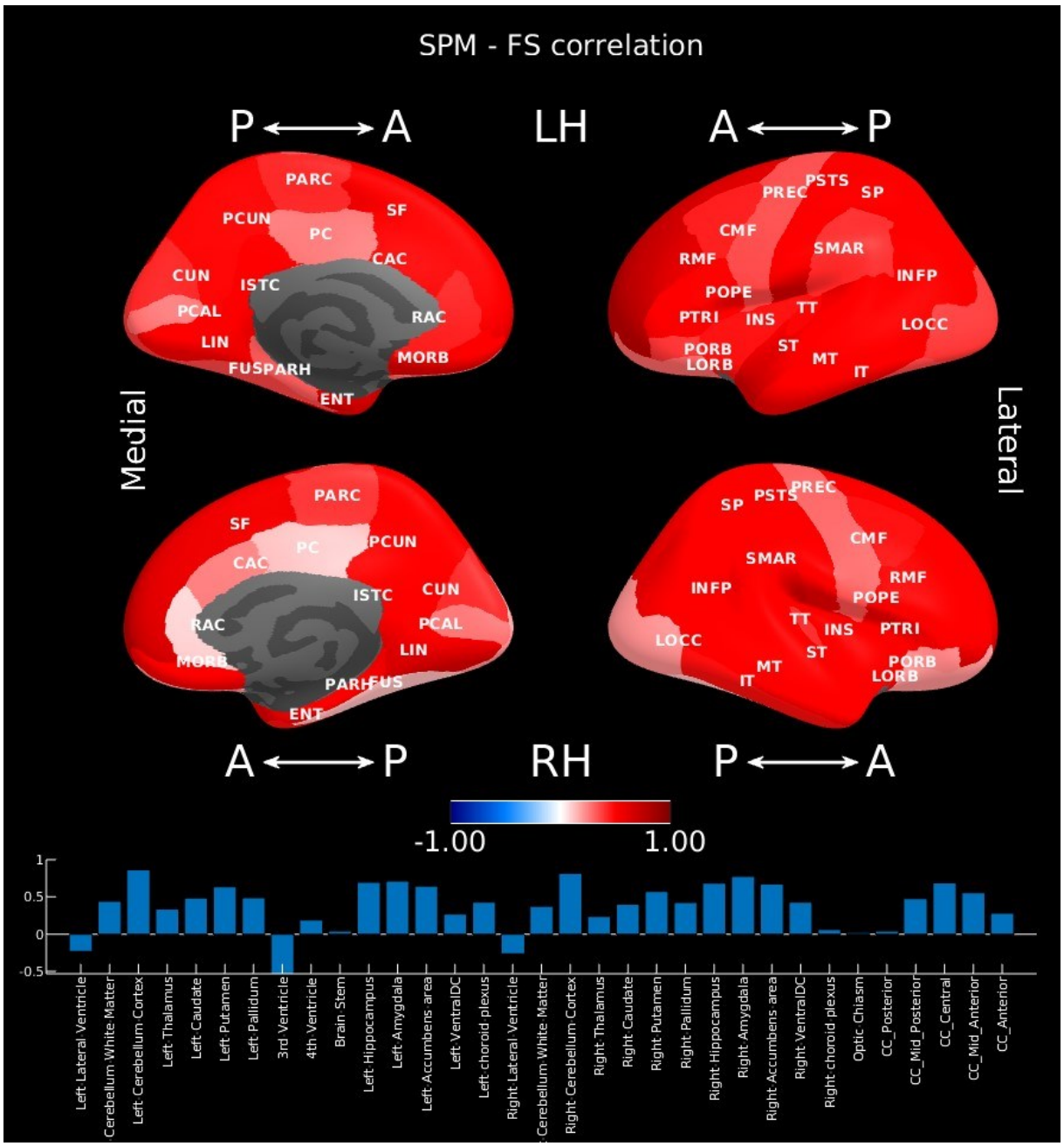

Figure 19: Pearson correlation coefficient for the comparison between normalized volumes calculated with SPM and FreeSurfer respectively. The correlation coefficients of the cortical areas are reported on the brain maps, while the subcortical ones in the diagram below. The two maps above represent the medial (left) and lateral (right) views of the left hemisphere, while the two maps below the medial (left) and lateral (right) views of the right hemisphere. The acronyms that identify the various brain volumes have the following meanings: AC: Caudal anterior cingulate, CMF: Caudal middle frontal, CUN: Cuneus, ENT: Entorhinal, FUS: Fusiform, INFP: Inferior parietal, INS: Insula, ISTC: Isthmus cingulate, IT: Inferior temporal, LIN: Lingual, LOCC: Lateral occipital, LORB: Lateral orbito-frontal, MORB: Medial orbito-frontal, MT: Middle temporal, PARC: Paracentral lobule, PARH: Parahippocampal, PC: Posterior cingulate, PCAL: Pericalcarine, PCUN: Precuneus, POPE: Pars opercularis, PORB: Pars orbitalis, PREC: Precentral, PSTS: Postcentral, PTRI: Pars triangularis, RAC: Rostral anterior cingulate, RMF: Rostral middle frontal, SF: Superior frontal, SMAR: Supramarginal, SP: Superior parietal, ST: Superior temporal, TT: Transverse temporal

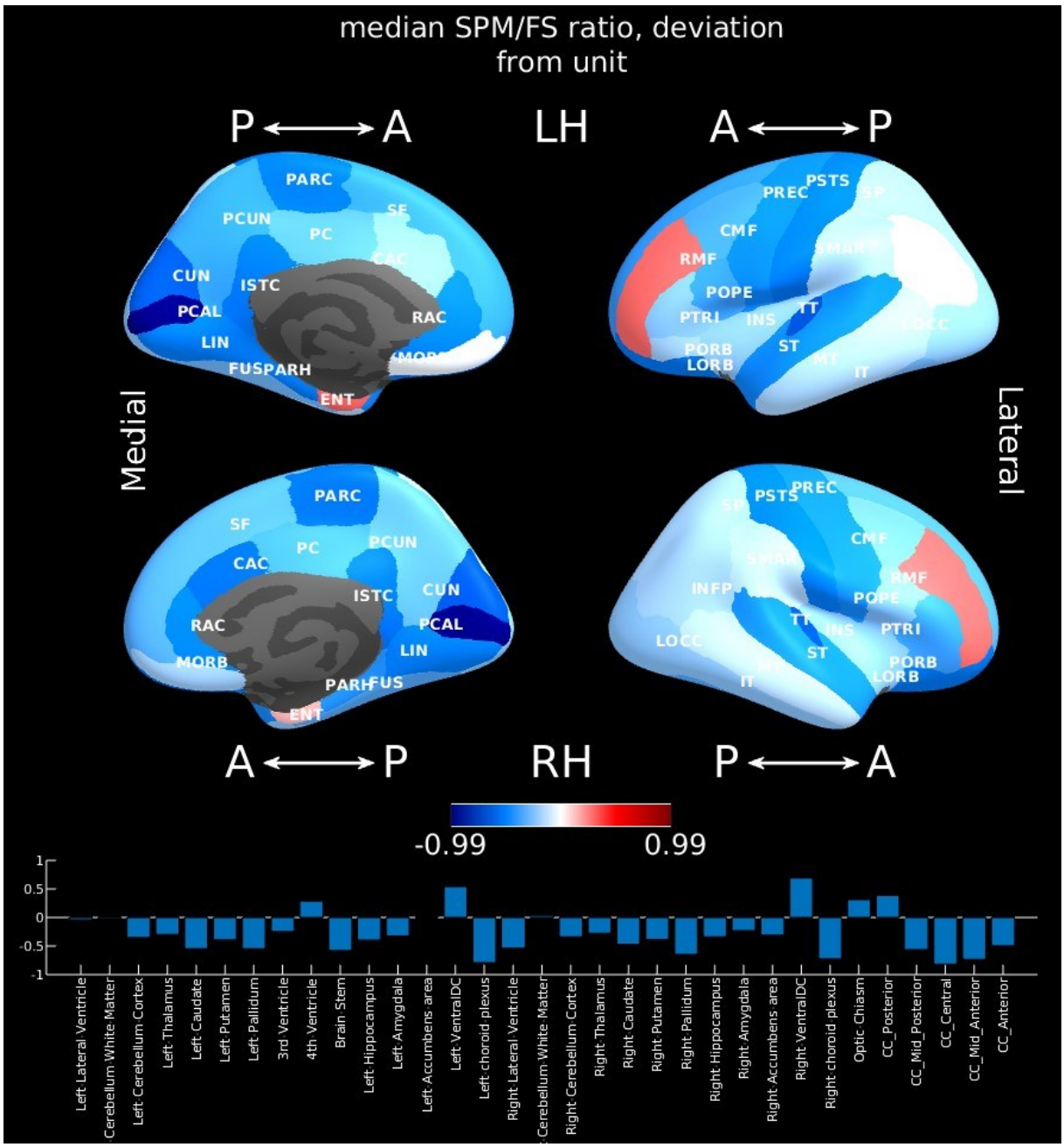

Figure 20: Values of the difference between the median of the ratio between volumes calculated with SPM and FreeSurfer, and unit value $[\left(median\ \frac{SPM_{volume}}{FreeSurfer_{volume}}\right) - 1]$. *Values below zero indicate larger values for FreeSurfer, while values above zero indicate larger values for SPM. Cortical areas deviation from zeros are reported on the brain maps, while the subcortical deviations in the diagram below. The two maps above represent the medial (left) and lateral (right) views of the left hemisphere, while the two maps below the medial (left) and lateral (right) views of the right hemisphere. The acronyms that identify the various brain volumes have the following meanings: AC: Caudal anterior cingulate, CMF: Caudal middle frontal, CUN: Cuneus, ENT: Entorhinal, FUS: Fusiform, INFP: Inferior parietal, INS: Insula, ISTC: Isthmus cingulate, IT: Inferior temporal, LIN: Lingual, LOCC: Lateral occipital, LORB: Lateral orbito-frontal, MORB: Medial orbito-frontal, MT: Middle temporal, PARC: Paracentral lobule, PARH: Parahippocampal, PC: Posterior cingulate, PCAL: Pericalcarine, PCUN: Precuneus, POPE: Pars opercularis, PORB: Pars orbitalis, PREC: Precentral, PSTS: Postcentral, PTRI: Pars triangularis, RAC: Rostral anterior cingulate, RMF: Rostral middle frontal, SF: Superior frontal, SMAR: Supramarginal, SP: Superior parietal, ST: Superior temporal, TT: Transverse temporal*

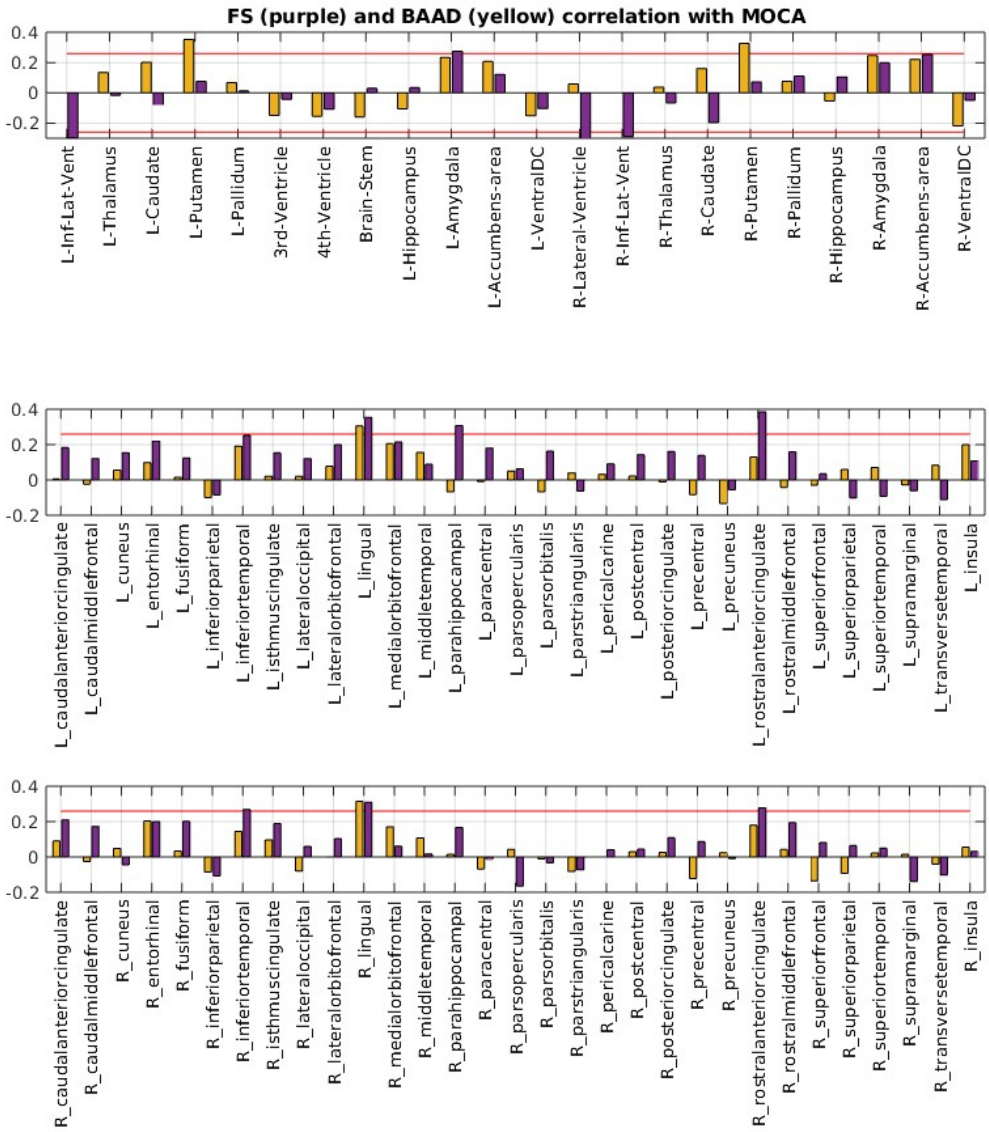

Figure 21: Spearman correlation coefficient values assumed, respectively, by FreeSurfer and BAAD (SPM) with MOCA. The correlation value calculated with FreeSurfer is purple, while the one calculated with SPM is yellow. The red line is the threshold for significance p=0.05.

4.4 MORPHOMETRY VERSUS BLOOD BIOMARKERS

Once the morphometric analysis had been carried out for the population considered, we then moved on to look for a connection among the volumes and the 4 biomarkers derived from blood analyses.

Firstly, to figure out what kind of correlation coefficient I could use, I ran a normality test on the biomarkers to see if it was possible to use the Person Correlation Coefficient. Since the analysis performed through One-sample Kolmogorov-Smirnov test on Matlab highlighted a non-normal distribution on all four biomarkers, it was not possible to use the calculation of the Pearson correlation coefficient.

Consequently, I performed a statistical nonparametric measure of correlation extracting Spearman correlation coefficients and the related p-values (figures 22, 24, 25, 26 and 27).

As it can be seen in the figure 22, the maximum values of the Spearman coefficient for each biomarker correspond respectively to 0.2588, 0.3096, 0.3056 and 0.3570, while the minimum values are -0.3416, -0.3421, -0.3276 and -0.3104. So, the percentage of linear relationship between brain volumes and biomarkers reaches its maximum positive and negative values around 30%. Thus, the data indicate that the relationship between brain volumes and biomarkers appears to be positively and/or negatively linear only around 30% for very few volumes, while, for the majority, the Spearman coefficient tends to zero (i.e. no linear relation between the data considered).

In figures from 24 to 27, the p-values greater than 0.05 were obscured, allowing us to have visibility of the areas in which we can reject the null hypothesis. For visualization purposes, p-values were transformed with an inverted logarithmic scale (-log10(p)). From the results in figures 24, 25, 26 and 27 it emerges that in most volumes there is no connection between the pathology and the biomarkers considered. However, it is also possible to note that in a limited number of areas the p-value is lower than 0.05. In particular, the volumes where it is possible to find these values below 5% are:

1. the link between NFL and SC_Optic-Chiasm, where the p-value is 0.0115 (Figure 24 and blue scatterplot in Figure 23)
2. the link between GFAP and SC_Left-vessel, where the p-value is 0.0113 (Figure 25 and green scatterplot in Figure 23)
3. the link between pTau181 and R_superiorfrontal, where the p-value is 0.0166 (Figure 26 and magenta scatterplot in Figure 23)
4. the link between GFAP/NFL and SC_Optic-Chiasm, where the p-value is 0.0081 (Figure 27 and cyan scatterplot in Figure 23)

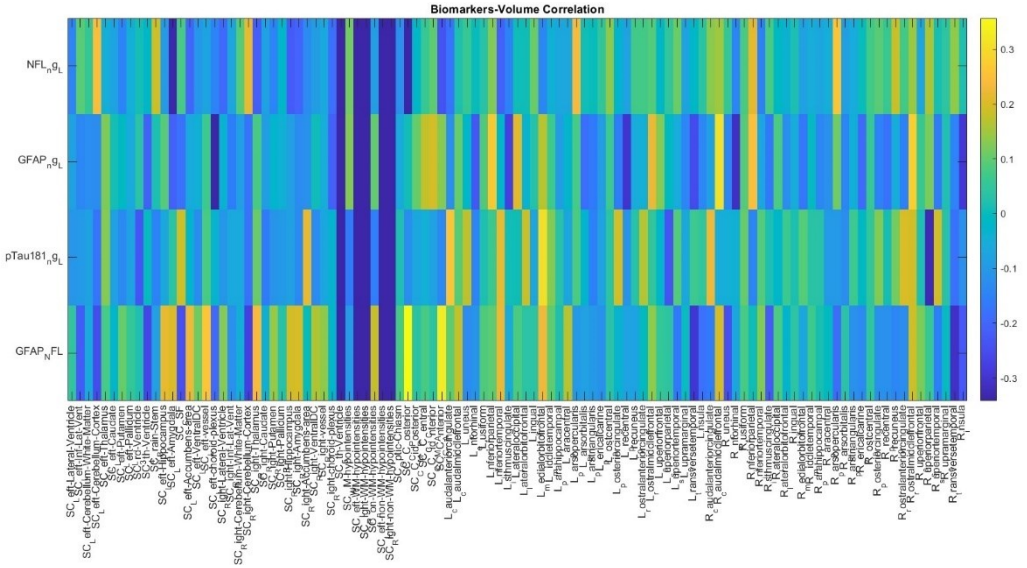

Figure 22: Spearman Correlation Coefficients between biomarkers and brain volumes. The matrix in figure shows the values of the Sperman correlation coefficient between each volume on the x-axis and the biomarkers on the y-axis. The correlation coefficients can vary between -1 and 1. The lowest values tend towards blue, while, moving away from them there are shades tending towards green, orange and yellow (highest values found)

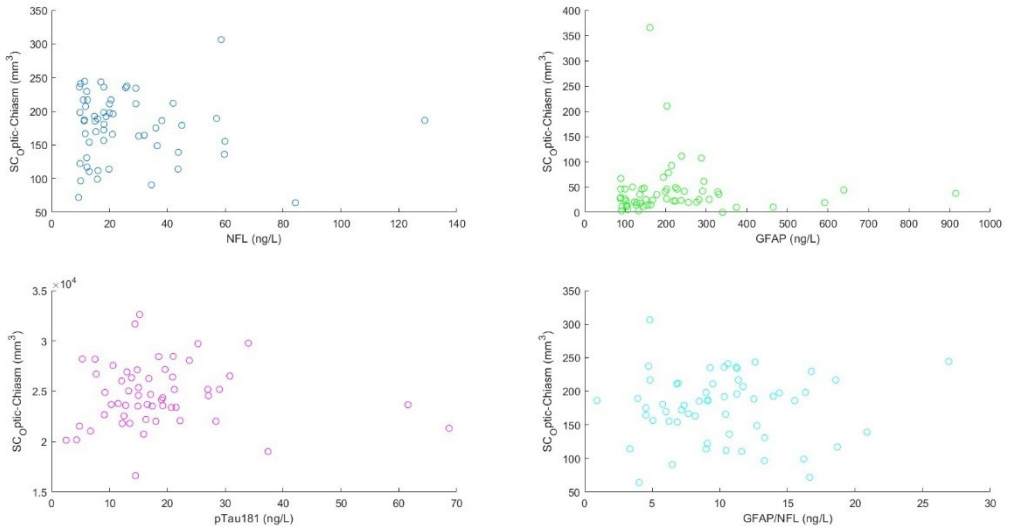

Figure 23: Scatterplots showing the biomarker-volume relationship for all brain volumes for which the p-value is lower than the significance level of the tests conducted. The NFL-SC_Optic-Chiasm relationship scatterplot for each patient is at the top left, with circles marked in blue. The GFAP-SC_Left-vessel relationship scatterplot for each patient is at the top right, with circles marked in green. The pTau181-R_superiorfrontal relationship scatterplot for each patient is at the bottom left, with circles marked in magenta. The GFAP/NFL-SC_Optic-Chiasm relationship scatterplot for each patient is at the bottom right, with circles marked in cyan.

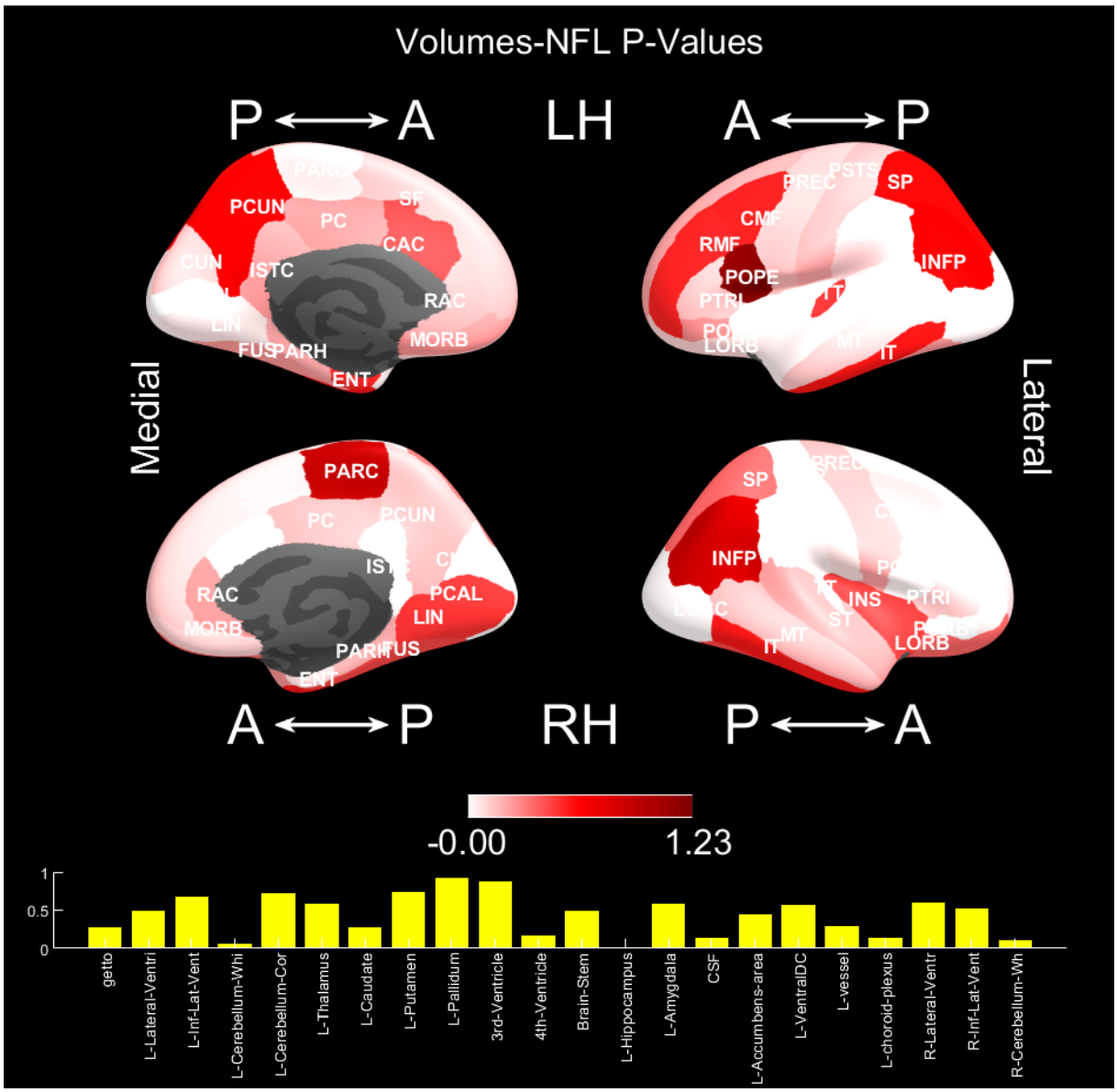

Figure 24:P-Values found between NFL and non-normalised brain volumes (Spearman). The acronyms that identify the various brain volumes have the following meanings: CAC: Caudal anterior cingulate, CMF: Caudal middle frontal, CUN: Cuneus, ENT: Entorhinal, FUS: Fusiform, INFP: Inferior parietal, INS: Insula, ISTC: Isthmus cingulate, IT: Inferior temporal, LIN: Lingual, LOCC: Lateral occipital, LORB: Lateral orbito-frontal, MORB: Medial orbito-frontal, MT: Middle temporal, PARC: Paracentral lobule, PARH: Parahippocampal, PC: Posterior cingulate, PCAL: Pericalcarine, PCUN: Precuneus, POPE: Pars opercularis, PORB: Pars orbitalis, PREC: Precentral, PSTS: Postcentral, PTRI: Pars triangularis, RAC: Rostral anterior cingulate, RMF: Rostral middle frontal, SF: Superior frontal, SMAR: Supramarginal, SP: Superior parietal, ST: Superior temporal, TT: Transverse temporal

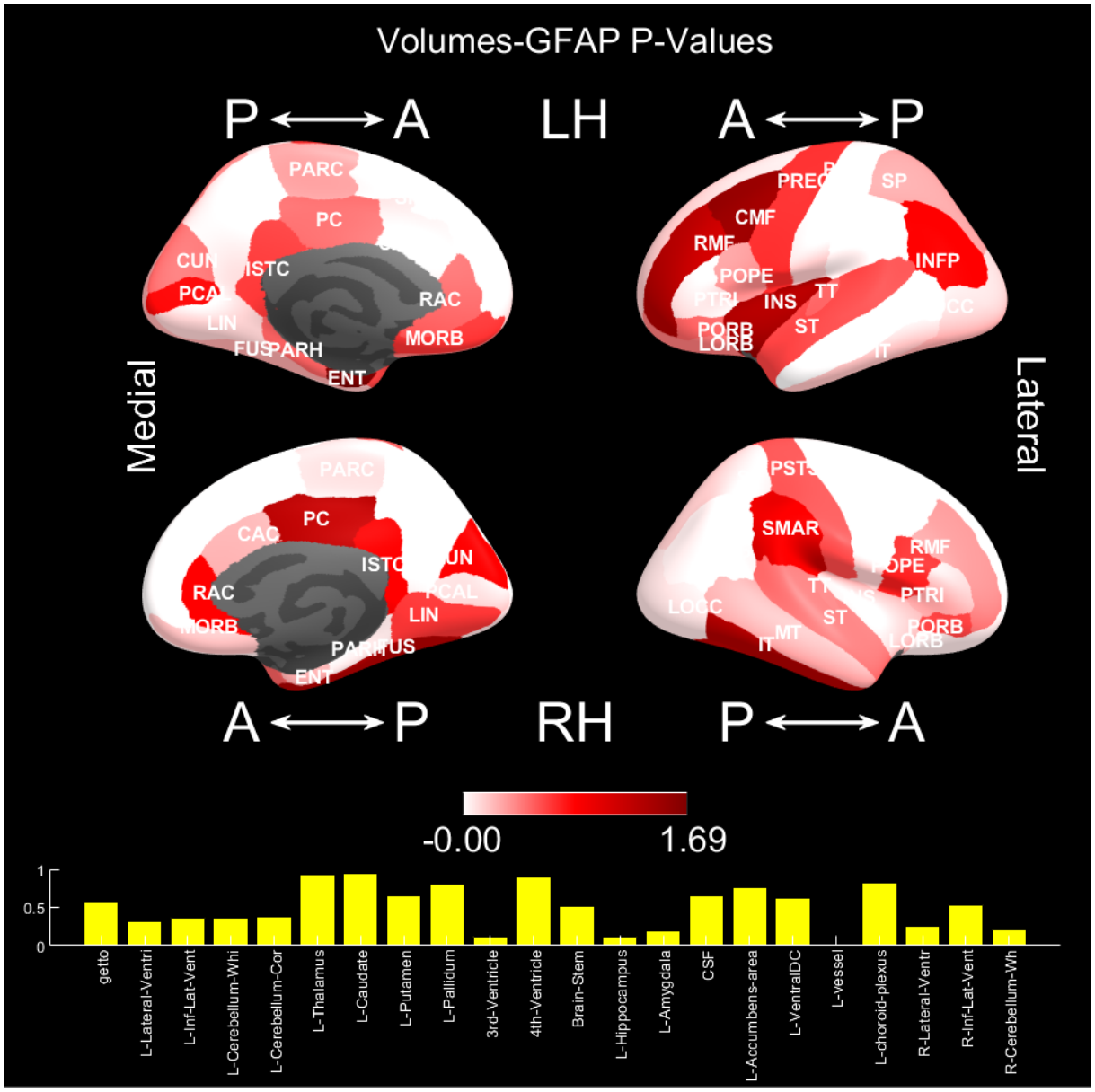

Figure 25: P-Values found between GFAP and non-normalised brain volumes (Spearman). The acronyms that identify the various brain volumes have the following meanings: CAC: Caudal anterior cingulate, CMF: Caudal middle frontal, CUN: Cuneus, ENT: Entorhinal, FUS: Fusiform, INFP: Inferior parietal, INS: Insula, ISTC: Isthmus cingulate, IT: Inferior temporal, LIN: Lingual, LOCC: Lateral occipital, LORB: Lateral orbito-frontal, MORB: Medial orbito-frontal, MT: Middle temporal, PARC: Paracentral lobule, PARH: Parahippocampal, PC: Posterior cingulate, PCAL: Pericalcarine, PCUN: Precuneus, POPE: Pars opercularis, PORB: Pars orbitalis, PREC: Precentral, PSTS: Postcentral, PTRI: Pars triangularis, RAC: Rostral anterior cingulate, RMF: Rostral middle frontal, SF: Superior frontal, SMAR: Supramarginal, SP: Superior parietal, ST: Superior temporal, TT: Transverse temporal

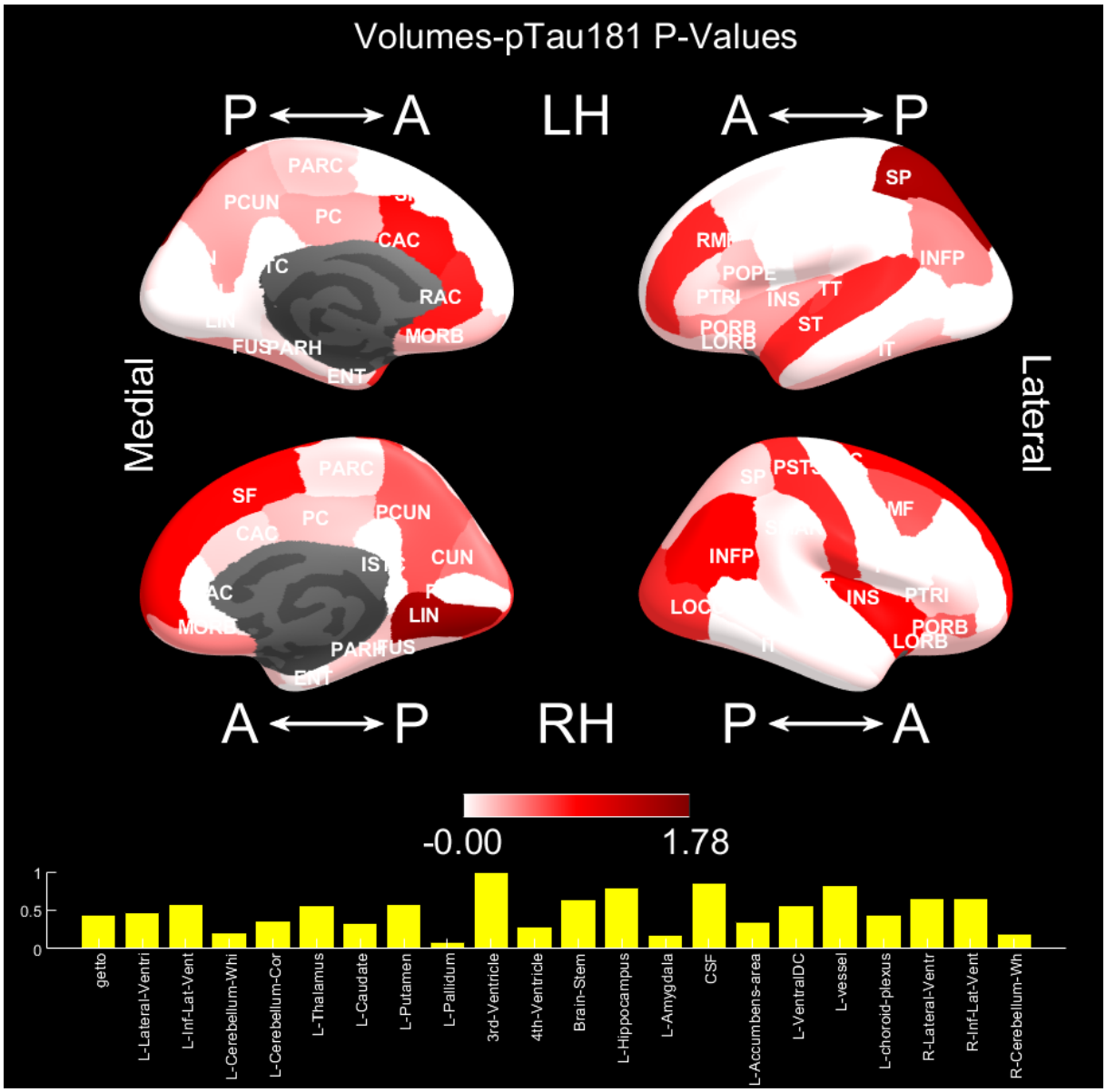

Figure 26: P-Values found between pTau181 and non-normalised brain volumes (Spearman). The acronyms that identify the various brain volumes have the following meanings: CAC: Caudal anterior cingulate, CMF: Caudal middle frontal, CUN: Cuneus, ENT: Entorhinal, FUS: Fusiform, INFP: Inferior parietal, INS: Insula, ISTC: Isthmus cingulate, IT: Inferior temporal, LIN: Lingual, LOCC: Lateral occipital, LORB: Lateral orbito-frontal, MORB: Medial orbito-frontal, MT: Middle temporal, PARC: Paracentral lobule, PARH: Parahippocampal, PC: Posterior cingulate, PCAL: Pericalcarine, PCUN: Precuneus, POPE: Pars opercularis, PORB: Pars orbitalis, PREC: Precentral, PSTS: Postcentral, PTRI: Pars triangularis, RAC: Rostral anterior cingulate, RMF: Rostral middle frontal, SF: Superior frontal, SMAR: Supramarginal, SP: Superior parietal, ST: Superior temporal, TT: Transverse temporal

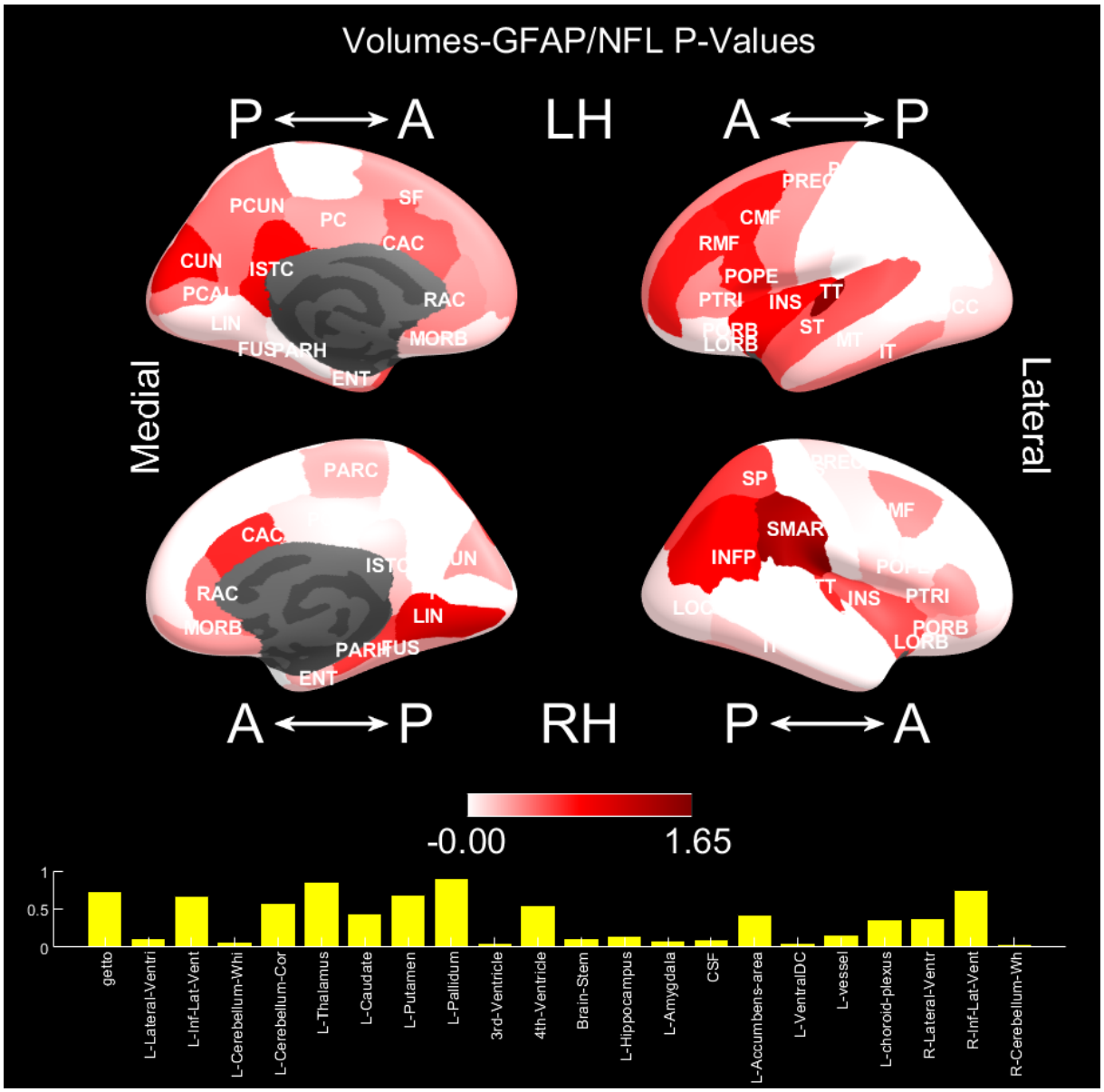

Figure 27: P-Values found between GFAP/NFL ratio and non-normalised brain volumes (Spearman). The acronyms that identify the various brain volumes have the following meanings: CAC: Caudal anterior cingulate, CMF: Caudal middle frontal, CUN: Cuneus, ENT: Entorhinal, FUS: Fusiform, INFP: Inferior parietal, INS: Insula, ISTC: Isthmus cingulate, IT: Inferior temporal, LIN: Lingual, LOCC: Lateral occipital, LORB: Lateral orbito-frontal, MORB: Medial orbito-frontal, MT: Middle temporal, PARC: Paracentral lobule, PARH: Parahippocampal, PC: Posterior cingulate, PCAL: Pericalcarine, PCUN: Precuneus, POPE: Pars opercularis, PORB: Pars orbitalis, PREC: Precentral, PSTS: Postcentral, PTRI: Pars triangularis, RAC: Rostral anterior cingulate, RMF: Rostral middle frontal, SF: Superior frontal, SMAR: Supramarginal, SP: Superior parietal, ST: Superior temporal, TT: Transverse temporal

Although some p-values were below 0.05, it is worth noting that no significance survives a correction for multiple tests performed using the Bonferroni-Holmes method.

Subsequently, I calculated the Spearman Correlation Coefficient and the related p-values on the normalized volumetric data. The volumes for which the p-value is lower than the significance level of 0.05 are:

1. SC_Left-Amygdala (p-value = 0,024) and L_parsopercularis (p-value = 0,0210), from the correlation made with NFL (see Figure 29 and Scatterplot in Figure 33)
2. L_inferiorparietal (p-value = 0,0074) and R_caudalmiddlefrontal (p-value = 0,026) R_entorhinal (p-value = 0,012), from the correlation made with GFAP (see Figure 30 and Scatterplot in Figure 34)
3. SC_Right-Caudate (p-value = 0,049) and R_supramarginal (p-value = 0,0333), from the correlation made with pTau181 (see Figure 31 and Scatterplot in Figure 35)
4. SC_Left-Accumbens-area (p-value = 0,046) SC_Right-Thalamus (p-value = 0,0206) R_transversetemporal (p-value = 0,045), from the correlation made with GFAP/NFL (see Figure 32 and Scatterplot in Figure 36)

As above, I visualized p-values using an inverted logarithmic transform of -log10(p).

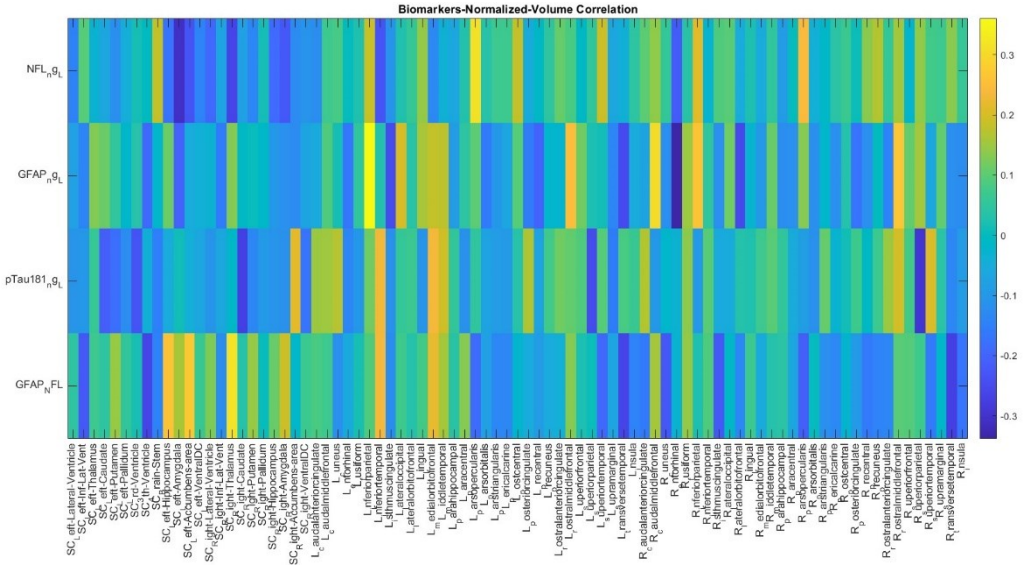

Figure 28:: Normalized Spearman Correlation Coefficients between biomarkers and normalized volumes. The matrix in figure shows the values of the Sperman correlation coefficient between each normalized volume on the x-axis and the biomarkers on the y-axis. The correlation coefficients can vary between -1 and 1. The lowest values tend towards blue, while, moving away from them there are shades tending towards green, orange and yellow (highest values found)

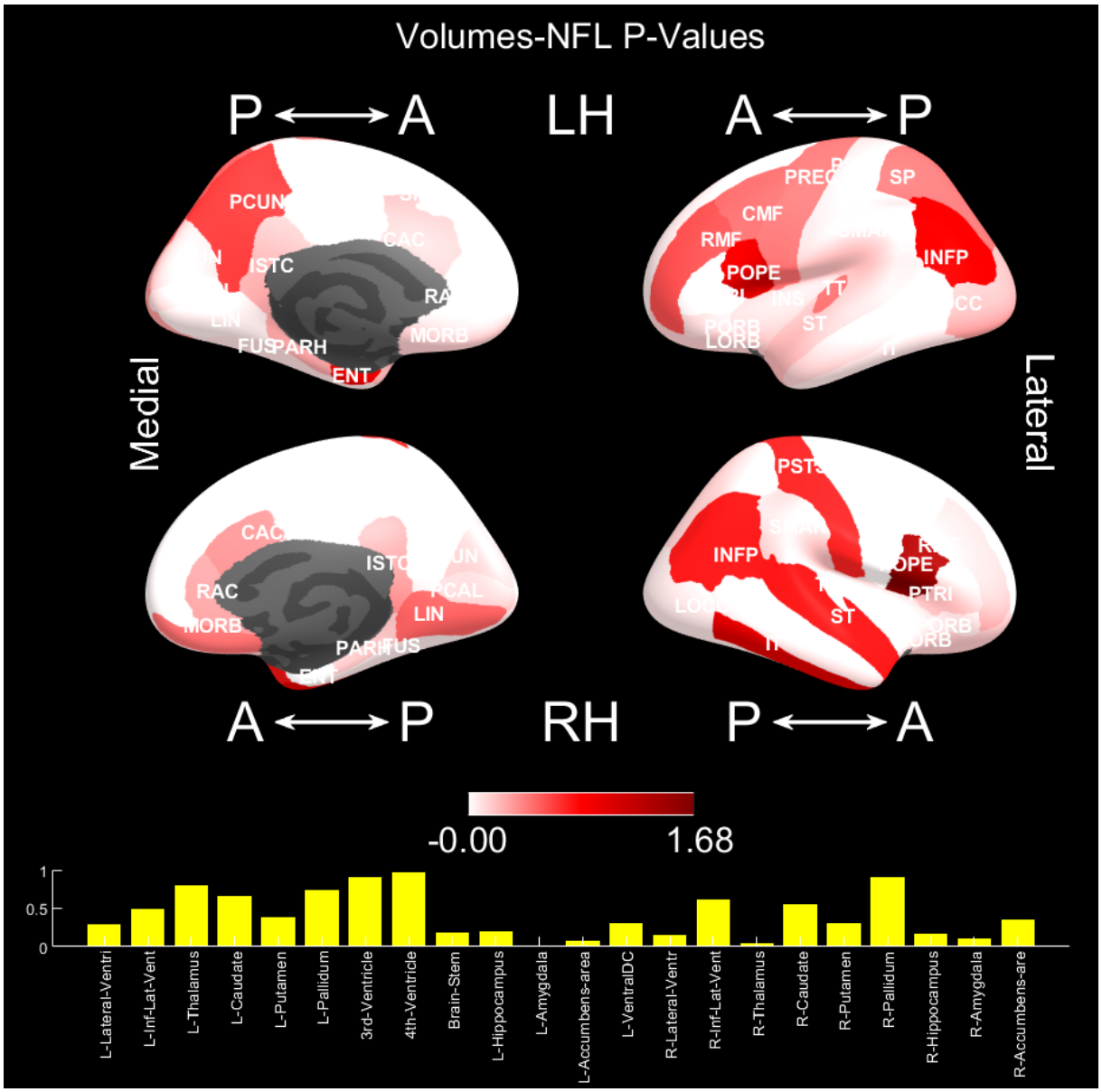

Figure 29: P-Values found between NFL and normalised brain volumes (Spearman). The acronyms that identify the various brain volumes have the following meanings: CAC: Caudal anterior cingulate, CMF: Caudal middle frontal, CUN: Cuneus, ENT: Entorhinal, FUS: Fusiform, INFP: Inferior parietal, INS: Insula, ISTC: Isthmus cingulate, IT: Inferior temporal, LIN: Lingual, LOCC: Lateral occipital, LORB: Lateral orbito-frontal, MORB: Medial orbito-frontal, MT: Middle temporal, PARC: Paracentral lobule, PARH: Parahippocampal, PC: Posterior cingulate, PCAL: Pericalcarine, PCUN: Precuneus, POPE: Pars opercularis, PORB: Pars orbitalis, PREC: Precentral, PSTS: Postcentral, PTRI: Pars triangularis, RAC: Rostral anterior cingulate, RMF: Rostral middle frontal, SF: Superior frontal, SMAR: Supramarginal, SP: Superior parietal, ST: Superior temporal, TT: Transverse temporal

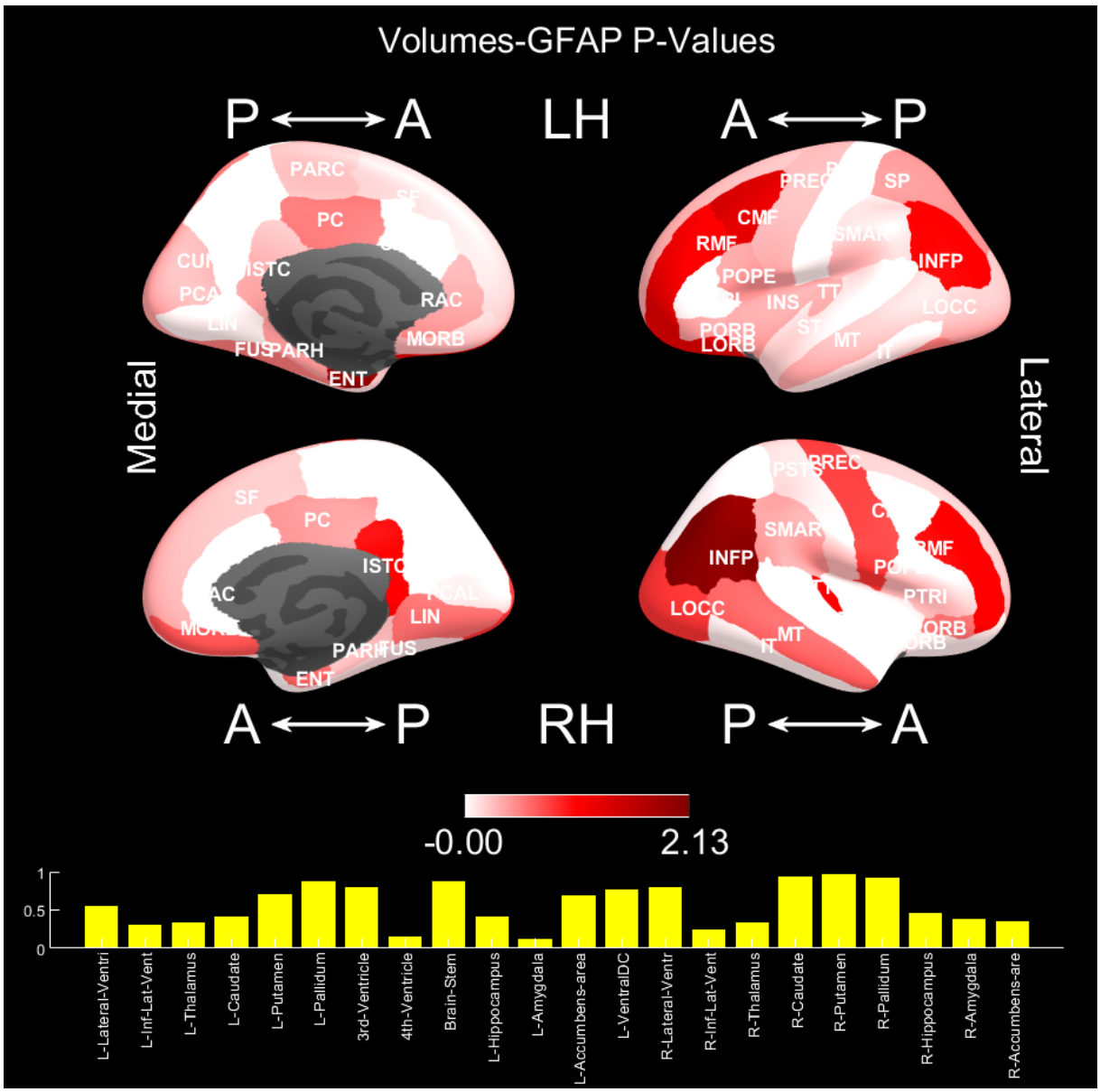

Figure 30: P-Values found between GFAP and normalised brain volumes (Spearman). The acronyms that identify the various brain volumes have the following meanings: CAC: Caudal anterior cingulate, CMF: Caudal middle frontal, CUN: Cuneus, ENT: Entorhinal, FUS: Fusiform, INFP: Inferior parietal, INS: Insula, ISTC: Isthmus cingulate, IT: Inferior temporal, LIN: Lingual, LOCC: Lateral occipital, LORB: Lateral orbito-frontal, MORB: Medial orbito-frontal, MT: Middle temporal, PARC: Paracentral lobule, PARH: Parahippocampal, PC: Posterior cingulate, PCAL: Pericalcarine, PCUN: Precuneus, POPE: Pars opercularis, PORB: Pars orbitalis, PREC: Precentral, PSTS: Postcentral, PTRI: Pars triangularis, RAC: Rostral anterior cingulate, RMF: Rostral middle frontal, SF: Superior frontal, SMAR: Supramarginal, SP: Superior parietal, ST: Superior temporal, TT: Transverse temporal

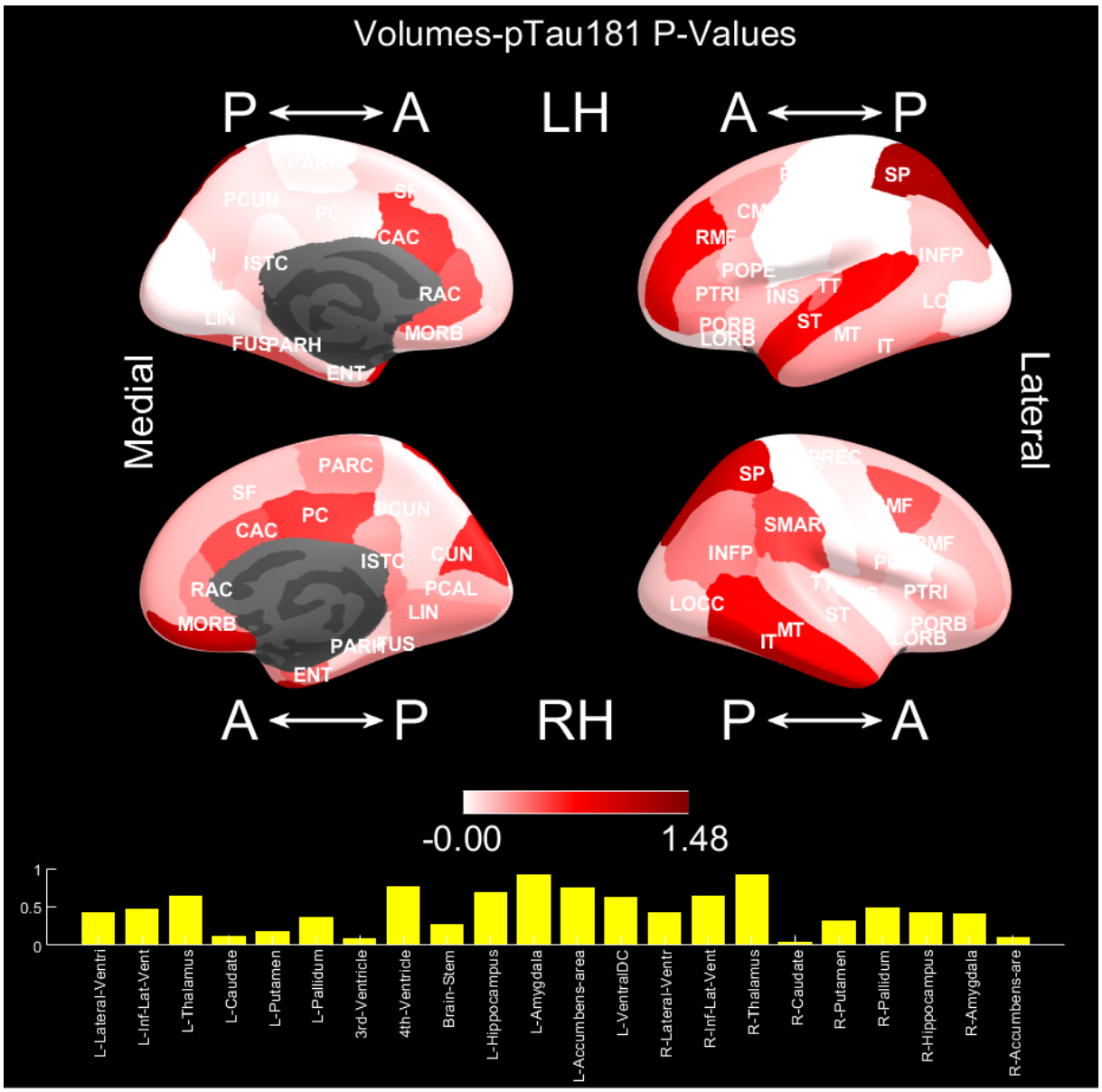

Figure 31: P-Values found between pTau181 and normalised brain volumes (Spearman).). The acronyms that identify the various brain volumes have the following meanings: CAC: Caudal anterior cingulate, CMF: Caudal middle frontal, CUN: Cuneus, ENT: Entorhinal, FUS: Fusiform, INFP: Inferior parietal, INS: Insula, ISTC: Isthmus cingulate, IT: Inferior temporal, LIN: Lingual, LOCC: Lateral occipital, LORB: Lateral orbito-frontal, MORB: Medial orbito-frontal, MT: Middle temporal, PARC: Paracentral lobule, PARH: Parahippocampal, PC: Posterior cingulate, PCAL: Pericalcarine, PCUN: Precuneus, POPE: Pars opercularis, PORB: Pars orbitalis, PREC: Precentral, PSTS: Postcentral, PTRI: Pars triangularis, RAC: Rostral anterior cingulate, RMF: Rostral middle frontal, SF: Superior frontal, SMAR: Supramarginal, SP: Superior parietal, ST: Superior temporal, TT: Transverse temporal

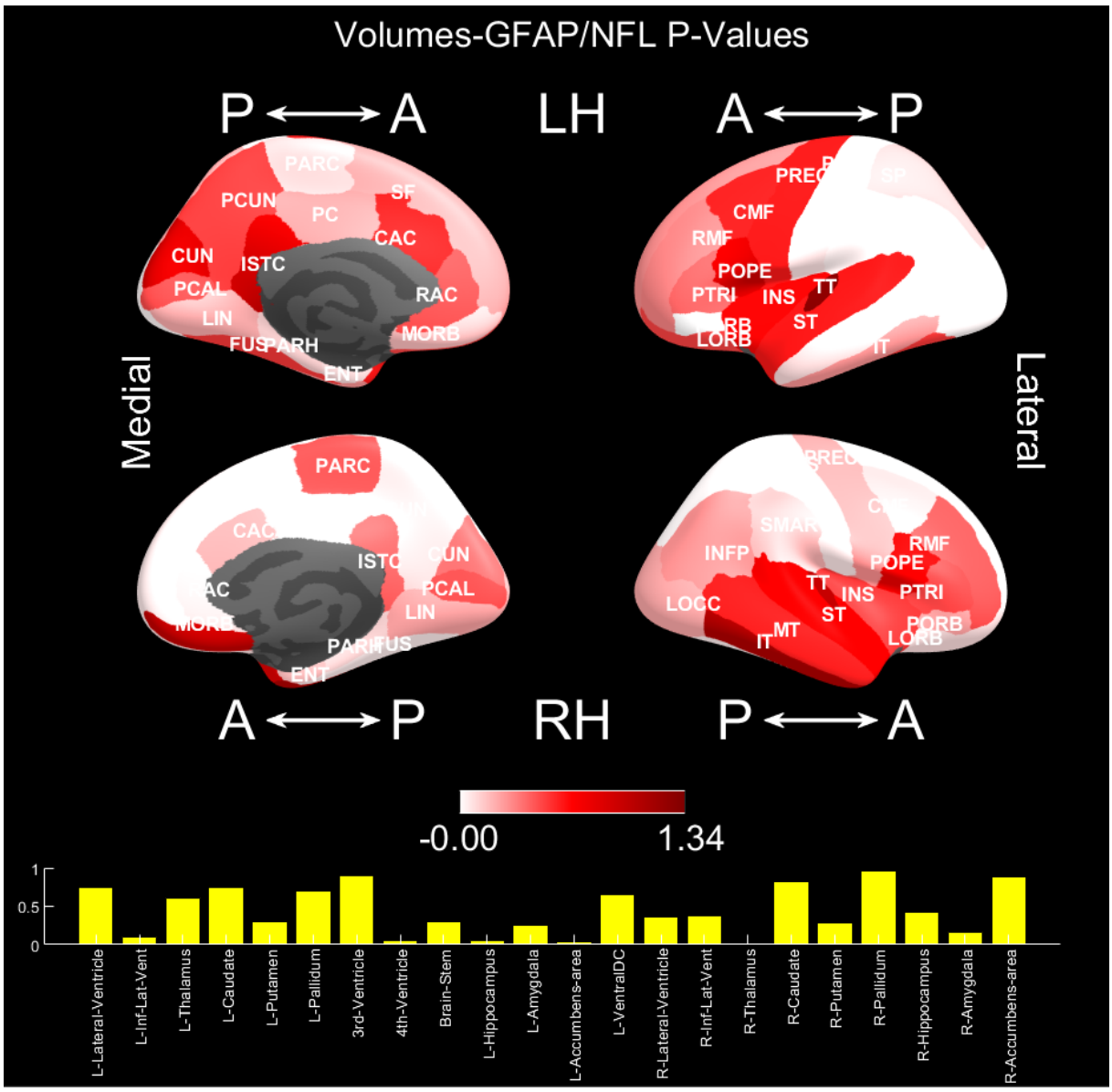

Figure 32: P-Values found between GFAP/NFL ratio and normalised brain volumes (Spearman).). The acronyms that identify the various brain volumes have the following meanings: CAC: Caudal anterior cingulate, CMF: Caudal middle frontal, CUN: Cuneus, ENT: Entorhinal, FUS: Fusiform, INFP: Inferior parietal, INS: Insula, ISTC: Isthmus cingulate, IT: Inferior temporal, LIN: Lingual, LOCC: Lateral occipital, LORB: Lateral orbito-frontal, MORB: Medial orbito-frontal, MT: Middle temporal, PARC: Paracentral lobule, PARH: Parahippocampal, PC: Posterior cingulate, PCAL: Pericalcarine, PCUN: Precuneus, POPE: Pars opercularis, PORB: Pars orbitalis, PREC: Precentral, PSTS: Postcentral, PTRI: Pars triangularis, RAC: Rostral anterior cingulate, RMF: Rostral middle frontal, SF: Superior frontal, SMAR: Supramarginal, SP: Superior parietal, ST: Superior temporal, TT: Transverse temporal

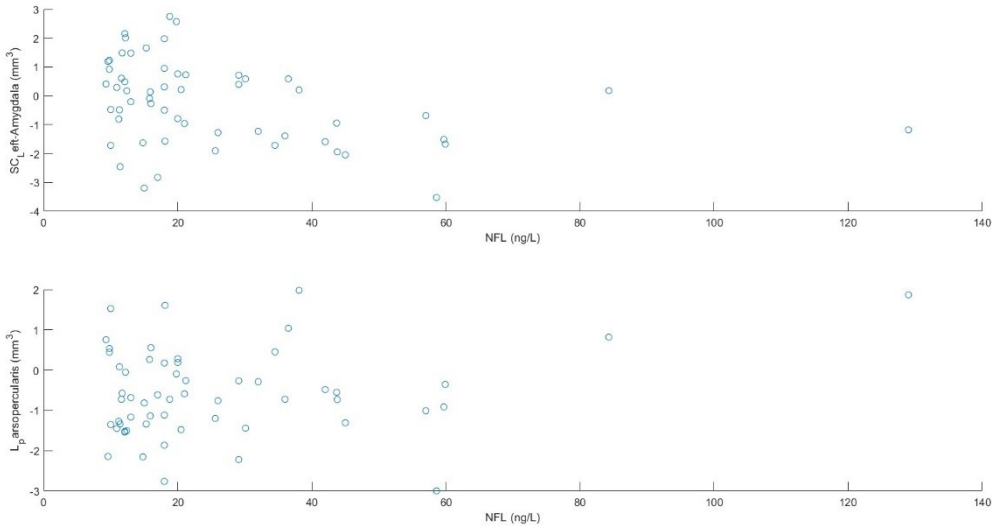

Figure 33: Scatterplots showing the NFL-volume relationship for the two brain volumes for which the p-value is lower than the significance level of the tests conducted. The NFL- SC_Left-Amygdala relationship scatterplot for each patient is at the top, while the NFL- SC_Left- L_parsopercularis relationship scatterplot for each patient is at the bottom.

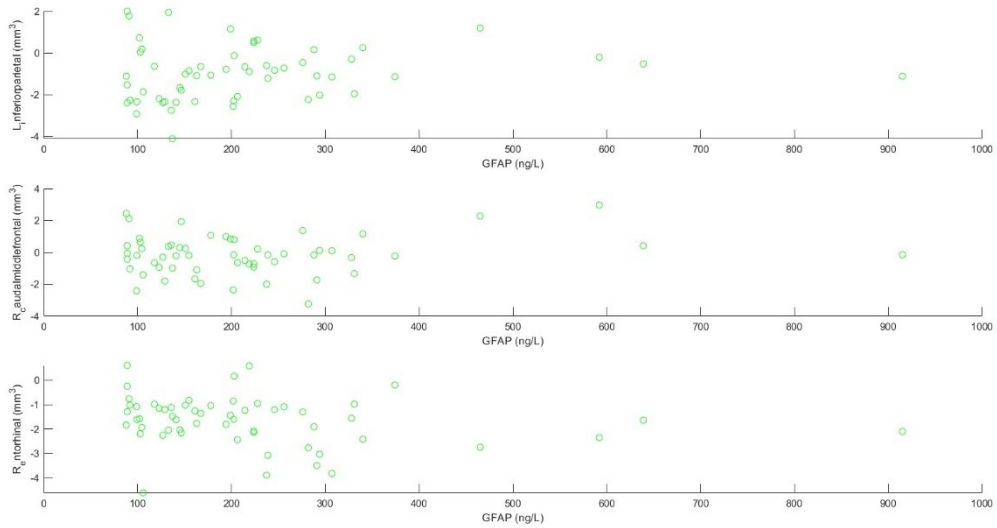

Figure 34: Scatterplots showing the GFAP-volume relationship for the three brain volumes for which the p-value is lower than the significance level of the tests conducted. The GFAP - L_inferiorparietal relationship scatterplot for each patient is at the top. The GFAP - R_caudalmiddlefrontal relationship scatterplot for each patient is in the middle. The GFAP - R_entorhinal relationship scatterplot for each patient is at the bottom.

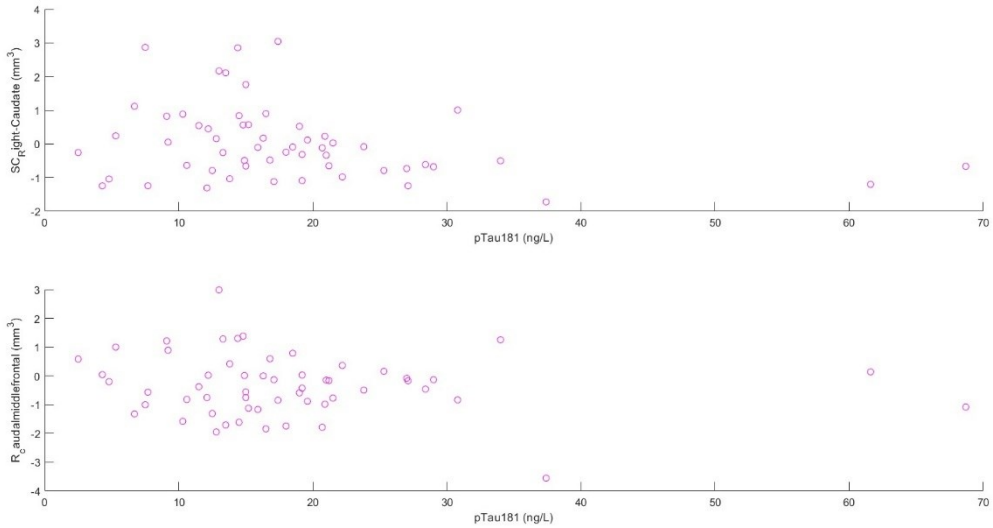

Figure 35: Scatterplots showing the pTau181-volume relationship for the two brain volumes for which the p-value is lower than the significance level of the tests conducted. The pTau181- SC_Right-Caudate relationship scatterplot for each patient is at the top, while the pTau181- R_supramarginal relationship scatterplot for each patient is at the bottom.

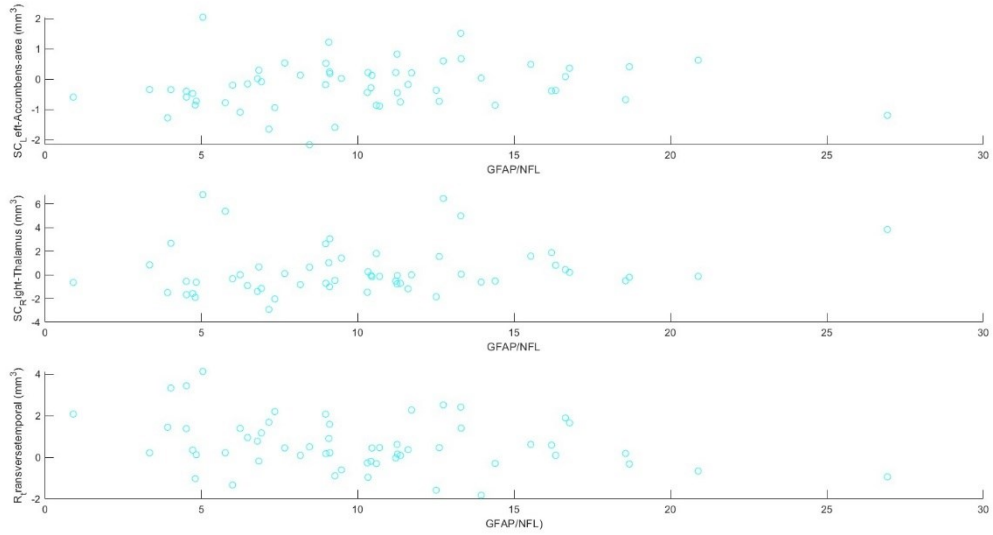

Figure 36: Scatterplots showing the GFAP/NFL-volume relationship for the three brain volumes for which the p-value is lower than the significance level of the tests conducted. The GFAP/NFL - SC_Left-Accumbens-area relationship scatterplot for each patient is at the top. The GFAP/NFL - SC_Right-Thalamus relationship scatterplot for each patient is in the middle. The GFAP/NFL - R_transversetemporal relationship scatterplot for each patient is at the bottom.

Also in this case, applying the Holm-Bonferroni method for multiple testing correction leads to no sub-threshold p-values.

Ultimately, I carried out a partial correlation analysis to evaluate whether the correction used to extract the volumes z-scores is adequate, or whether instead partial correlation could be a

relevantly better approach to exclude effects of age, gender and eTIV (figure 37). From figure 38 to figure 41 it's possible to see that the results obtained with partial correlation on absolute volumes are similar to those obtained with simple correlation on normalized volumes.

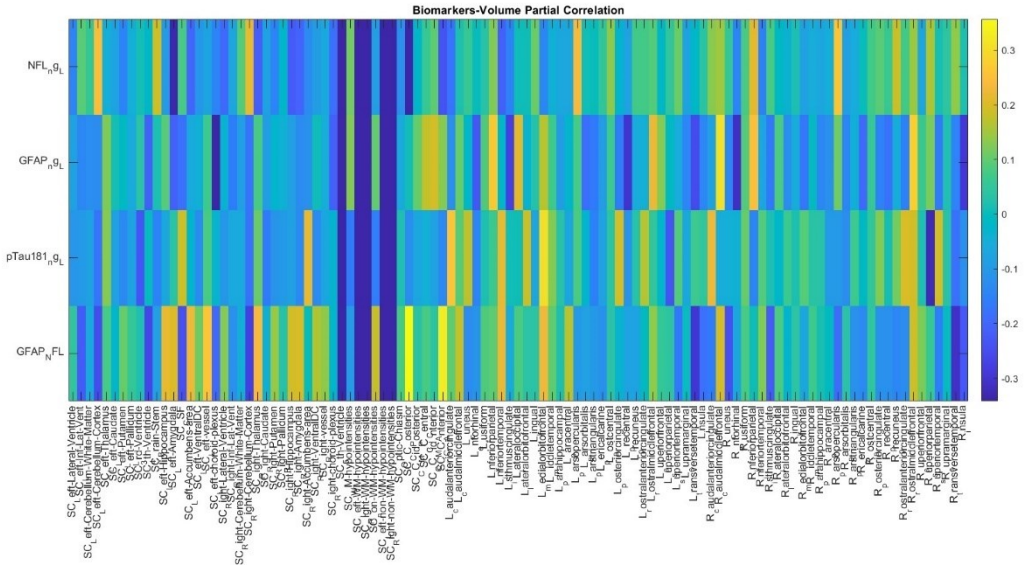

Figure 37: Spearman Partial Correlation Coefficients between biomarkers and volumes. The matrix in figure shows the values of the Sperman partial correlation coefficient between each volume on the x-axis and the biomarkers on the y-axis. The correlation coefficients can vary between -1 and 1. The lowest values tend towards blue, while, moving away from them there are shades tending towards green, orange and yellow (highest values found)

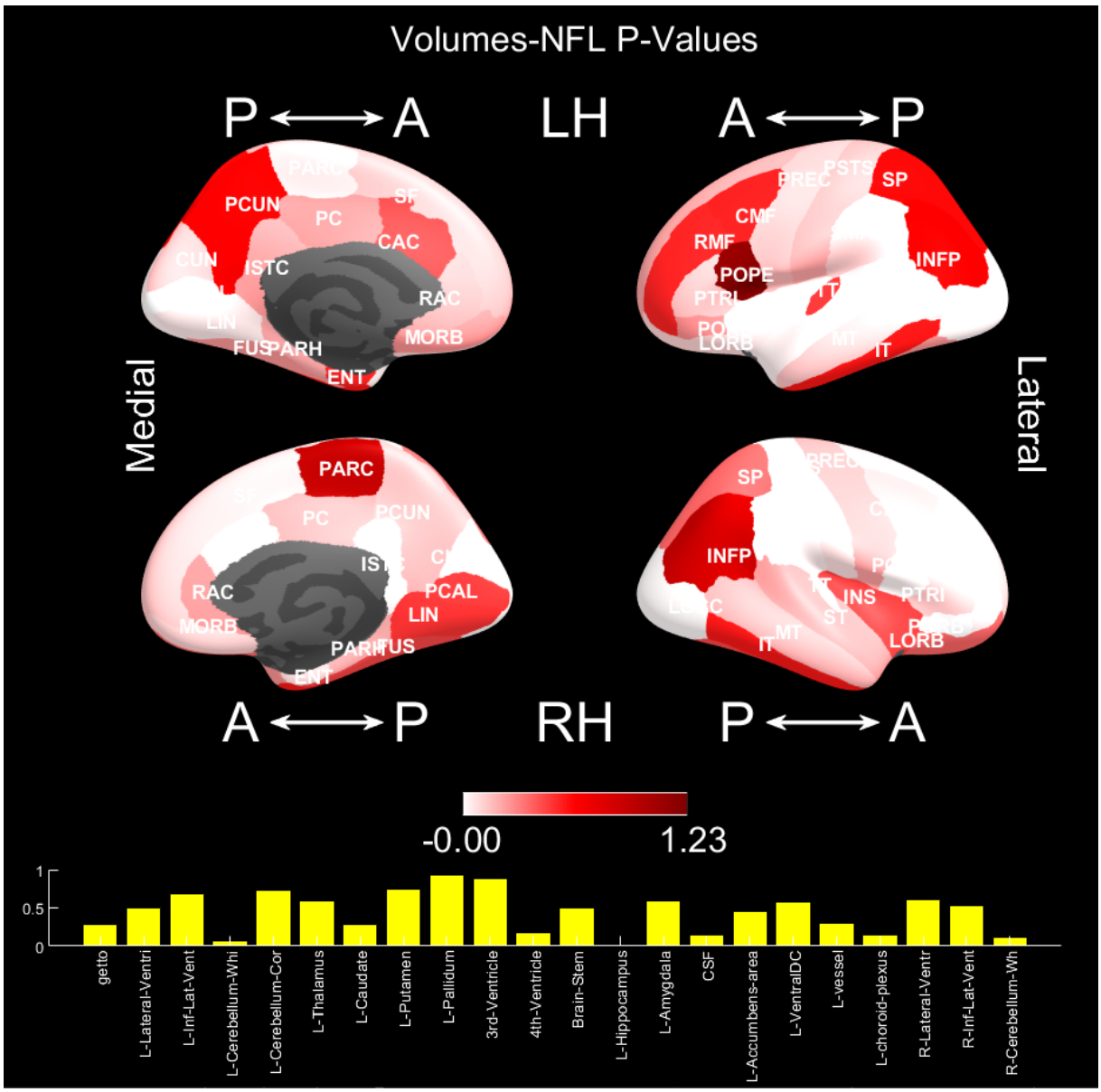

Figure 38: P-Values found between NFL and brain volumes through Spearman Partial Correlation. The acronyms that identify the various brain volumes have the following meanings: CAC: Caudal anterior cingulate, CMF: Caudal middle frontal, CUN: Cuneus, ENT: Entorhinal, FUS: Fusiform, INFP: Inferior parietal, INS: Insula, ISTC: Isthmus cingulate, IT: Inferior temporal, LIN: Lingual, LOCC: Lateral occipital, LORB: Lateral orbito-frontal, MORB: Medial orbito-frontal, MT: Middle temporal, PARC: Paracentral lobule, PARH: Parahippocampal, PC: Posterior cingulate, PCAL: Pericalcarine, PCUN: Precuneus, POPE: Pars opercularis, PORB: Pars orbitalis, PREC: Precentral, PSTS: Postcentral, PTRI: Pars triangularis, RAC: Rostral anterior cingulate, RMF: Rostral middle frontal, SF: Superior frontal, SMAR: Supramarginal, SP: Superior parietal, ST: Superior temporal, TT: Transverse temporal

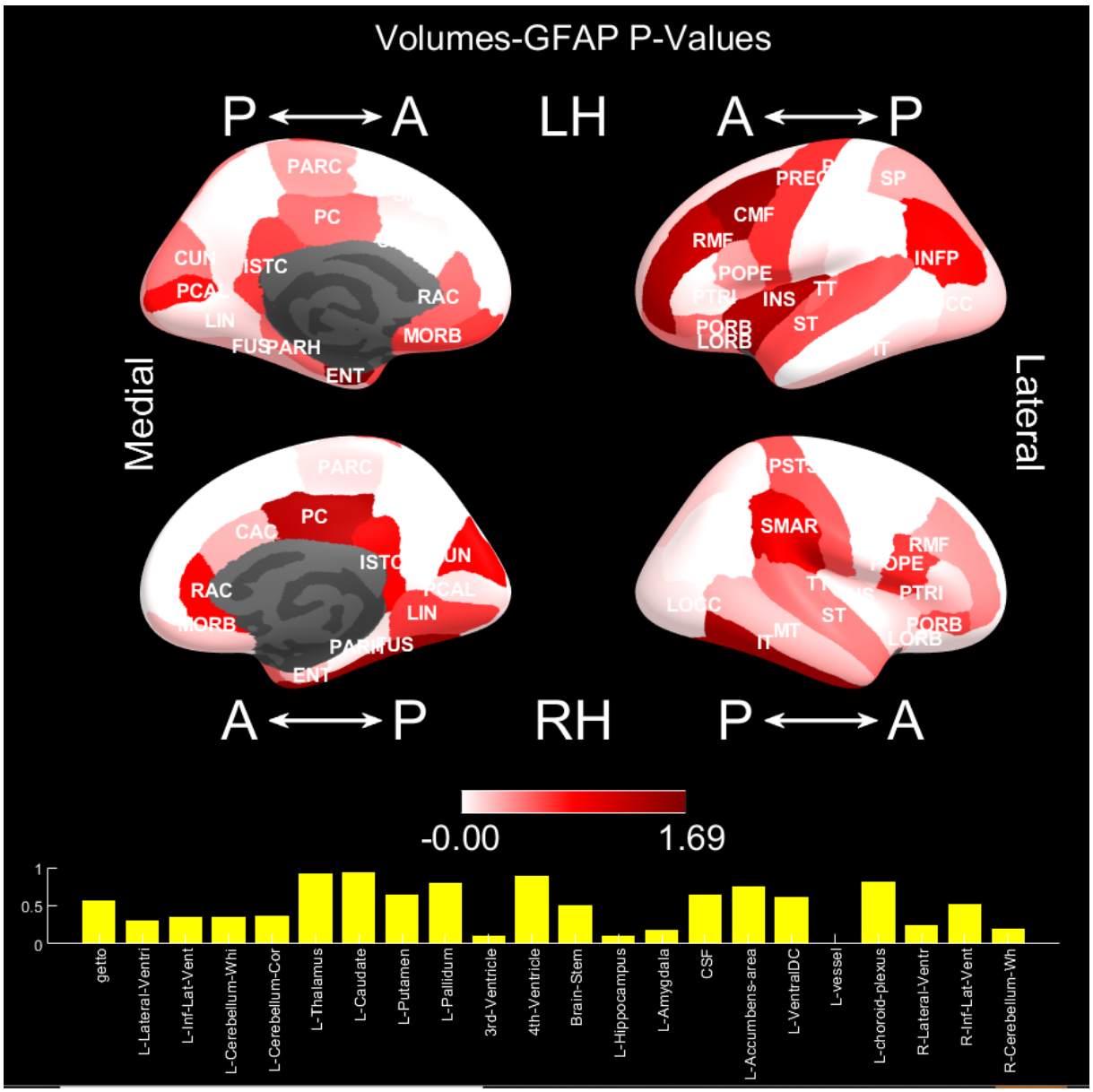

Figure 39: P-Values found between GFAP and brain volumes through Spearman Partial Correlation. The acronyms that identify the various brain volumes have the following meanings: CAC: Caudal anterior cingulate, CMF: Caudal middle frontal, CUN: Cuneus, ENT: Entorhinal, FUS: Fusiform, INFP: Inferior parietal, INS: Insula, ISTC: Isthmus cingulate, IT: Inferior temporal, LIN: Lingual, LOCC: Lateral occipital, LORB: Lateral orbito-frontal, MORB: Medial orbito-frontal, MT: Middle temporal, PARC: Paracentral lobule, PARH: Parahippocampal, PC: Posterior cingulate, PCAL: Pericalcarine, PCUN: Precuneus, POPE: Pars opercularis, PORB: Pars orbitalis, PREC: Precentral, PSTS: Postcentral, PTRI: Pars triangularis, RAC: Rostral anterior cingulate, RMF: Rostral middle frontal, SF: Superior frontal, SMAR: Supramarginal, SP: Superior parietal, ST: Superior temporal, TT: Transverse temporal

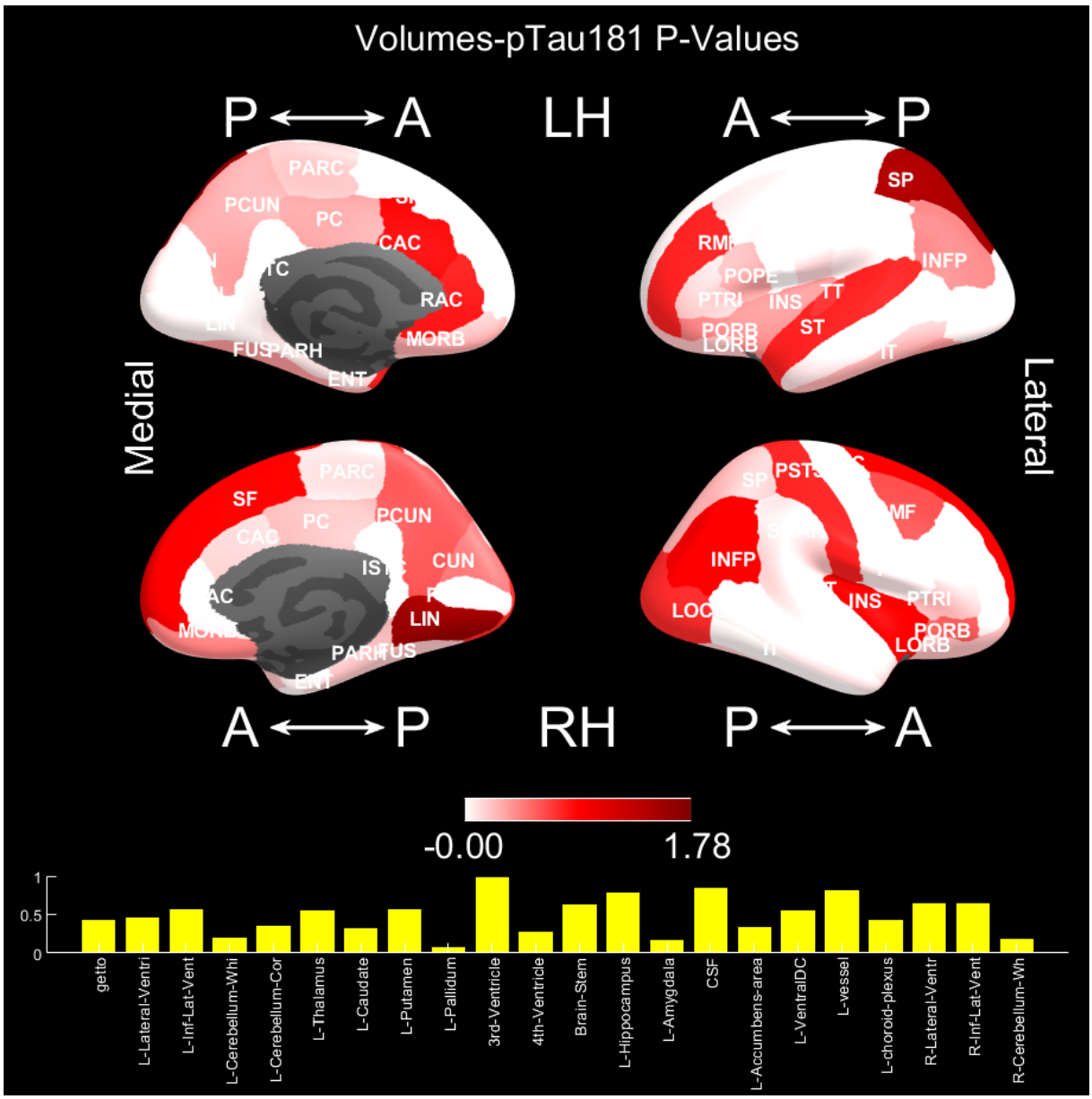

Figure 40: P-Values found between pTau181 and brain volumes through Spearman Partial Correlation. The acronyms that identify the various brain volumes have the following meanings: CAC: Caudal anterior cingulate, CMF: Caudal middle frontal, CUN: Cuneus, ENT: Entorhinal, FUS: Fusiform, INFP: Inferior parietal, INS: Insula, ISTC: Isthmus cingulate, IT: Inferior temporal, LIN: Lingual, LOCC: Lateral occipital, LORB: Lateral orbito-frontal, MORB: Medial orbito-frontal, MT: Middle temporal, PARC: Paracentral lobule, PARH: Parahippocampal, PC: Posterior cingulate, PCAL: Pericalcarine, PCUN: Precuneus, POPE: Pars opercularis, PORB: Pars orbitalis, PREC: Precentral, PSTS: Postcentral, PTRI: Pars triangularis, RAC: Rostral anterior cingulate, RMF: Rostral middle frontal, SF: Superior frontal, SMAR: Supramarginal, SP: Superior parietal, ST: Superior temporal, TT: Transverse temporal

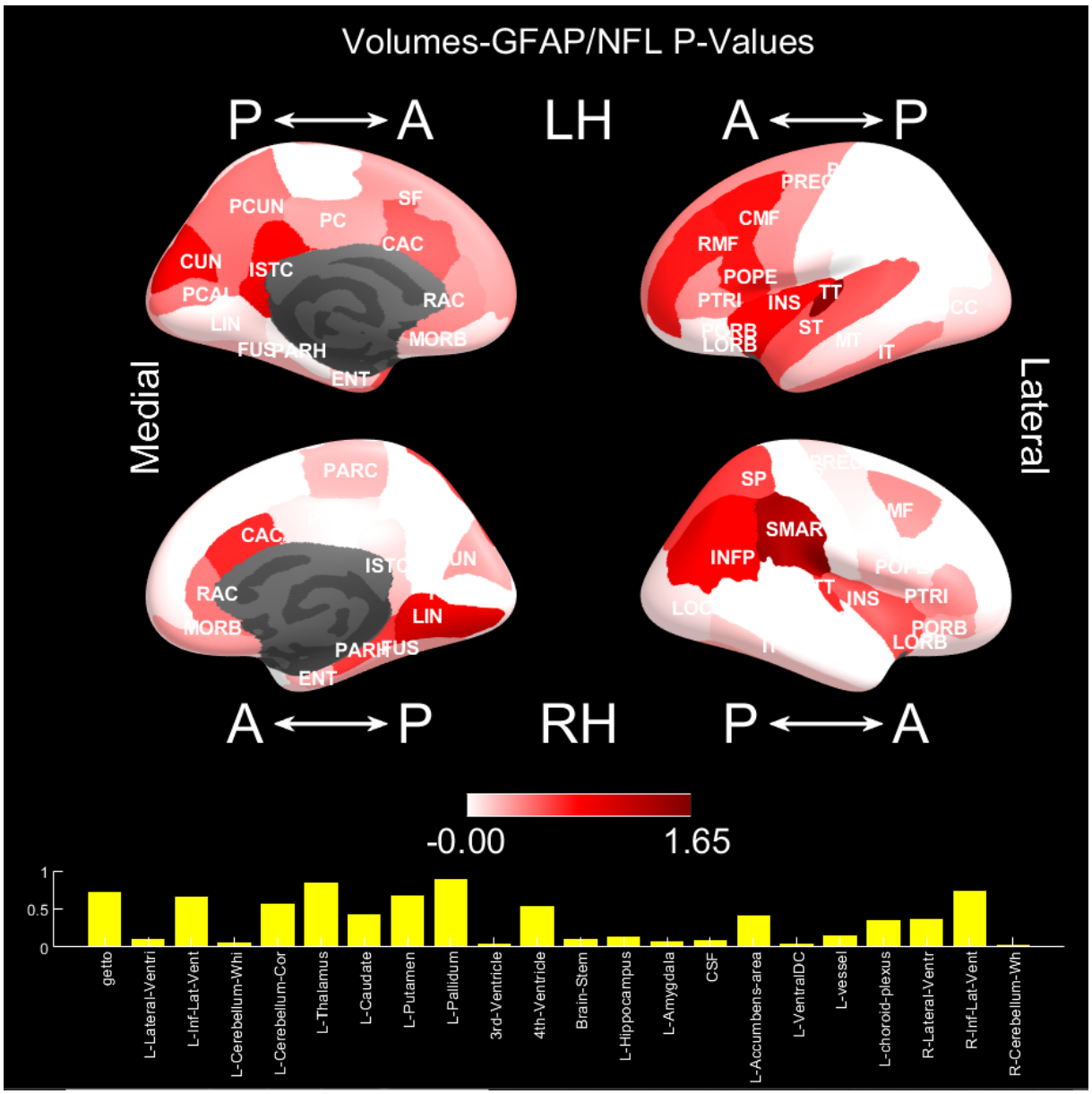

Figure 41: P-Values found between GFAP/NFL and brain volumes through Spearman Partial Correlation. The acronyms that identify the various brain volumes have the following meanings: CAC: Caudal anterior cingulate, CMF: Caudal middle frontal, CUN: Cuneus, ENT: Entorhinal, FUS: Fusiform, INFP: Inferior parietal, INS: Insula, ISTC: Isthmus cingulate, IT: Inferior temporal, LIN: Lingual, LOCC: Lateral occipital, LORB: Lateral orbito-frontal, MORB: Medial orbito-frontal, MT: Middle temporal, PARC: Paracentral lobule, PARH: Parahippocampal, PC: Posterior cingulate, PCAL: Pericalcarine, PCUN: Precuneus, POPE: Pars opercularis, PORB: Pars orbitalis, PREC: Precentral, PSTS: Postcentral, PTRI: Pars triangularis, RAC: Rostral anterior cingulate, RMF: Rostral middle frontal, SF: Superior frontal, SMAR: Supramarginal, SP: Superior parietal, ST: Superior temporal, TT: Transverse temporal

4.5 BLOOD BIOMARKERS, DEMOGRAPHICS AND COGNITIVE STATES

After having divided the dataset by sex and cognitive state, I carried out comparisons (T-tests) between the populations obtained to verify any differences in biomarkers values, due to belonging to a particular domain.

In the following tables it's possible to see the results of these tests for uncorrected p-values. Each table is associated with one of the four biomarkers studied. I used a different table color to distinguish each biomarker (blue for GFAP, green for pTau181, gray for NFL, yellow for GFAP/NFL). The tables show the mean and standard deviation values of the populations compared, while alongside I have reported the p-value obtained from the test.

In Figure 42, I have drawn up boxplots of the compared populations, having a p-value less than or equal to 0.05

As it's possible to see from the tables and boxplots in Figure 42, the p-values below the significance threshold are:

1) the p-value found for comparison between PD-NC men and women, related to their GFAP levels (Table 6). The comparison between the two groups can be found in the boxplot at the top left of Figure 42.
2) the p-value found for comparison between PD-MCI men and women, related to their pTau181 levels (Table 10). The comparison between the two groups can be found in the boxplot at the top right of Figure 42.
3) the p-value found for comparison between PD men and women, related to their NFL levels (Table 14). The comparison between the two groups can be found in the boxplot at the bottom left of Figure 42.
4) the p-value found for comparison between PD-MCI and PD-NC women, related to their GFAP/NFL levels (Table 21). The comparison between the two groups can be found in the boxplot at the bottom right of Figure 42.

By correcting the significance of the tests with the method discussed previously, bringing it back to the case of multiple tests, no p-value below the threshold was found.

	Male Mean	Male STD	Female Mean	Female STD	P-value
MCI	220,15	129,55	199,64	104,28	0,71
NC	176,00	71,77	307,60	243,66	0,02
TOT	191,22	94,61	266,47	205,70	0,06

Table 6: GFAP table divided by gender and cognitive state

	MCI Mean	MCI STD	NC Mean	NC STD	P-value
Male and Female Subjects	211,95	117,60	223,52	166,44	0,78

Table 7: GFAP table divided by cognitive state

	MCI Mean	MCI STD	NC Mean	NC STD	P-value
Male Subjects	220,15	129,55	176,00	71,77	0,20

Table 8: GFAP values for male subjects

	MCI Mean	MCI STD	NC Mean	NC STD	P-value
Female Subjects	199,64	104,28	307,60	243,66	0,25

Table 9: GFAP values for female subjects

	Male Mean	Male STD	Female Mean	Female STD	P-value
MCI	22,15	14,18	10,61	5,16	0,04
NC	17,90	7,35	20,85	16,44	0,47
TOT	19,28	10,15	16,95	14,05	0,48

Table 10: pTau181 table divided by gender and cognitive state

	MCI Mean	MCI STD	NC Mean	NC STD	P-value
Male and Female Subjects	17,54	12,64	18,99	11,44	0,66

Table 11: pTau181 table divided by cognitive state

	MCI Mean	MCI STD	NC Mean	NC STD	P-value
Male Subjects	22,15	14,18	17,90	7,35	0,25

Table 12: pTau181values for male subjects

	MCI Mean	MCI STD	NC Mean	NC STD	P-value
Female Subjects	10,61	5,16	20,85	16,44	0,11

Table 13: pTau181values for female subjects

	Male Mean	Male STD	Female Mean	Female STD	P-value
MCI	25,65	14,62	43,28	42,34	0,20
NC	19,90	12,41	27,08	17,67	0,16
TOT	21,79	13,10	33,25	29,66	0,05

Table 14: NFL table divided by gender and cognitive state

	MCI Mean	MCI STD	NC Mean	NC STD	P-value
Male and Female Subjects	32,70	29,37	22,49	14,70	0,09

Table 15: NFL table divided by cognitive state

	MCI Mean	MCI STD	NC Mean	NC STD	P-value
Male Subjects	25,65	14,62	19,90	12,41	0,23

Table 16: NFL values for male subjects

	MCI Mean	MCI STD	NC Mean	NC STD	P-value
Female Subjects	43,28	42,34	27,08	17,67	0,23

Table 17: NFL values for female subjects

	Male Mean	Male STD	Female Mean	Female STD	P-value
MCI	9,90	4,63	7,33	3,74	0,21
NC	10,63	5,53	11,32	4,41	0,70
TOT	10,79	5,11	9,80	4,53	0,67

Table 18: GFAP/NFL table divided by gender and cognitive state

	MCI Mean	MCI STD	NC Mean	NC STD	P-value
Male and Female Subjects	8,88	4,39	10,88	5,10	0,15

Table 19: GFAP/NFL table divided by cognitive state

	MCI Mean	MCI STD	NC Mean	NC STD	P-value
Male Subjects	9,90	4,63	10,63	5,53	0,70

Table 20: GFAP/NFL values for male subjects

	MCI Mean	MCI STD	NC Mean	NC STD	P-value
Female Subjects	7,33	3,74	11,32	4,41	0,05

Table 21: GFAP/NFL values for female subjects

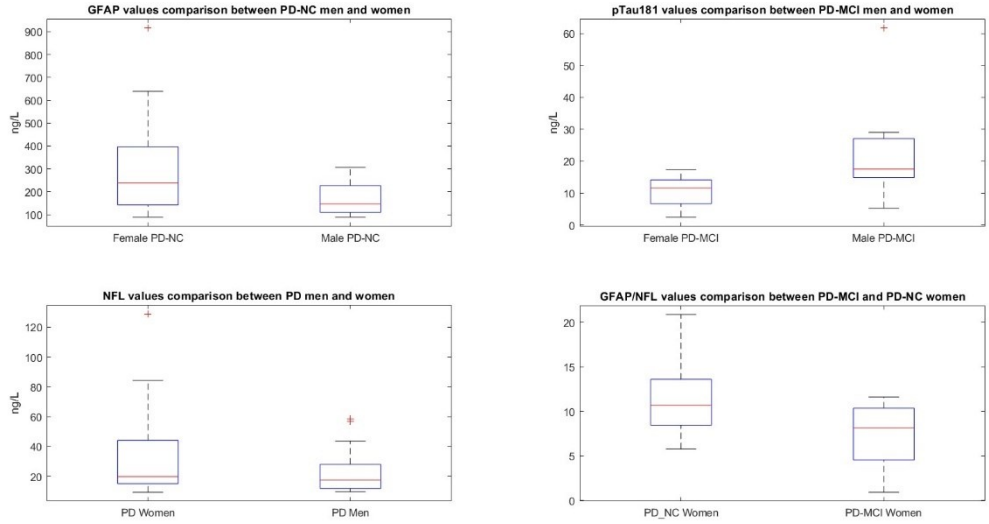

Figure 42: Population comparisons boxplots with significant p-values. The figure shows the boxplots of the populations compared in the previous tables, with p-values lower than or equal to the threshold value. On each box, the central mark indicates the median, and the bottom and top edges of the box indicate the 25th and 75th percentiles, respectively. The whiskers extend to the most extreme data points not considered outliers, and the outliers are plotted individually using the '+' marker symbol.

Finally, I calculated the Spearman correlation coefficient between the serological data and two cognitive scales: the MOCA (Montreal Cognitive Assessment) and the MMSE (Mini-Mental State Examination). Also in this case, it was not possible to calculate the Pearson coefficient because the MOCA and MMSE values do not follow a normal distribution, so I performed a non-parametric test.

The results of this correlation analysis between biomarkers and cognitive tests are presented in table 22. In the same table it's possible to see, under every correlation coefficient, the corresponding p-value in brackets.

	NFL (ng/L)	**GFAP (ng/L)**	**pTau181 (ng/L)**	**GFAP/NFL**
MOCA	-0,008 (0,95)	0,052 (0,05)	-0,001 (1,00)	0,153 (0,26)
MMSE	-0,048 (0,77)	0,041 (0,80)	0,014 (0,93)	0,139 (0,39)

Table 22: Spearman correlation coefficients between cognitive scales and biomarkers. Under each coefficient the corresponding p-value is reported in brackets

Also in this case, the significance level of the test was set at 5%, but no significant correlation was found with this threshold level.

Chapter 5

DISCUSSIONS

In this work I used voxel-based and surface-based morphometry algorithms to estimate the volume of subcortical and cortical structures in the brains of 57 PD patients from T1-weighted and T2-weighted FLAIR magnetic resonance images. These measures were related to blood biomarkers to evaluate possible correlations between structural changes and levels of NFL, GFAP or pTau181. Differences between the presence and absence of cognitive impairment were also tested. An entirely voxel-based algorithm for brain morphometry analysis, based on SPM CAT12, was used to perform a comparison between the two techniques.

The dataset numerosity is biased towards males and normal cognition, which is consistent with the distribution of Parkinson's disease which shows a higher prevalence in the male population (88).

From the results of the morphometry and, in particular, from the comparison of normalized volumes vs. zero, it emerges that the parts of the brain most affected by the disease are: the cingulate cortex, the paracentral lobule, the entorhinal cortex, the fusiform cortex, the parahippocampal gyrus, Broca's area and the temporal cortex. Thus, the most affected areas perfectly coincide with those indicated in the literature (89–93). Moreover, the morphological alterations found are in line with the regions of altered connectivity (94).

In our analysis we found differences with p-values below the significance level of 0.05 in the rostral anterior cingulate, supramarginal and transversetemporal cortexes. The p-values do not survive corrections for multiple comparisons, which might be ascribed to a low sample size, nonetheless, the involvement of the volumetric contraction of the cingulate cortex in cognitive decline is confirmed in literature, as well of that of parietal structures highlighted in Figure 17 (95). The involvement of the parahippocampal cortex in our case is not significant but is relatively close to the threhsold.

Regarding the correlation analysis between volumes and biomarkers, the significant values found in single tests were not confirmed through correction methods for multiple tests, despite falling short by very small fractions. Interesting differences were found in biomarker values during comparisons between the MCI and NC groups, divided by gender. As regards the pTau181 values, in particular, from the comparison between PD-MCI male and female subjects,

a significant difference on uncorrected p-values emerges in the median values, which are higher in favor of men. If we consider the values of the GFAP/NFL ratio, instead, a significant difference (again on uncorrected p-values) can be found between PD-MCI and PD-NC females subjects, also in this case confirmed by diversity of medians with higher values for PD-MCI.

Again, from the analysis of the relations between blood biomarkers and brain morphometry, more widespread differences across brain regions emerged when considering volumes normalized using normative values rather than analysing non-normalized volumes. This clearly speaks in favour of the need to correct for gender, age and eTIV differences when performing morphometry analysis. This correction was also attempted using partial correlation, i.e., trying to estimate covariates effects from our data. Interestingly, the results obtained using partial correlation showed no relevant difference with respect to those obtained on non-normalized data. Consequently, normalization was more effective than partial correlation in cleaning the results from the effect of irrelevant covariates for the purpose of pursuing a link between morphometric parameters and biomarkers.

Regarding the differences between FreeSurfer and BAAD, the correlations with MOCA scores suggest that the former provides a better parcellation of the cortical area, while the latter seems to obtain a more accurate segmentation of the subcortical area. The differences of the results that the two software obtain in the subcortex (Figure19) and, in particular, the absence of correlation for the ventricles and the brainstem, could depend on the fact that they use two different algorithms to perform the skullstrip. Indeed, the masks used to perform the skullstrip in the FreeSurfer pipeline are constructed to cut the medulla and ventricles at a consistent level across subjects, while no control is performed for the SPM pipeline. So, the lack of correlation visible in Figure 19 could be due to the fact that each of the two algorithms cuts more or less a certain portion of these parts. From the deviations shown in figure 20, instead, it emerges that probably one or both the algorithms tend to underestimate and/or overestimate some of the brain volumes. The deviation of the null value of the quantity considered (the difference between the median of the ratio between volumes calculated with BAAD and FreeSurfer and one), in fact, implies that, for each volume, either one of the two sofware underestimates its value, or one of the two software overestimates its value, or that when one underestimates its value the other overestimates it and vice versa. Further comparisons with normative values computed with SPM and with gold-standard manual segmentation are needed to assess the ground truth.

5.1 LIMITATIONS

Notably, we observed close-to-significant differences for the values of biomarkers in women and men. To my knowledge, no gender-based standardization exists in literature for blood biomarkers.

Among the limitations of the study, we report again the unbalanced dataset towards NC male subjects. This deficiency not only does not allow for homogeneous comparisons regarding the differences between those with and without a cognitive deficit, but it also does not allow us to fully understand whether there are relevant differences in the evolution of Parkinson's disease between the male population and the female one.

In addition, I observed a significant difference in terms of age between MCI males and NC males, which might have an impact on the results since age is a known factor affecting brain atrophy.

More generally, the sample size at my disposal is not very large, therefore the statistics found could undergo significant variations if a higher number of subjects were available to study. Other limitations could be individuated in the cortical parcellation used, the Desikan-Killiany, composed of relatively few regions of interest (ROI), and in not having investigated the possible existence of non-linear correlations between biomarkers and volumes, for example using maximal information coefficient.

5.2 FUTURE DIRECTIONS

We can try to imagine useful improvements for this line of research. Given the observed gender bias in the distributions of blood biomarkers, further acquisitions of blood biomarkers in healthy subjects should be oriented towards finding a relation with demographics, in order to allow researchers to extract gender- and age-independent z-scores.

As possible developments of future studies it might be considered the FreeSurfer's feature of segmenting white matter lesions (96). In this way, it could be assessed if there is a possible correlation between the lesions and the biomarkers. We also note that distributions of blood biomarkers were observed in this work to be non-gaussian, but the use of logarithmic transforms could be useful in normalizing these data and therefore in increasing the power of our statistics.

According to Hugo C. Baggio and Carme Junqué functional magnetic resonance imaging (fMRI) has been used for several years to study alterations of cognitive patterns in PD subjects (97). In particular, these studies have shown that different types of cognitive deficits linked to

Parkinson's disease are associated with an alteration of brain connectivity, analyzed during the resting state (97). Despite movement and space artifacts, the fMRI could provide a more complete picture of dementia and mild cognitive impairment aetiology, allowing us to investigate more thoroughly the association between the neurophysiological alterations caused by Parkinson's and the onset of cognitive deficits.

Last but not least, diffusion MRI could also play a key role for future studies. Because of its ability to detect changes in the microstructure of the brain damage (98), studying diffusive images could be a valid support on two fronts. First, it would certainly help to complete and detail the morphometric analysis, enriching it with details on the variations in the structure of the brain and thus increasing knowledge of the way in which the disease develops. Secondly, microstructural variations could be related to biomarkers and/or cognitive states in order to investigate possible links.

Chapter 6

CONCLUSIONS

In conclusion, this thesis aimed at evaluating the relation between brain morphometry and blood biomarkers in a cohort of Parkinson's disease patients stratified by presence of cognitive impairment. Surface based morphometry revealed alterations in PD with respect to normative data in line with literature, on cingulate, insular and temporal cortexes. The limited sample size did not allow to fully confirm the relations between atrophy and cognitive impairment, but it was still possible to provide a first glimpse of the associations between Neurofilaments, GFAP and pTau181 and patterns of brain atrophy in PD. This line of research could reveal new insights in the specificity of these biomarkers, if further studies will be able to define on larger cohorts the patterns linked to each biomarker, paving new paths in the search for non-invasive, cheap and reliable detectors of neurodegeneration.

BIBLIOGRAPHY

1. Filler A, Filler A. The History, Development and Impact of Computed Imaging in Neurological Diagnosis and Neurosurgery: CT, MRI, and DTI. Nature Precedings [Internet]. 13 luglio 2009 [citato 15 aprile 2024]; Disponibile su: https://precedings.nature.com/doifinder/10.1038/npre.2009.3267

2. Middei S. Neuroimaging Applications for Diagnosis and Therapy of Pathologies in the Central and Peripheral Nervous System. Brain Sciences. 1 febbraio 2022;12(2):207.

3. Aderinto N, Olatunji D, Abdulbasit M, Edun M. The essential role of neuroimaging in diagnosing and managing cerebrovascular disease in Africa: a review. Annals of Medicine. 12 dicembre 2023;55(2):2251490.

4. Yen C, Lin CL, Chiang MC. Exploring the Frontiers of Neuroimaging: A Review of Recent Advances in Understanding Brain Functioning and Disorders. Life. 29 giugno 2023;13(7):1472.

5. O'Donnell LJ, Westin CF. An Introduction to Diffusion Tensor Image Analysis. Neurosurgery Clinics of North America. aprile 2011;22(2):185–96.

6. Henderson TA, Van Lierop MJ, McLean M, Uszler JM, Thornton JF, Siow YH, et al. Functional Neuroimaging in Psychiatry—Aiding in Diagnosis and Guiding Treatment. What the American Psychiatric Association Does Not Know. Front Psychiatry. 15 aprile 2020;11:276.

7. Abellaneda-Pérez K, Miquel L, Lusilla-Palacios P, Gual A. Estimulación cerebral no invasiva combinada con neuroimagen: Hacia una medicina de precisión en el tratamiento de las adicciones. Adicciones. 1 gennaio 2023;35(1):3.

8. Bloomfield PS, Brigadoi S, Rizzo G, Veronese M, curatori. Basic neuroimaging: a guide to the methods and their applications. First edition. Erscheinungsort nicht ermittelbar: Verlag nicht ermittelbar; 2017. 305 p.

9. Currie S, Hoggard N, Craven IJ, Hadjivassiliou M, Wilkinson ID. Understanding MRI: basic MR physics for physicians. Postgraduate Medical Journal. 1 aprile 2013;89(1050):209–23.

10. Tariq H, Burney A. Brain MRI literature review for interdisciplinary studies. JBGC. 11 novembre 2014;4(4):p41.

11. Gerber AJ, Peterson BS, Giedd JN, Lalonde FM, Celano MJ, White SL, et al. Anatomical Brain Magnetic Resonance Imaging of Typically Developing Children and Adolescents. Journal of the American Academy of Child & Adolescent Psychiatry. maggio 2009;48(5):465–70.

12. Tofts P. Quantitative MRI of the brain: measuring changes caused by disease. Chichester: John Wiley; 2003.

13. Pan JW, Moon CH, Hetherington HP. Cerebrospinal fluid–suppressed T $_2$ -weighted MR imaging at 7 T for human brain. Magnetic Resonance in Med. maggio 2019;81(5):2924–36.

14. Chavhan GB, Babyn PS, Thomas B, Shroff MM, Haacke EM. Principles, Techniques, and Applications of T2*-based MR Imaging and Its Special Applications. RadioGraphics. settembre 2009;29(5):1433–49.

15. Tillema JM, Pirko I. Neuroradiological evaluation of demyelinating disease. Ther Adv Neurol Disord. luglio 2013;6(4):249–68.

16. Saranathan M, Worters PW, Rettmann DW, Winegar B, Becker J. Physics for clinicians: Fluid-attenuated inversion recovery (FLAIR) and double inversion recovery (DIR) Imaging. Magnetic Resonance Imaging. dicembre 2017;46(6):1590–600.

17. Soares JM, Magalhães R, Moreira PS, Sousa A, Ganz E, Sampaio A, et al. A Hitchhiker's Guide to Functional Magnetic Resonance Imaging. Front Neurosci [Internet]. 10 novembre 2016 [citato 1 ottobre 2024];10. Disponibile su: http://journal.frontiersin.org/article/10.3389/fnins.2016.00515/full

18. Whitten L. Functional Magnetic Resonance Imaging (fMRI): An Invaluable Tool in Translational Neuroscience [Internet]. Research Triangle Park, NC: RTI Press; 2012 dic [citato 1 ottobre 2024]. Disponibile su: http://www.rti.org/publication/functional-magnetic-resonance-imaging-fmri-invaluable-tool-translational-neuroscience

19. Huisman TAGM. Diffusion-weighted and diffusion tensor imaging of the brain, made easy. Cancer Imaging. 2010;10(1A):S163–71.

20. Lerma-Usabiaga G, Liu M, Paz-Alonso PM, Wandell BA. Reproducible Tract Profiles 2 (RTP2) suite, from diffusion MRI acquisition to clinical practice and research. Sci Rep. 12 aprile 2023;13(1):6010.

21. Friston KJ, curatore. Statistical parametric mapping: the analysis of funtional brain images. 1st ed. Amsterdam ; Boston: Elsevier/Academic Press; 2007. 647 p.

22. Good CD, Johnsrude IS, Ashburner J, Henson RNA, Friston KJ, Frackowiak RSJ. A Voxel-Based Morphometric Study of Ageing in 465 Normal Adult Human Brains. NeuroImage. luglio 2001;14(1):21–36.

23. Gonzalez RC, Woods RE. Digital image processing. 3. ed. Upper Saddle River, NJ: Pearson/Prentice Hall; 2007. 954 p.

24. Goto M, Abe O, Hagiwara A, Fujita S, Kamagata K, Hori M, et al. Advantages of Using Both Voxel- and Surface-based Morphometry in Cortical Morphology Analysis: A Review of Various Applications. MRMS. 2022;21(1):41–57.

25. Tucholka A, Fritsch V, Poline JB, Thirion B. An empirical comparison of surface-based and volume-based group studies in neuroimaging. NeuroImage. novembre 2012;63(3):1443–53.

26. Parkinson J. An Essay on the Shaking Palsy. JNP. maggio 2002;14(2):223–36.

27. Sheng L, Zhao P, Ma H, Radua J, Yi Z, Shi Y, et al. Cortical thickness in Parkinson's disease: a coordinate-based meta-analysis. Aging. 15 febbraio 2021;13(3):4007–23.

28. Marras C, Chaudhuri KR. Nonmotor features of Parkinson's disease subtypes. Movement Disorders. agosto 2016;31(8):1095–102.

29. Moustafa AA, Chakravarthy S, Phillips JR, Gupta A, Keri S, Polner B, et al. Motor symptoms in Parkinson's disease: A unified framework. Neuroscience & Biobehavioral Reviews. settembre 2016;68:727–40.

30. Tibar H, El Bayad K, Bouhouche A, Ait Ben Haddou EH, Benomar A, Yahyaoui M, et al. Non-Motor Symptoms of Parkinson's Disease and Their Impact on Quality of Life in a Cohort of Moroccan Patients. Front Neurol. 4 aprile 2018;9:170.

31. DeMaagd G, Philip A. Parkinson's Disease and Its Management: Part 1: Disease Entity, Risk Factors, Pathophysiology, Clinical Presentation, and Diagnosis. P T. agosto 2015;40(8):504–32.

32. Fengler S, Liepelt-Scarfone I, Brockmann K, Schäffer E, Berg D, Kalbe E. Cognitive changes in prodromal Parkinson's disease: A review. Movement Disorders. dicembre 2017;32(12):1655–66.

33. Kehagia AA, Barker RA, Robbins TW. Neuropsychological and clinical heterogeneity of cognitive impairment and dementia in patients with Parkinson's disease. The Lancet Neurology. dicembre 2010;9(12):1200–13.

34. Goldman JG, Litvan I. Mild cognitive impairment in Parkinson's disease. Minerva Med. dicembre 2011;102(6):441–59.

35. Aarsland D, Batzu L, Halliday GM, Geurtsen GJ, Ballard C, Ray Chaudhuri K, et al. Parkinson disease-associated cognitive impairment. Nat Rev Dis Primers. 1 luglio 2021;7(1):47.

36. Degirmenci Y, Angelopoulou E, Georgakopoulou VE, Bougea A. Cognitive Impairment in Parkinson's Disease: An Updated Overview Focusing on Emerging Pharmaceutical Treatment Approaches. Medicina. 1 ottobre 2023;59(10):1756.

37. Pedersen KF, Larsen JP, Tysnes OB, Alves G. Natural course of mild cognitive impairment in Parkinson disease: A 5-year population-based study. Neurology. 21 febbraio 2017;88(8):767–74.

38. Brooks DJ. Morphological and functional imaging studies on the diagnosis and progression of Parkinson's disease. J Neurol. 10 aprile 2000;247(S2):II11–8.

39. Jokinen P, Brück A, Aalto S, Forsback S, Parkkola R, Rinne JO. Impaired cognitive performance in Parkinson's disease is related to caudate dopaminergic hypofunction and hippocampal atrophy. Parkinsonism & Related Disorders. febbraio 2009;15(2):88–93.

40. Meijer FJA. Brain MRI in Parkinson s disease. Front Biosci. 2014;6(2):360–9.

41. Burton EJ. Cerebral atrophy in Parkinson's disease with and without dementia: a comparison with Alzheimer's disease, dementia with Lewy bodies and controls. Brain. 14 gennaio 2004;127(4):791–800.

42. Pletcher C, Dabbs K, Barzgari A, Pozorski V, Haebig M, Wey S, et al. Cerebral cortical thickness and cognitive decline in Parkinson's disease. Cerebral Cortex Communications. 6 gennaio 2023;4(1):tgac044.

43. Summerfield C, Junqué C, Tolosa E, Salgado-Pineda P, Gómez-Ansón B, Martí MJ, et al. Structural Brain Changes in Parkinson Disease With Dementia: A Voxel-Based Morphometry Study. Arch Neurol. 1 febbraio 2005;62(2):281.

44. Postuma RB, Berg D, Stern M, Poewe W, Olanow CW, Oertel W, et al. MDS clinical diagnostic criteria for Parkinson's disease: MDS-PD Clinical Diagnostic Criteria. Mov Disord. ottobre 2015;30(12):1591–601.

45. Goetz CG, Tilley BC, Shaftman SR, Stebbins GT, Fahn S, Martinez-Martin P, et al. Movement Disorder Society-sponsored revision of the Unified Parkinson's Disease Rating Scale (MDS-UPDRS): Scale presentation and clinimetric testing results. Movement Disorders. 15 novembre 2008;23(15):2129–70.

46. Ravina B, Marek K, Eberly S, Oakes D, Kurlan R, Ascherio A, et al. Dopamine transporter imaging is associated with long-term outcomes in Parkinson's disease. Movement Disorders. 15 settembre 2012;27(11):1392–7.

47. Li T, Le W. Biomarkers for Parkinson's Disease: How Good Are They? Neurosci Bull. febbraio 2020;36(2):183–94.

48. Li D, Mielke MM. An Update on Blood-Based Markers of Alzheimer's Disease Using the SiMoA Platform. Neurol Ther. dicembre 2019;8(S2):73–82.

49. Yamashita KY, Bhoopatiraju S, Silverglate BD, Grossberg GT. Biomarkers in Parkinson's disease: A state of the art review. Biomarkers in Neuropsychiatry. dicembre 2023;9:100074.

50. Youssef P, Hughes L, Kim WS, Halliday GM, Lewis SJG, Cooper A, et al. Evaluation of plasma levels of NFL, GFAP, UCHL1 and tau as Parkinson's disease biomarkers using multiplexed single molecule counting. Sci Rep. 30 marzo 2023;13(1):5217.

51. Khalil M, Teunissen CE, Otto M, Piehl F, Sormani MP, Gattringer T, et al. Neurofilaments as biomarkers in neurological disorders. Nat Rev Neurol. ottobre 2018;14(10):577–89.

52. Tönges L, Buhmann C, Klebe S, Klucken J, Kwon EH, Müller T, et al. Blood-based biomarker in Parkinson's disease: potential for future applications in clinical research and practice. J Neural Transm. settembre 2022;129(9):1201–17.

53. Marques TM, Van Rumund A, Oeckl P, Kuiperij HB, Esselink RAJ, Bloem BR, et al. Serum NFL discriminates Parkinson disease from atypical parkinsonisms. Neurology [Internet]. 26 marzo 2019 [citato 18 novembre 2024];92(13). Disponibile su: https://www.neurology.org/doi/10.1212/WNL.0000000000007179

54. Pilotto A, Imarisio A, Conforti F, Scalvini A, Masciocchi S, Nocivelli S, et al. Plasma NfL, clinical subtypes and motor progression in Parkinson's disease. Parkinsonism & Related Disorders. giugno 2021;87:41–7.

55. Yang Z, Wang KKW. Glial fibrillary acidic protein: from intermediate filament assembly and gliosis to neurobiomarker. Trends in Neurosciences. giugno 2015;38(6):364–74.

56. Pereira JB, Janelidze S, Smith R, Mattsson-Carlgren N, Palmqvist S, Teunissen CE, et al. Plasma GFAP is an early marker of amyloid-β but not tau pathology in Alzheimer's disease. Brain. 16 dicembre 2021;144(11):3505–16.

57. Lin J, Ou R, Li C, Hou Y, Zhang L, Wei Q, et al. Plasma glial fibrillary acidic protein as a biomarker of disease progression in Parkinson's disease: a prospective cohort study. BMC Med. 6 novembre 2023;21(1):420.

58. Che N, Ou R, Li C, Zhang L, Wei Q, Wang S, et al. Plasma GFAP as a prognostic biomarker of motor subtype in early Parkinson's disease. npj Parkinsons Dis. 1 marzo 2024;10(1):48.

59. Lantero Rodriguez J, Karikari TK, Suárez-Calvet M, Troakes C, King A, Emersic A, et al. Plasma p-tau181 accurately predicts Alzheimer's disease pathology at least 8 years prior to post-mortem and improves the clinical characterisation of cognitive decline. Acta Neuropathol. settembre 2020;140(3):267–78.

60. Pagonabarraga J, Pérez-González R, Bejr-kasem H, Marín-Lahoz J, Horta-Barba A, Martinez-Horta S, et al. Dissociable contribution of plasma NfL and p-tau181 to cognitive impairment in Parkinson's disease. Parkinsonism & Related Disorders. dicembre 2022;105:132–8.

61. Smith C, Malek N, Grosset K, Cullen B, Gentleman S, Grosset DG. Neuropathology of dementia in patients with Parkinson's disease: a systematic review of autopsy studies. J Neurol Neurosurg Psychiatry. 23 agosto 2019;jnnp-2019-321111.

62. Fiorenzato E, Antonini A, Camparini V, Weis L, Semenza C, Biundo R. Characteristics and progression of cognitive deficits in progressive supranuclear palsy vs. multiple system atrophy and Parkinson's disease. J Neural Transm. novembre 2019;126(11):1437–45.

63. Litvan I, Goldman JG, Tröster AI, Schmand BA, Weintraub D, Petersen RC, et al. Diagnostic criteria for mild cognitive impairment in Parkinson's disease: *Movement* Disorder Society Task Force guidelines. Movement Disorders. marzo 2012;27(3):349–56.

64. Dubois B, Burn D, Goetz C, Aarsland D, Brown RG, Broe GA, et al. Diagnostic procedures for Parkinson's disease dementia: Recommendations from the movement disorder society task force. Movement Disorders. 15 dicembre 2007;22(16):2314–24.

65. Nasreddine ZS, Phillips NA, Bédirian V, Charbonneau S, Whitehead V, Collin I, et al. The Montreal Cognitive Assessment, MoCA: A Brief Screening Tool For Mild Cognitive Impairment. J American Geriatrics Society. aprile 2005;53(4):695–9.

66. Santangelo G, Siciliano M, Pedone R, Vitale C, Falco F, Bisogno R, et al. Normative data for the Montreal Cognitive Assessment in an Italian population sample. Neurol Sci. aprile 2015;36(4):585–91.

67. Folstein MF, Folstein SE, McHugh PR. "Mini-mental state". Journal of Psychiatric Research. novembre 1975;12(3):189–98.

68. Magni E, Binetti G, Bianchetti A, Rozzini R, Trabucchi M. Mini-Mental State Examination: a normative study in Italian elderly population. Euro J of Neurology. maggio 1996;3(3):198–202.

69. Rissin DM, Kan CW, Campbell TG, Howes SC, Fournier DR, Song L, et al. Single-molecule enzyme-linked immunosorbent assay detects serum proteins at subfemtomolar concentrations. Nat Biotechnol. giugno 2010;28(6):595–9.

70. Dahnke R, Ziegler G, Grosskreutz J, Gaser C. Quality Assurance in Structural MRI. 2015 [citato 27 settembre 2024]; Disponibile su: http://rgdoi.net/10.13140/RG.2.2.16267.44321

71. Reuter M, Schmansky NJ, Rosas HD, Fischl B. Within-subject template estimation for unbiased longitudinal image analysis. NeuroImage. luglio 2012;61(4):1402–18.

72. Ishida M. Brain MRI as a Biomarker of Alzheimer's Disease: Prediction of the Pathology by Machine Learning. 13 ottobre 2021;

73. Shinohara RT, Sweeney EM, Goldsmith J, Shiee N, Mateen FJ, Calabresi PA, et al. Statistical normalization techniques for magnetic resonance imaging. NeuroImage: Clinical. 2014;6:9–19.

74. Oliveira FPM, Tavares JMRS. Medical image registration: a review. Computer Methods in Biomechanics and Biomedical Engineering. 25 gennaio 2014;17(2):73–93.

75. Kellner E, Dhital B, Kiselev VG, Reisert M. Gibbs-ringing artifact removal based on local subvoxel-shifts. Magnetic Resonance in Med. novembre 2016;76(5):1574–81.

76. Juntu J, Sijbers J, Dyck D, Gielen J. Bias Field Correction for MRI Images. In: Kurzyński M, Puchała E, Woźniak M, Żołnierek A, curatori. Computer Recognition Systems [Internet]. Berlin, Heidelberg: Springer Berlin Heidelberg; 2005 [citato 12 agosto 2024]. p. 543–51. (Advances in Soft Computing; vol. 30). Disponibile su: http://link.springer.com/10.1007/3-540-32390-2_64

77. Dovrou A, Nikiforaki K, Zaridis D, Manikis GC, Mylona E, Tachos N, et al. A segmentation-based method improving the performance of N4 bias field correction on T2weighted MR imaging data of the prostate. Magnetic Resonance Imaging. settembre 2023;101:1–12.

78. Hoopes A, Mora JS, Dalca AV, Fischl B, Hoffmann M. SynthStrip: skull-stripping for any brain image. NeuroImage. ottobre 2022;260:119474.

79. Lutkenhoff ES, Rosenberg M, Chiang J, Zhang K, Pickard JD, Owen AM, et al. Optimized Brain Extraction for Pathological Brains (optiBET). Wu X, curatore. PLoS ONE. 16 dicembre 2014;9(12):e115551.

80. Ashburner J, Friston KJ. Unified segmentation. NeuroImage. luglio 2005;26(3):839–51.

81. Friston KarlJ, Ashburner J, Frith CD, Poline J -B., Heather JD, Frackowiak RSJ. Spatial registration and normalization of images. Human Brain Mapping. gennaio 1995;3(3):165–89.

82. Evans AC, Kamber M, Collins DL, MacDonald D. An MRI-Based Probabilistic Atlas of Neuroanatomy. In: Shorvon SD, Fish DR, Andermann F, Bydder GM, Stefan H, curatori. Magnetic Resonance Scanning and Epilepsy [Internet]. Boston, MA: Springer US; 1994 [citato 13 agosto 2024]. p. 263–74. Disponibile su: http://link.springer.com/10.1007/978-1-4615-2546-2_48

83. Alexander B, Loh WY, Matthews LG, Murray AL, Adamson C, Beare R, et al. Desikan-Killiany-Tourville Atlas Compatible Version of M-CRIB Neonatal Parcellated Whole Brain Atlas: The M-CRIB 2.0. Front Neurosci. 5 febbraio 2019;13:34.

84. Gaser C, Dahnke R, Thompson PM, Kurth F, Luders E, the Alzheimer's Disease Neuroimaging Initiative. CAT: a computational anatomy toolbox for the analysis of structural MRI data. GigaScience. 2 gennaio 2024;13:giae049.

85. Potvin O, Mouiha A, Dieumegarde L, Duchesne S. Corrigendum to: “FreeSurfer subcortical normative data” [Data in Brief 9 (2016) 732–736]. Data in Brief. aprile 2019;23:103704.

86. Potvin O, Dieumegarde L, Duchesne S. Normative morphometric data for cerebral cortical areas over the lifetime of the adult human brain. NeuroImage. agosto 2017;156:315–39.

87. Aickin M, Gensler H. Adjusting for multiple testing when reporting research results: the Bonferroni vs Holm methods. Am J Public Health. maggio 1996;86(5):726–8.

88. Zirra A, Rao SC, Bestwick J, Rajalingam R, Marras C, Blauwendraat C, et al. Gender Differences in the Prevalence of Parkinson’s Disease. Movement Disord Clin Pract. gennaio 2023;10(1):86–93.

89. Vogt BA. Cingulate cortex in Parkinson’s disease. In: Handbook of Clinical Neurology [Internet]. Elsevier; 2019 [citato 25 novembre 2024]. p. 253–66. Disponibile su: https://linkinghub.elsevier.com/retrieve/pii/B9780444641960000133

90. Wei X, Wang Z, Zhang M, Li M, Chen YC, Lv H, et al. Brain Surface Area Alterations Correlate With Gait Impairments in Parkinson’s Disease. Front Aging Neurosci. 27 gennaio 2022;14:806026.

91. Deng JH, Zhang HW, Liu XL, Deng HZ, Lin F. Morphological changes in Parkinson’s disease based on magnetic resonance imaging: A mini-review of subcortical structures segmentation and shape analysis. World J Psychiatry. 19 dicembre 2022;12(12):1356–66.

92. Li J, Zhang Y, Huang Z, Jiang Y, Ren Z, Liu D, et al. Cortical and subcortical morphological alterations in motor subtypes of Parkinson’s disease. npj Parkinsons Dis. 5 dicembre 2022;8(1):167.

93. Radziunas A, Deltuva VP, Tamasauskas A, Gleizniene R, Pranckeviciene A, Petrikonis K, et al. Brain MRI morphometric analysis in Parkinson’s disease patients with sleep disturbances. BMC Neurol. dicembre 2018;18(1):88.

94. Deng X, Liu Z, Kang Q, Lu L, Zhu Y, Xu R. Cortical Structural Connectivity Alterations and Potential Pathogenesis in Mid-Stage Sporadic Parkinson’s Disease. Front Aging Neurosci. 31 maggio 2021;13:650371.

95. Hwang KS, Beyer MK, Green AE, Chung C, Thompson PM, Janvin C, et al. Mapping Cortical Atrophy in Parkinson’s Disease Patients with Dementia. Journal of Parkinson’s Disease. 2013;3(1):69–76.

96. Hotz I, Deschwanden PF, Liem F, Mérillat S, Malagurski B, Kollias S, et al. Performance of three freely available methods for extracting white matter hyperintensities: FREESURFER , UBO Detector, and BIANCA. Human Brain Mapping. aprile 2022;43(5):1481–500.

97. Baggio HC, Junqué C. Functional MRI in Parkinson’s Disease Cognitive Impairment. In: International Review of Neurobiology [Internet]. Elsevier; 2019 [citato 25 novembre 2024]. p. 29–58. Disponibile su: https://linkinghub.elsevier.com/retrieve/pii/S0074774218301107

98. Oliveira RVD, Pereira JS. The role of diffusion magnetic resonance imaging in Parkinson’s disease and in the differential diagnosis with atypical parkinsonism. Radiol Bras. agosto 2017;50(4):250–7.

Ringraziamenti

Il primo ringraziamento lo rivolgo alla Prof.ssa Alessandra Bertoldo per avermi dato l'opportunità di svolgere la tesi di laurea su un argomento da me scelto, appoggiando e promuovendo il mio interesse nell'approfondirlo. Non mi ha, infatti, soltanto inserito in un progetto di ricerca di grande rilievo, ma si è anche assicurata di garantirmi le migliori condizioni di studio e lavoro, avendo preziosa considerazione dei grandi cambiamenti personali e professionali che stavo attraversando.

È doveroso sottolineare l'importanza assunta dal mio correlatore, il dott. Simone Cauzzo, a cui va un mio particolare ringraziamento. Mi ha accompagnato passo per passo in questi mesi di lavoro, chiarendo dubbi ed incertezze, mostrandosi sempre disponibile, aiutandomi nelle difficoltà ed incoraggiandomi di fronte agli ostacoli incontrati. Le correzioni da lui impartitemi sono state sempre orientate al mio miglioramento e mai al giudizio. Ed è per questo che oggi voglio augurare a lui ogni bene e la realizzazione di tutti gli obiettivi, auspicandogli di non perdere mai la sua propensione alla divulgazione scientifica che è nobile strumento di arricchimento dell'altro e mai mezzo di esaltazione di sé.

A mia madre. Non esiste modo in cui possa ringraziarti adeguatamente. Sei sempre stata e sarai sempre il mio riferimento cardine in ogni aspetto della mia vita, da quello affettivo a quello professionale. Sei stata la persona che, più di tutte, mi ha sostenuto nel mio percorso esistenziale. Dal mio primo vagito, passando per tutte le difficoltà del mio percorso accademico e della vita in generale, mi hai stretto a te e mi hai dato calore e conforto. Sei stata la sola persona che ha sempre creduto in me, l'unica che, nonostante i fallimenti, mi ha sempre visto come qualcosa di bello, qualcosa per cui valesse la pena sacrificarsi anche quando il mondo sembrava volesse rigettarmi. Sei stata la mia prima e più importante insegnante. È vivido il ricordo di quando mi rincorrevi per farmi studiare alle elementari e di quando, tornata stanca da lavoro, mi aiutavi a ripetere i compiti delle scuole medie e del liceo. Perché, nonostante la stanchezza e le grandi difficoltà che non ti sono mai mancate nella vita, avevi una lezione importante da impartirmi, la più importante di tutte: che per me si può fare! Perché il tuo amore per me non è mai stato in discussione, neanche nei momenti in cui, invero, non me lo sarei meritato. Ti sono riconoscente non solo per la mia vita ma anche per le mie vittorie, che non appartengono ad altri se non a te e a Dio. Ogni volta che sono caduto tu eri lì a risollevarmi. Ogni volta che mi sentivo una nullità tu eri lì a darmi conforto e a ricordarmi quanto valessi. Hai reso ogni mio fallimento l'esperienza più bella, perché ciò che mi è rimasto non è quanto possa essere stata dura la vita, ma quanto sia stato bello avere te accanto in quei momenti. In questa vita ho imparato molte cose, ma le più belle me le hai insegnate tu. A te la dedica di questo traguardo. Grazie di tutto mamma, ti voglio un mondo di bene!

A mia sorella Valeria. Lo sai già, insieme a mamma ci sei tu! Entrambe siete i miei affetti più cari. Sei arrivata circa due anni dopo di me, ma sei stata ogni volta davanti a me. Sin da quando eri piccola ti ho guardata con ammirazione, sei da sempre la mia sorellina bellissima, il gioiello di casa nostra che andava difeso, protetto, tutelato. O almeno così ho provato a fare, secondo quanto raccontano i nostri genitori, come quando, appena nata, mi sono accostato a fare la guardia alla tua culla. Le cose, poi, sappiamo, non sono andate proprio così. Sei sempre stata la più forte e saggia dei due. Quella che aveva maggiore capacità di reazione, quella che fin da subito ha saputo affrontare con coraggio e sapienza la vita. Quella che non aveva paura di mostrare apertura verso gli altri perché già salda nella consapevolezza delle proprie qualità e determinata nei suoi desideri ed obiettivi. Con la tua forza d'animo e sapienza davi sicurezza a tutti, al punto che, anche quando avresti avuto anche tu bisogno di una coccola e/o una carezza, non te la si offriva perché rispetto a me sembravi molto meno bisognosa e scalfibile. Dovevo vegliare io su di te, ma essendo tu troppo più di me, alla fine le cose sono andate al contrario. Sei stata una roccia ed un riferimento per me. A te devo la mia conversione, la ritrovata consapevolezza delle mie qualità ed una visione più chiara dei veri valori della vita. Lo so! Non ti è costato poco in termini emotivi e mentali darmi il tuo sostegno in questi anni e non è stato nemmeno giusto che ti caricassi di quest'onere. Il risultato di oggi va anche a te, ma spero di ricevere la grazia da Dio di poter ripagare, un giorno, tutto il bene che mi hai regalato. Sono, però, consapevole che non ci sarà mai modo, per me, di poter ripagare Lui del regalo che ci ha fatto con te. Io non sono riuscito ad essere il miglior fratello maggiore, ma tu sei rimasta un gioiello prezioso. Ringrazio che tu sia davanti a me e spero tu lo sia sempre, perché così mi basterà solo guardare avanti per vedere la cosa più bella e questo è il vero premio. Hai visto! Alla fine, ho vinto io!

A mio padre. Sei stato la figura battagliera a cui per molto tempo avrei voluto somigliare. Il tuo modo di approcciare alle cose, deciso e senza esitazione, mi ha colpito sin da piccolo. Ho sempre stimato la sicurezza che hai avuto nell'approcciare pragmaticamente ai problemi e la resilienza che hai mostrato nelle avversità della vita. Non mi è riuscito bene emularti, ma d'altra parte ho sempre avuto un temperamento ed un'indole diversi dai tuoi. Dal non riuscire ad uniformarmi a te e dal confronto, non sempre tranquillo, che mi hai dato possibilità di avere, ho imparato a comprendere meglio me stesso e le sfaccettature della mia personalità. Non sono stato capace di seguire la tua linea, ma senza dubbio ti sono debitore per avermi insegnato a seguire la mia. Grazie per i saggi consigli sul piano universitario e professionale che non sempre ho saputo seguire. Grazie per avermi aiutato a capire che la vita non deve essere perfetta per meritare di essere vissuta. Che, quando le cose vanno male, è necessario armarsi della giusta corazza ed affrontarle, evitando così di subirle. Da te ho ereditato la predisposizione per la matematica e la fisica, senza cui, non sarei mai riuscito ad arrivare fin qui. Per questa ed altre cose c'è anche il tuo contributo che mi ha consentito di diventare non solo dottore in ingegneria, ma anche l'uomo che sono. Grazie papà!

A mia zia Maria Carmela. Sei per me un pilastro fondamentale, un riferimento senza il quale la mia vita non avrebbe lo stesso significato. Lo sei sicuramente da prima che sapessi leggere, quando, ho memorizzato, per la prima volta, un numero di telefono: quello di casa di nonno, ricordando la sequenza di tasti da premere. Ma non stavo chiamando casa di nonno, stavo chiamando zia Carmela. Da che ho memoria non c'è stato un momento in cui non ti avessi in considerazione, in cui non fossi consapevole di avere in te una seconda madre a cui appoggiarmi, in caso, tutto intorno a me sembrasse crollare. Era così quando, litigando da bambino con i miei, li minacciavo di andarmene di casa e alla loro domanda su dove avrei pensato di andare potevo rispondere in sicurezza: da mia zia! Sei stata la mia scialuppa di salvataggio durante questi anni di vita, lo sei oggi e lo sarai sempre. Grazie per tutti gli amorevoli sì che mi hai regalato. Grazie per tutto il sostegno che mi hai reso. Grazie per avermi capito quando nessuno sembrava poterlo fare. Grazie per tutto il bene che mi hai donato e per la figura affettiva che hai rappresentato e rappresenti per me. Hai chiarito e consolidato in me il significato di molti valori, da quello degli affetti familiari a quello della cultura. Sei un esempio di integrità, rigorosità e professionalità a cui mi sono ispirato e a cui mi ispererò sempre. Di te non conservo altro che bei ricordi e spero, con questo traguardo, di averne regalato uno anche a te.

Alla famiglia Caiola. Siete e sarete sempre la mia famiglia. Il posto in cui sicuramente voglio abitare, quello dove sono cresciuto, dove so di potermi sentire a casa. Grazie a voi ho capito cosa sono e chi voglio essere. Pensare a voi mi ha dato una mano, nei momenti difficili, a ritrovare me stesso. Grazie per tutti i momenti belli che ho trascorso insieme a voi, in questi anni. Grazie per gli insegnamenti che mi avete dato. Grazie per il calore, conforto e riparo che mi avete regalato. Voi siete la mia famiglia e io sono uno di voi. Il mio sangue è il vostro sangue. Considerate, quindi, come vostro, anche questo traguardo. Grazie a tutte le mie zie, i miei zii e la mia prozia Anna. Grazie a mia nonna Maria e a mio nonno Corrado, per aver costruito una così bella famiglia, dove ho avuto la possibilità di crescere. Vi voglio tutti bene!

Al mio amico Gennaro. Insieme ne abbiamo passate tante. Già dal liceo e per tutto il percorso universitario, ci siamo spalleggiati ed aiutati l'un l'altro. Dal confronto con te ho imparato tante cose. Ti ho sempre stimato per il tuo grande valore intellettuale ed umano. È stato un onore ed un privilegio per me averti accanto in questi anni e poter godere del tuo consiglio e supporto. Grazie per tutti i momenti spensierati e divertenti trascorsi assieme a te. Ti ringrazio per essere l'amico che sei stato e che sei. A te auguro tutto il bene che Dio possa offrirti in questa vita!

Alla mia amica Jessica. Sei stata la sorpresa della mia esperienza patavina. La tua compagnia, durante le giornate di studio, mi ha regalato tanta gioia ed entusiasmo nell'affrontare gli ultimi esami. Sei stata un esempio di determinazione e caparbietà imprescindibile per aiutarmi a superare prove che altrimenti avrei fallito. Grazie per tutti i momenti belli, le risate e l'affetto che mi hai regalato. Ti voglio tanto bene e spero che la vita possa regalarti tutto ciò che desideri.

Anche perché già so che, se la vita pensasse di non concedertelo, te lo prenderesti con la forza. Che Dio ti benedica amica mia!

A David, Federica, Riccardo ed Alessandra. Per voi è necessario un ringraziamento congiunto. Dopo tutto, siete diventati una parte importante della mia vita nello stesso momento. Con voi ho vissuto tante belle esperienze, dal Rotaract fino all'organizzazione delle serate e dei fine settimana da trascorrere assieme. Ma, cosa più importante, siete stati veri amici anche nei momenti difficili e nelle incomprensioni. Stando insieme a voi ho imparato molto, ma l'insegnamento più importante che mi avete dato è che, nonostante le differenze o le divergenze, quello che conta più per me è l'affetto che nutro per voi.

Alla mia amica Annarita. Grazie per tutti i consigli che mi hai dato in questi anni. Grazie per avermi dato un punto di vista diverso e per avermi aiutato ad ampliare le mie vedute. Grazie per l'affetto che mi hai mostrato pur vedendo le mie miserie. Ti voglio bene!

A tutti gli amici che ho incontrato in questi anni. Grazie per aver arricchito la mia vita di bei ricordi e di momenti trascorsi assieme, dal valore inestimabile. Grazie per aver reso questo mio percorso meno arduo e più piacevole da vivere. Grazie per avermi aiutato a trovare un obiettivo quando, nei momenti di aridità, sembrava non potessi riuscire a scorgerne uno.

A tutti coloro che mi hanno ostacolato e mi hanno fatto del male in questi anni. Grazie perché solo nel buio si apprezza lo splendore delle poche luci preziose che illuminano l'universo. Mi avete fatto comprendere meglio quanto io sia fortunato. Mi avete dato una migliore comprensione di quello che di veramente bello ed importante risiede in questa vita. Mi avete aiutato a crescere e diventare una persona più forte e determinata. Sono onorato e grato per aver incontrato anche voi, perché la vera crescita non si ha nei momenti in cui va tutto bene, ma quelli in cui va tutto male. Mi avete dato delle occasioni a cui, con la consapevolezza di oggi, non sarei disposto a rinunciare. A voi auguro ogni bene e offro, con l'aiuto di Dio, il mio perdono e ringraziamento.

Alla mia fidanzata Anna. Ultima, ma non per importanza sei tu! Sei stata un dono per il mio cuore. Riparo per le mie afflizioni. Caposaldo contro molti miei dubbi. Sei arrivata nel momento giusto e hai conferito tanta gioia e amore alla mia vita. Hai dato un significato ed una declinazione diversi a questi ultimi due anni: non sono stati solo gli anni in cui mi sono laureato e ho iniziato a lavorare, ma sono stati gli anni in cui è iniziata la mia storia con te. Sei stata il raggio di sole che ha penetrato le nuvole della mia vita. Sei stata la nota iniziale di una melodia dolcissima. Stando con te sono cambiato molto e parte di quello che ero non lo sarò più. Sei stato uno dei passaggi più significativi della mia esistenza, la risposta di Dio ad una mia necessità. Non ti sarò mai abbastanza grato per quello che hai fatto. Ti ringrazio di tutto il supporto, l'amore e la consolazione di cui mi hai fatto dono. Ti ringrazio per avermi aiutato a

capire le parti positive del mio carattere e modificare quelle negative. Grazie per avermi dato maggiore consapevolezza di me stesso. Con te ho imparato ad apprezzare cose che non avrei mai pensato mi potessero piacere e a rifiutare altre che, non avrei mai pensato essere, per me, così deleterie. L'affetto e l'amore che ho per te non cambieranno mai, nel mio cuore ci sarà sempre posto per te. Hai plasmato la mia vita in una maniera incontrovertibile sei stata la cura a tante mie ferite. Spero solo che, vedendomi conseguire questo traguardo, tu riesca a percepire quello che è il frutto delle tue immense qualità, che mi hanno dato un aiuto prezioso a raggiungerlo. Grazie di tutto mia amata!